TWO-DIMENSIONAL BOUNDARY ELEMENT ANALYSIS OF SEISMIC CRACKING IN CONCRETE GRAVITY DAMS

Vinod Batta

A Thesis

in

The Department

of

Civil Engineering

Presented in Partial Fulfillment of the Requirements
for the Degree of Doctor of Philosophy at
Concordia University
Montreal, Quebec, Canada

February 1995

ISBN 0-612-01273-5

Canada

ABSTRACT

TWO-DIMENSIONAL BOUNDARY ELEMENT ANALYSIS OF SEISMIC CRACKING IN CONCRETE GRAVITY DAMS

Vinod Batta, Ph. D.
Concordia University, Montreal

A two-dimensional formulation based on the boundary element method is presented to investigate earthquake induced fracture in concrete gravity dams. The cracking is represented by the discrete approach wherein each crack surface is modelled in a separate dam domain employing the concept of multi-domain discretization. The principles of linear elastic fracture mechanics are used to define the stress field in front of the crack tip and the stress singularity occurring at the ''p is captured utilizing traction singular quarter-point boundary elements placed on each side. Stability of cracks under dynamic loads is monitored employing a propagation criterion based on the maximum tensile strain theory. The dynamic analysis is carried out by direct integration of the equations of motion. The ability of the formulation to predict correctly the stress singularity at the crack tip is demonstrated. Also verified is the ability of the formulation to simulate and monitor a changing crack profile under dynamic loading through comparison with available experimental data.

Seismic cracking of the prototype Koyna dam is investigated in detail employing both single and multiple fracture models. For the single fracture model, a parametric investigation is conducted to determine the influence of various analytical and material parameters on the fracture response of a gravity dam subjected to an earthquake. Refinement of the numerical modelling of the dam by means of internal collocation is studied and the adopted dual-reciprocity approach is shown to be adequate for seismic fracture analysis of dams. In order to obtain an enhanced database, the seismic cracking response of a monolith of the Pine Flat dam, which represents a more standard gravity-

type dam, is also studied. It is demonstrated that the final pattern of cracking, as well as the fracture process itself, is largely unaffected by the geometrical properties of the cross-section. Furthermore, an attempt is made to examine the likelihood of hydrodynamic pressure build-up in cracks on the water retaining face of a dam. To this end, the corresponding opening/closing data during various phases of the dam response is analyzed. It is found that the dynamic water pressure is more likely to influence response during the post-rupture phase, rather than affect the behavior prior to rupture.

Finally, noting that the fracture investigations undertaken herein assume fixed conditions for the dam base, a time-domain boundary element procedure is proposed to allow future dam/foundation coupling in the dynamic crack propagation analysis of concrete dams.

ACKNOWLEDGEMENTS

The author acknowledges with gratitude the guidance, support and encouragement provided by his thesis supervisor, Professor O. A. Pekau, during the entire course of this research. His critical reviews, together with his excellent sense of engineering judgement, have proved invaluable to the quality of this work.

The initial introduction to this problem by Professor Zhang Chuhan of Tsinghua University, Beijing, and subsequent fruitful discussions during his visits to Concordia University are also gratefully acknowledged.

The financial support for this work was provided by Natural Sciences and Engineering Research Council of Canada under Grant No. A8258. The excellent computing facilities provided at the Civil Engineering Department at Concordia University, largely because of the efforts of Professor Pekau, have been very useful in conducting this research. Thanks are also due to SNC-Lavalin Inc. for allowing the author to take time off from work to complete this research.

Among his friends, the author wishes to mention Denis, the two Richards and Tony for their friendship and support.

The deepest gratitude goes to the family of the author and his Bhua for their inspiration, support and encouragement throughout his studies. Finally, the utmost patience and understanding demonstrated by author's wife Sumeera deserve greatest appreciation. Her help in the preparation of this thesis is also acknowledged thankfully. Of course, these acknowledgements will not be complete without an affectionate mention of author's six month old son Varun, who has been a continuous source of joy during the final stretch of this work.

TO MY PARENTS

CHIRANJILAL JI AND KAUSHALYA DEVI

TABLE OF CONTENTS

LIST OF FIGURES

LIST OF TABLES

LIST OF NOTATIONS

a_0	frequency factor ($\omega b/c_2$)
b	half-width of strip footing or loading
c_1	velocity of dilatation wave
$[c_{11}]$	Rayleigh damping matrix
c_2	velocity of shear wave
f^j	spatial functions used to transform inertial domain integral
[k]	stiffness matrix
k_s	spring stiffness
[m]	mass matrix
n	number of nodes on dam boundary excluding dam-rock interface
(n)	unit outward vector normal to Γ
n_h	number of nodes on dam-rock interface
p_i	component of traction
p^*_{ki}	traction component of static fundamental solution
r	distance between x and ξ
s	$\tan\theta_c/2$
t	time
$t_{(n)i}$	component of traction
$\bar{t}_{(n)ik}$	traction component of dynamic fundamental solution
u_i	component of displacement
$\dot{u}_i$	component of velocity
$\ddot{u}_i$	component of acceleration
$\bar{u}_{ik}$	displacement component of dynamic fundamental solution
u^*_{ki}	displacement component of static fundamental solution
u_r	relative displacement

$\ddot{u}^0$	imposed support acceleration
x	source point
C_{ij}	dynamic compliance of the half-space
C_{kl}	constant coefficients in the boundary integral equation
[E]	inverse of matrix [F]
[G]	boundary element system matrix
[H]	boundary element system matrix
K	combined mode stress intensity factor
K_{ij}	dynamic stiffness of the half-space
K_I	opening mode stress intensity factor
K_{II}	sliding mode stress intensity factor
K_{Id}	fracture toughness of material
M	number of boundary elements in the discretization
[M]	generalized mass matrix
N	total number of time steps
N_i	shape functions
P_i	components of dynamic force under the footing
{Q}	nodal force vector
R	width of discretization on each side of footing; also load vector
R_e	receiver element
S_e	source element
α	Rayleigh damping coefficient
α_i^j	time-dependent functions used to transform inertial domain integral
β	Rayleigh damping coefficient
δ_{ik}	Kronecker's delta
ε_θ	circumferential strain
$\bar{\varepsilon}_\theta$	circumferential strain factor

η^j_{li}	components of traction corresponding to $\tau^j_{lim,\,m}$
κ	material constant related to ν
λ	constant used to obtain spring stiffness k_s
μ	shear modulus of material
ν	Poisson's ratio
θ	angle measured from crack tip
θ_c	crack extension angle
ρ	mass density
$\tau^j_{lim,\,m}$	stress tensor
ω	forcing frequency
Ψ^j_{li}	displacement field corresponding to $\tau^j_{lim,\,m}$
ξ	field point; also generalized coordinate
Δl	length of each boundary element
Δt	time step size
Γ	boundary of the region
Ω	domain of the region

CHAPTER I

INTRODUCTION

1.1 OBJECTIVE AND SCOPE

Accurate prediction of the performance of concrete gravity dams under strong ground motions poses significant analytical challenge. The coupled dam-foundation-reservoir system requires a proper modelling of each sub-system including the inherent non-linearities which may arise from cracking of the dam concrete, non-linear behavior of the foundation material and/or cavitation at the dam-reservoir interface. The present study investigates primarily the first of these problems, namely the cracking behavior of concrete gravity dams under external excitation. The problem is of considerable importance because a large number of existing gravity dams are 50 years or more in age and were designed using the uniform seismic coefficient method which is no longer considered adequate (Chopra 1987). Moreover, for many of these dam sites the seismic codes have been scaled-up, which further necessitates a re-evaluation of the safety of these structures. Since the past experience - cracking of Koyna, Hsigfenkiang and Sefidrud dams (Ahmadi and Khoshrang 1992) - has shown that the dam concrete may crack significantly under an earthquake with strong enough ground shaking, such safety evaluations entail proper crack propagation analysis. The question to be addressed is to what extent a crack of known size and location will grow, since this generally will determine the operational safety of a dam under the dynamic loadings resulting from a future earthquake.

The principal objective of the current research is to develop an efficient and accurate numerical procedure for analyzing seismic cracking in concrete gravity dams and to perform a detailed investigation of their fracture behavior under earthquakes.

Employing the analytical procedure developed in this study, a parametric evaluation involving various analytical and physical parameters is conducted to examine their influence on the fracture response of dams. Since the interaction of reservoir water within a crack on the water retaining face of a dam is of considerable importance, an attempt is made to study the crack opening/closing behavior and relate it to the possible effect of water pressure on fracture process itself.

In addition, independent of the above investigation, a formulation is presented also for the two-dimensional soil-structure interaction problem typically encountered at the base of a gravity dam. In this regard, it has been demonstrated (Chopra 1987) that the response of a dam subjected to earthquake induced vibrations is affected significantly by the interaction with the foundation rock. However, since most of the formulations developed for modelling such interaction (Vaish and Chopra 1974; Dasgupta and Chopra 1979; Abdalla 1984) work in the frequency domain, they cannot be incorporated in the analysis of dams undergoing crack propagation. The non-linearity inherent in such analyses necessitates that the stiffness or compliance functions of the foundation medium be derived in the time domain. A procedure is therefore developed in the time domain so that it can be integrated in the seismic crack propagation analysis of dams. The boundary element method, which offers many advantges over the finite element method in the modelling of infinite domains, is adopted for this formulation also.

1.2 REVIEW OF EXISTING LITERATURE

1.2.1 Preliminary remarks

In carrying out a dynamic crack propagation analysis three distinct aspects of the problem arise: namely, the choice of an appropriate numerical tool, proper modelling of the crack itself and, finally, the selection of a suitable criterion for crack extension. In order to formulate an accurate and yet efficient methodology to solve this complex problem, a proper blending of these features is required.

Current numerical techniques employed in fracture analysis comprise the finite element and the boundary element methods. In either method, a proper representation of the strain discontinuity imposed by the presence of cracks in the domain is imperative. The available alternatives consist of explicitly representing the crack as a physical separation of the nodes or else modelling the formation of a crack by altering the stress-strain relationship in the cracked zone in such a way that no tensile stress develops perpendicular to the crack. These alternative techniques are, respectively, known as the discrete and the smeared crack approaches. While the finite element method is capable of easily integrating either of these approaches in its formulation, the boundary element technique poses certain difficulties when used in conjunction with the smeared crack approach and thus exhibits limitations when applied to structures which have a cluster of small cracks situated in specific zones. On the other hand, in analyzing the propagation of a discrete crack, the finite element method requires complete remeshing of the domain around the original and the propagated cracks. This redefinition of the mesh enlarges the system and destroys its bandwidth. Alternative use of boundary element discretization requires only the addition of elements to represent the extended crack profile.

1.2.2 Past investigations

The available studies of seismic cracking in concrete gravity dams have employed mostly the finite element method together with either smeared or discrete modelling of the crack. The smeared crack model combined with tensile strength propagation criterion was employed in early studies of earthquake induced cracking (Pal 1976; Mlakar 1987; Graves and Derucher 1987). However, as demonstrated by Bazant and Cedolin (1979), the method lacks objectivity because the force required to propagate the crack after initiation depends upon the size of the finite elements in front of the crack. To overcome this spurious mesh dependence it was suggested that the cracking model must incorporate the principles of fracture mechanics so that the fracture energy can be conserved during the

cracking process. This procedure was subsequently employed by Vargas-Loli and Fenves (1989) to study the effect of cracking on the earthquake response of gravity dams. In order to circumvent the limit on the size of the finite elements, the size reduced strength criterion proposed by Bazant and Cedolin (1979) was used. Although objective results were obtained, the analysis could only predict diffused crack patterns, which is the expected limitation of smeared crack procedures. Improvements in the form of localization of the crack band (Bazant and Oh 1983) and the use of a coaxial rotating crack model (Rots 1991) have been attempted and the latter was recently adopted by Bhattacharjee and Leger (1993) to study cracking of concrete dams under static and dynamic loads. The formulation employs nonlinear fracture mechanics and relies on constitutive modelling for crack initiation as well as for the propagation behaviour. The procedure, however, limits the maximum size of the finite elements which can be used in the mesh and thereby introduces a computational disadvantge when analyzing large dams.

The above considerations have prompted the use of discrete crack models. Discrete models provide a better physical representation of cracks and, in the case of hydraulic structures such as dams, also permit modelling of the water pressure within the crack. Employed in a finite element procedure the model requires a remapping of the mesh at each stage of crack extension. Employing a semi-adaptive mesh updating procedure and a strength-based criterion for the cracking process Skrikerud and Bachmann (1986) were the first to apply discrete crack model in analyzing cracking in dams. However, results for the Koyna dam showed that the predicted cracking was strongly mesh dependent. The procedure was subsequently refined by Feltrin et al. (1992) who modified the discrete crack model to incorporate strain softening of the concrete but found this refinement to be of minor importance.

Discrete crack propagation based on linear elastic fracture mechanics was proposed by Ayari and Saouma (1990). A contact-impact model for crack closure was developed and seismic cracking analysis of Koyna dam was presented. Unfortunately,

results were presented for only an unrealisticly high value of the concrete fracture toughness. Chapuis et al. (1985), on the other hand, used a material model derived with particular regard to the effect of strain rate and seismic loading history for analyzing cracking of the Pine Flat dam. However, the hybrid smeared-discrete crack model used in following the crack trajectory requires two sets of analyses. More recently, Zhou and Lin (1992) employed an idealized sliding structural model to study the seismic cracking of the Fongman dam in China. The analytical results were also corroborated by model testing on a shake table.

In recent years discrete crack propagation analysis procedures have also been developed using the boundary element method, although for the dynamic case the literature is scarce. The general advantages of adopting a boundary approach, particularly the reduction of the dimensions of the problem, are now well established. Furthermore, the two-dimensional problem posed by the present fracture analysis of a gravity dam monolith requires only the use of line elements. Modelling and propagation of discrete cracks is thus considerably facilitated as the rediscretization process involves only realigning the line elements along the new crack profile. Moreover, since the method requires discretization only of the boundary of the structure and utilizes the exact solution of the governing differential equation in the interior, it offers a more accurate solution for fracture problems than the finite element technique. However, unlike the latter, the boundary element method yields a set of equations which is neither symmetric nor sparse, although it is dimensionally much smaller than the corresponding finite element system.

Application of the boundary element method to the analysis of cracked structures poses an analytical difficulty resulting from the identical coordinates of nodes along the two crack surfaces, which lead to a singular system of equations. Various strategies have been proposed in the literature (Cruse 1978; Snyder and Cruse 1975; Blandford et al. 1981) to overcome this limitation. Of these, the multidomain discretization proposed by Blandford et al. (1981) and employed by Ingreffea et al. (1989) provides the most accurate

mathematical representation of the crack but was limited therein to fracture analysis under static loads. For dynamic fracture mechanics, a brief summary of previous applications of the boundary element method is presented by Manolis and Beskos (1988), which reveals that most of these attempts (Fan and Hahn 1985; Mettu and Nicholson 1988; Dominguez and Chirino 1986) are restricted to the analysis of stationary cracks under dynamic loads and thus do not include crack propagation.

To the author's knowledge, the only available boundary-element-based dynamic crack propagation analysis formulation is by Feng (1994). The dynamic analysis procedure, however, employed the mode superposition technique for obtaining the time-step response and was therefore not very efficient for the present non-linear analysis, as the eigenvalue problem was required to be solved after each modification to the crack geometry. The formulation also relied on the assumption of a hypothetical cracked structure wherein overlap of the crack surfaces was permitted during crack closure in order to maintain unchanged the elastic stiffness of the structure. Change in stiffness accompanying crack closure was simulated by load pulses applied at the contact nodes. An alternative crack closure scheme was also suggested employing an iterative force method, which further reduced the efficiency. In addition, the formulation was limited to the treatment of a single crack propagating through the dam.

1.3 ORGANIZATION OF THE THESIS

In the present study, the multidomain boundary element method has been adopted for structural idealization. The discrete crack approach is employed for fracture modelling and the crack propagation procedure is generalized to account for the presence of multiple cracks. Principles of linear elastic fracture mechanics are used to conduct a time-history analysis of crack propagation. Although normally nonlinear fracture mechanics, accounting for the fracture process zone in front of the crack tip, is recommended for concrete structures, for large structures such as dams linear elastic fracture mechanics is

considered appropriate (Bruhwiler et al. 1991). It is argued that, in the case of concrete dams, the size of fracture process zone is small compared to the size of the structure. Brittle fracture thus dominates the cracking since the fracture energy contribution to the total energy is not significant (Feltrin et al. 1992; Bhattacharjee and Léger 1993).

Implementation of the boundary element procedure for dynamic crack propagation analysis is presented in Chapter II. Techniques for modelling the crack and monitoring its stability are also described in this Chapter, together with the procedure used for remeshing after each crack extension. The accuracy of the dynamic boundary element formulation in capturing the crack tip stress singularity in a dynamic environment is verified using a classical solution. The capability of the developed procedure to conduct a time step-by-step crack propagation analysis and to accurately predict the crack profile is demonstrated by comparing the analytical results with those available for a laboratory specimen of a gypsum cantilever beam tested on a shake table.

Application of the developed procedure to study earthquake induced cracking in a concrete gravity dam is presented in Chapter III. Also discussed is a refinement to the transient boundary element formulation in the form of internal collocation within a domain in order to permit a better representation of the inertia of the system. Necessity of internal collocation for fracture analysis of dams is evaluated and the influence of various analytical and physical parameters on the cracking response of dams is investigated. Results are presented for the Koyna dam with a single crack propagating from the downstream face.

In Chapter IV the above procedure is extended to a more general case where the occurrence and simultaneous propagation of multiple cracks can be simulated. A detailed examination of the cracking process for the Koyna dam employing both single and multiple fracture models is conducted. Particular attention is focussed on the patterns of rupture predicted by these fracture models, as well as on the associated crack opening behaviors.

Chapter V presents a time-domain boundary element formulation for two-dimensional elastodynamic foundation problems. The developed procedure is verified by computing the response of the half-space, representing the soil medium, to external dynamic stresses and comparing the results with available analytical solutions. The applicability and usefulness of the formulation for future dynamic interaction problems is established through successful analyses of surface as well as embedded rigid strip foundations. Future implementation of the procedure to incorporate foundation interaction effects in the crack propagation analysis of concrete gravity dams is also discussed in this Chapter.

Finally, the significant conclusions of the present research are summarized in Chapter VI. Recommendations for future work in the area are also given in this Chapter.

CHAPTER II

IMPLEMENTATION OF BOUNDARY ELEMENT METHOD FOR CRACK PROPAGATION ANALYSIS

2.1 INTRODUCTION

The present Chapter formulates the problem of dynamic crack propagation using boundary elements. Multidomain boundary discretization is adopted to model the structure and a procedure is developed to study the extension of an existing crack under external excitation. Analysis is conducted by means of a time marching scheme and the extent, direction and time of propagation of the crack is determined employing the principles of linear elastic fracture mechanics theory. In addition to the direct integration of the equations of motion, the formulation proposed herein avoids also the hypothetical cracked structure of Feng (1994). To simulate closure of the crack, dimensionless springs are employed to avoid overlap, thus providing closer analytical modelling of the physical situation. Comparison with the available experimental results for a gypsum cantilever beam tested on a shaking table under quasi-harmonic excitation confirms the good performance of the dynamic crack propagation analysis proposed herein.

2.2 BOUNDARY ELEMENT FORMULATION

The boundary element formulation, also known as boundary integral equation analysis, redefines a problem in terms of quantities assigned to the boundary of the structure only and thus reduces the integral operations by one step. The governing equations are replaced by a boundary integral operator using Betti's reciprocal work theorem. In the multidomain boundary element method, the structure is divided into subdomains by the crack profile in such a way that the two crack surfaces are represented

as traction free boundaries belonging to two separate domains. The integral equations are then formulated for each domain and assembled. Beyond the crack tip these domains are analytically separated by a line extending from the crack tip. Continuity and equilibrium conditions are satisfied along this arbitrary line.

For static problems the boundary integral expressions are widely available; however, their use in a dynamic analysis is limited because of the additional requirement of formulating the mass matrix as a function of the boundary nodes only. Earlier attempts to use the boundary solutions in elastodynamics, typically that of Cruse and Rizzo (1968), work in transformed domain and require back-transformation to obtain the time-dependent solution. Alternatively, transient boundary solutions have been proposed by Nardini and Brebbia (1982) and Ahmad and Banerjee (1985) formulated using the frequency-independent functions and particular solution approach. The procedure of Nardini and Brebbia (1982) is adopted for the present formulation and is briefly summarized below.

The boundary integral expression for a 2-D isotropic, homogeneous and linear elastic body Ω with boundary Γ can be written as

$$-C_{ki}(\xi)\,u_i(\xi) + \int_\Gamma u^*_{ki}(\xi, x)\,p_i(x)\,d\Gamma - \int_\Gamma p^*_{ki}(\xi, x)\,u_i(x)\,d\Gamma - \rho \int_\Omega \ddot{u}_i(x, t)\,u^*_{ki}(\xi, x)\,d\Omega = 0 \qquad (2.1)$$

where ρ is the mass density; ξ and x are the source and field points, respectively; C_{ki} denote constants uniquely defined by the position of point ξ with respect to the boundary; u_i and p_i represent displacements and tractions on the boundary; $\ddot{u}_i$ denote the components of acceleration; u^*_{ki} and p^*_{ki} comprise the frequency independent fundamental solution defined in Appendix A. In equation (2.1) standard tensor notation, with a repeated subscript implying summation, is adopted. A comma denotes spatial differentiation, while

temporal differentiation is denoted by an overhead dot. In order to transform the inertial integral, an approximation for acceleration $\ddot{u}_i$ within the domain is employed. Expressing the time-dependent displacements $u_i(x,t)$ as the sum of m spatial functions $f^j(x)$ multiplied by the unknown time-dependent functions $\alpha_i^j(t)$ yields

$$u_i(x,t) = \alpha_i^j(t) f^j(x); \quad (j = 1 \text{ to } m) \tag{2.2}$$

The acceleration $\ddot{u}_i(x,t)$ can then be written as

$$\ddot{u}_i(x,t) = \ddot{\alpha}_i^j(t) f^j(x) \tag{2.3}$$

Defining a displacement field ψ_{li}^j such that the corresponding stress tensor is given by

$$\tau_{lim,m}^j = \delta_{li} f^j \tag{2.4}$$

where δ_{li} is the Kronecker delta, and utilizing equation (2.2), permits expressing the inertial domain integral of equation (2.1) as

$$\rho \int_\Omega \ddot{u}_i(x,t)\, u_{ki}^*(\xi,x)\, d\Omega = \rho \ddot{\alpha}_l^j(t) \{ - C_{ki}(x)\, \psi_{li}^j(x) + \int_\Gamma u_{ki}^*(\xi,x)\, \eta_{li}^j(x)\, d\Gamma - \int_\Gamma p_{ki}^*(\xi,x)\, \psi_{li}^j(x)\, d\Gamma \} \tag{2.5}$$

where η_{li}^j are the tractions corresponding to the stress field τ_{lim}^j.

Combining equations (2.5) and (2.1) yields the following expression:

$$C_{ki}(\xi)\, u_i(\xi) + \int_\Gamma p_{ki}^*(\xi,x)\, u_i(x)\, d\Gamma - \int_\Gamma u_{ki}^*(\xi,x)\, p_i(x)\, d\Gamma - \rho \ddot{\alpha}_l^j(t) \{ C_{ki}(\xi)\, \psi_{li}^j(x) + \int_\Gamma p_{ki}^*(\xi,x)\, \psi_{li}^j(x)\, d\Gamma - \int_\Gamma u_{ki}^*(\xi,x)\, \eta_{li}^j(x)\, d\Gamma \} = 0 \tag{2.6}$$

This is the governing integral equation which, in the multidomain formulation, is applied to the boundary of each subdomain. It should be noted that the representation of the internal displacement field by equation (2.2) introduces an approximation because the functions $f^j(x)$ result in displacements ψ^j_{li} and the corresponding stresses τ^j_{lim} which satisfy only static equilibrium given by equation (2.4). On the other hand, the procedure of Ahmad and Banerjee (1985) eliminates this approximation by employing a domain displacement field that satisfies more closely the differential equation of a dynamic problem. This is achieved by considering also the inertial effect in defining the displacement field. The need for this, or similar refinement such as the introduction of interior point collocation, is discussed in the next Chapter.

2.3 BOUNDARY DISCRETIZTION AND NUMERICAL SOLUTION

Numerical solution of integral equation (2.6) is obtained by discretizing boundary Γ into a finite number of elements. Displacements and tractions within these boundary elements may be expressed as interpolation functions using standard isoparametric formulation. Since use of these elements in the vicinity of the crack tip does not account for the true variation of displacements and stresses, special crack tip boundary elements are used.

2.3.1 Crack tip boundary elements

Linear elastic fracture mechanics theory suggests that the displacements and tractions, respectively, exhibit $\sqrt{r}$ and $1/\sqrt{r}$ variation in the vicinity of the crack tip, where r is the distance from the tip. The required displacement variation is achieved by moving the mid-point node of the quadratic element to the quarter point, as is commonly done in the corresponding finite element formulation. This process is shown in Figure 2.1. Thus, the displacement variation within the crack tip element is expressed by

$$u = a_0 + a_1\sqrt{\xi} + a_2\xi = \sum_{i=1}^{3} N_i(\xi)\, u_i \tag{2.7}$$

where a_0, a_1 and a_2 are coefficients; ξ is the normalized coordinate; $N_i(\xi)$ represent the element shape functions; and u_i are the nodal displacements. For the quarter-point element of Figure 2.1(b), shape functions $N_i(\xi)$ are given by

$$\begin{aligned} N_1(\xi) &= 1 - 3\sqrt{\xi} + 2\xi \\ N_2(\xi) &= 4(\sqrt{\xi} - \xi) \\ N_3(\xi) &= -\sqrt{\xi} + 2\xi \end{aligned} \tag{2.8}$$

For the element tractions, however, the quarter-point boundary elements require additional modification of the interpolation functions. This is because the boundary element method requires the displacements and tractions to be independently represented, unlike the finite element method where the traction singularity is inherently obtained by differentiating the displacement shape functions. The correct traction shape functions, representing the analytical singularity, are obtained in this case by multiplying the displacement shape function by $1/\sqrt{\xi}$. Thus, the traction variation over the crack tip element becomes

$$t = (a_0 + a_1\sqrt{\xi} + a_2\xi)/\sqrt{\xi} = \sum_{i=1}^{3} \frac{1}{\sqrt{\xi}} N_i(\xi)\, t_i \tag{2.9}$$

where t_i represent the nodal values of traction.

The traction singular quarter-point boundary elements defined above are introduced only at the crack tip, whereas the elements adjoining these are of the standard isoparametric type.

2.3.2 Discretized boundary equations

A discretized matrix form of equation (2.6) can now be written as

$$[M]\{\ddot{u}\} + [H]\{u\} = [G]\{p\} \tag{2.10}$$

where [H] and [G] are the system matrices of the corresponding static problem; {u}, {ü} and {p} are the displacement, acceleration and traction vectors, respectively; and [M] represents the generalized mass matrix which has the form

$$[M] = \rho([G][\eta] - [H][\psi])E \tag{2.11}$$

with $[E] = [F]^{-1}$, where [F] is the matrix of values of functions $f^1(x)$ evaluated at the boundary nodes. Various choices for the class of functions f^1 have been proposed in Nardini and Brebbia (1982). Since these functions are used to formulate the inertial matrix only and noting that the mass integral does not involve derivatives, simple interpolation functions provide reasonable accuracy. Herein, functions $f^1 = C - R(\xi_j, x)$ are adopted, where $R(\xi_j, x)$ is the distance between point ξ_j and x, and C is a suitably chosen constant. The common value for C is unity and this is also employed herein. The corresponding expressions for the displacements ψ^j_{li} and tractions η^j_{li} are given in Appendix A.

Equation (2.10) is the governing discretized boundary integral equation for the dynamic system. Since use of nodal forces is preferred over nodal tractions {p} for most engineering applications, a general transformation of this equation is carried out. For distribution matrix [N], with coefficients derived from element interpolation functions, the nodal forces {Q} can be expressed as

$$\{Q\} = [N]\{p\} \tag{2.12}$$

Using equation (2.12) and premultiplying equation (2.10) by $[N][G]^{-1}$, one obtains

$$[m]\{\ddot{u}\} + [k]\{u\} = \{Q\} \tag{2.13}$$

where

$$\begin{aligned} [k] &= [N][G]^{-1}[H] \\ [m] &= [N][G]^{-1}[M] \end{aligned} \tag{2.14}$$

In equation (2.14), [k] and [m] represent the stiffness and mass matrices of the system, respectively. It should be noted that equation (2.13) is valid over the entire boundary of the system.

In most practical applications, the forcing functions are in the form of external excitations or support movements acting over only certain portions of the boundary. If subscript '1' is used to identify those portions of the boundary on which no kinematic excitations act, equation (2.13) can be partitioned and rewritten as

$$[m_{11}]\{\ddot{u}_r\} + [k_{11}]\{u_r\} = [m_o]\{\ddot{u}^o\} + \{Q_1\} \tag{2.15}$$

in which $\ddot{u}^o$ denotes the vector of imposed support accelerations, $[m_0]$ is a suitably transformed inertial matrix; and $\{u_r\}$ represents the unknown relative displacement vector with respect to the support movement.

2.3.3 Simulation of crack closure

Discrete cracks require special modelling in a dynamic environment. This is because a cracked structure subjected to external excitation experiences alternate opening and closing of the crack. During the opening phase, the two surfaces separate and become traction free over the open portion of the crack. On the other hand, when the crack is in the process of closing the surfaces come into contact and bear against each other over the closed length of the crack. In modelling the crack by an analytical technique such as the present multidomain boundary element method, the two crack surfaces are represented as

traction free boundaries. Thus, the correct representation of the opening phase is inherent in the analytical model; however, in representing crack closure the model allows overlap of the surfaces. This limitation arises because, once a certain number of nodes on the two crack flanks have come into contact, they are not prevented from moving past one another when the structure undergoes subsequent deformation.

The above analytical limitation is overcome by employing a series of non-dimensional and massless springs of high stiffness between adjacent nodes of the two crack flanks. Stiffness properties of these springs are determined such that overlap is prevented. A brief description of the solution procedure used for equation (2.15) and the required modifications to prevent overlap is given below.

2.3.4 Solution procedure

Equation (2.15) represents dynamic equilibrium for the boundary element system without damping. With the introduction of viscous damping equation (2.15) becomes

$$[m_{11}]\{\ddot{u}_r\} + [c_{11}]\{\dot{u}_r\} + [k_{11}]\{u_r\} = [m_o]\{\ddot{u}^o\} + \{Q_1\} \qquad (2.16)$$

where $[c_{11}]$ is the Rayleigh damping matrix which has the well-known form

$$[c_{11}] = \alpha[m_{11}] + \beta[k_{11}]$$

in which α and β represent the Rayleigh damping coefficients. Although the system matrices $[m_{11}]$ and $[k_{11}]$ are not symmetric, it is nonetheless possible to decouple equation (2.16) into component modes (Feng 1994). Coefficients α and β can thus be obtained from standard procedure by relating them to the assumed damping in two selected modes of vibration.

Equation (2.16) is solved to obtain the unknown displacement $\{u_r\}$ for a given

external excitation $\{\ddot{u}^o\}$ and external forces $\{Q_1\}$. The choice of the appropriate integration technique is, however critical. Direct time step-by-step integration using the Houbolt method is employed in the present study. Not only does the method provide numerical damping for the higher modes it also, as discussed later, avoids the additional assumptions required to carry out the dynamic crack propagation analysis.

For convenience, various subscripts in equation (2.16) are dropped and it is re-written as

$$[m]\{\ddot{u}\} + [c]\{\dot{u}\} + [k]\{u\} = \{R\} \tag{2.17}$$

for the linear case where no crack propagation is considered. The load vector $\{R\} = ([m_o]\{\ddot{u}^o\} + \{Q\})$. In the nonlinear analysis involving a propagating crack, the term [k]{u} in equation (2.17) is replaced by the nonlinear restoring force vector $\{p_r\}$. Thus, equation (2.17) becomes

$$[m]\{\ddot{u}\} + [c]\{\dot{u}\} + \{p_r\} = \{R\} \tag{2.17a}$$

in which the restoring force vector $\{p_r\}$ is updated after each stage of crack propagation based on the current tangent stiffness matrix of the cracked dam obtained as discussed in Appendix A.

At the $(n+1)^{th}$ time step, displacement $\{u_{n+1}\}$ can be written as

$$\{u_{n+1}\} = \{u_n\} + \{\delta u_n\} \tag{2.18}$$

where $\{\delta u_n\}$ is the incremental displacement at the $(n+1)^{th}$ time step. Using the backward difference expressions for acceleration and velocity and utilizing equation (2.18), equation (2.17a) can be written as

$$\begin{aligned}\left(\frac{2}{\Delta t^2}[m] + \frac{11}{6\Delta t}[c] + [k]\right)\{\delta u_n\} &= \left(\frac{3}{\Delta t^2}[m] + \frac{7}{6\Delta t}[c]\right)\{u_n\} \\ -\left(\frac{4}{\Delta t^2}[m] + \frac{3}{2\Delta t}[c]\right)\{u_{n-1}\} &+ \left(\frac{1}{\Delta t^2}[m] + \frac{1}{3\Delta t}[c]\right)\{u_{n-2}\} + \{R_{n+1}\}\end{aligned} \tag{2.19}$$

in which Δt is the time step size. Equation (2.19) is solved to obtain the incremental displacement $\{\delta u_n\}$. Thus,

$$\delta u_n = [\hat{k}]^{-1} \{\hat{R}_{n+1}\} \tag{2.20}$$

where the effective stiffness matrix $[\hat{k}]$ is expressed as

$$[\hat{k}] = \frac{2}{\Delta t^2}[m] + \frac{11}{6\Delta t}[c] + [k]$$

and the pseudo load vector $\{\hat{R}_{n+1}\}$ is given by

$$\{\hat{R}_{n+1}\} = \{R_{n+1}\} + [m]\,(3\{u_n\} - 4\{u_{n-1}\} + \{u_{n-2}\})/\Delta t^2$$
$$+ [c]\,(\frac{7}{6}\{u_n\} - \frac{3}{2}\{u_{n-1}\} + \frac{1}{3}\{u_{n-2}\})/\Delta t$$

Since the solution for δu_n requires knowledge of u_n, u_{n-1} and u_{n-2}, the solution for the first two time steps is obtained by employing the central difference explicit scheme with a fraction of Δt as the time step.

Once the boundary displacement vector $\{u_{n+1}\}$ is obtained from equation (2.18), relative displacements are calculated for all the pairs of nodes situated along the crack. Thus, if 'i' and 'j' denote a pair of nodes belonging to the upper and lower crack flanks (Figure 2.2), overlap is said to occur if

$$u_{ri} < u_{rj} \tag{2.21}$$

where u_{ri} and u_{rj} are the normal components of displacements at nodes i and j, respectively. If equation (2.21) is satisfied, a dimensionless spring is introduced between these nodes to account for the bearing force acting on the crack surfaces. The system stiffness matrix [k] of equation (2.17) is correspondingly modified as follows for spring stiffness k_s introduced between contact nodes i and j:

$$[\bar{k}] = \begin{bmatrix} k_{11} & k_{12} & & & & k_{1m} \\ k_{21} & k_{22} & & & & \\ & & k_{ii}+k_s & & k_{ij}-k_s & \\ & & & k_{(i+1)\,(i+1)} & & \\ & & k_{ji}-k_s & & k_{jj}+k_s & \\ k_{m1} & & & & & k_{mm} \end{bmatrix}$$

Spring stiffness k_s is given a numerically large value based on the average stiffness associated with the nodal pair connected by the spring. Thus,

$$k_s = \lambda \left(\frac{k_{ii}+k_{jj}}{2}\right) \tag{2.22}$$

The value for λ is obtained by trial in order to minimize the overlap. (For the example cantilever structure to follow $\lambda = 4$).

Two methods are available to complete the numerical solution of the crack closure process. One is to check for overlap at each node starting from the crack tip and to introduce the spring at the first such location; then the response is re-calculated for the current time step. The procedure is repeated for all nodes lying along the crack interface. However, this approach becomes inefficient if a large number of nodes is present on the crack line, since a new stiffness matrix has to be formed and decomposed in each cycle. In the present analysis the equilibrium unbalance method (Kanaan and Powell 1973), formulated for non-linear problems, is employed instead. This method is based on the fact that, even if there occurs a stiffness change during a time step, the deformations obtained with the previous stiffness are reasonably accurate because the time step is short, and also because the response of the structure is affected substantially by inertia and damping effects. Following this approach, the stiffness matrix is modified once for all the nodes where overlap is detected and a corresponding unbalance load is added to the force vector

for the next time step.

The relative displacements for all nodal pairs along the crack line are monitored at each step. If the crack tends to open at a particular location where a spring already exists, the latter is removed and the stiffness matrix and the force vector are correspondingly modified. In order to improve the solution accuracy and to avoid the development of numerical instability, an iterative scheme is applied in a time step subsequent to a stiffness change. The iterative sequence used is the generalized Newton process.

2.4 CRACK PROPAGATION

2.4.1 Computation of stress intensity factors

After the nodal displacements are obtained at each time step, the displacement correlation technique is employed to obtain the stress intensity factors in order to monitor the crack propagation.

For mixed-mode crack propagation (i.e. opening and sliding type), the displacement field near the tip (for r<<a, where 'a' represents the length of the crack) can be expressed in terms of stress intensity factors as follows:

$$u_x = \frac{K_I}{4\mu}\sqrt{\frac{r}{2\pi}}\left[(2\kappa-1)\cos\frac{\theta}{2}-\cos\frac{3\theta}{2}\right]+\frac{K_{II}}{4\mu}\sqrt{\frac{r}{2\pi}}\left[(2\kappa+3)\sin\frac{\theta}{2}+\sin\frac{3\theta}{2}\right]$$

$$u_y = \frac{K_I}{4\mu}\sqrt{\frac{r}{2\pi}}\left[(2\kappa-1)\sin\frac{\theta}{2}-\sin\frac{3\theta}{2}\right]-\frac{K_{II}}{4\mu}\sqrt{\frac{r}{2\pi}}\left[(2\kappa-3)\cos\frac{\theta}{2}+\cos\frac{3\theta}{2}\right] \qquad (2.23)$$

where r and θ are defined in Figure 2.3(a); K_I and K_{II} are mode I and mode II stress intensity factors, respectively; μ is the shear modulus; and κ is a material constant defined in terms of Poisson's ratio υ: $\kappa = (3 - 4\upsilon)$ for plane strain; and $\kappa = (3 - \upsilon)/(1 + \upsilon)$ for plane stress.

Using equations (2.23), expressions for the stress intensity factors can be obtained in terms of the relative displacements at the nodes of the crack tip elements (Kanninen and Popelar 1985). Depending upon the number of nodes, different formulae result. A simple 'one-point' formula is obtained if equations (2.23) are evaluated for $\theta = \pm 180^o$ (Smith and Mason 1982). Thus,

$$K_I = \frac{2\mu}{(\kappa+1)}\sqrt{\frac{\pi}{2r}}(V_D - V_B)$$
$$K_{II} = \frac{2\mu}{(\kappa+1)}\sqrt{\frac{\pi}{2r}}(U_D - U_B) \qquad (2.24)$$

where V_D, V_B and U_D, U_B are the V and U direction displacements for nodes D and B, respectively, as shown in Figure 2.3(b). The above expressions yield reasonably accurate values for the stress intensity factors for small values of r. Higher order formulae involving more than one nodal pair can also be derived (Smith and Mason 1982).

2.4.2 Criterion for crack extension

The stress intensity factors obtained above determine the time and direction of crack propagation. While simpler crack extension models such as the one based on Griffith's theory apply only to self-similar crack growths, a more comprehensive criterion needs to be applied in situations where the crack turns or curves under general loading conditions. Available criteria for such crack extension include the maximum tensile stress theory postulated by Erdogan and Sih (1963) and the maximum strain energy density criterion proposed by Sih and Macdonald (1974). The latter criterion has been favored by many researchers because of its simplicity and consistent performance to account for load time history effects regardless of geometry, material or loading type. A more recent and equally simple criterion which is ideally suited for crack growth in brittle materials, proposed by Fan (1983), is adopted in the present formulation. This criterion is based on

the maximum tensile strain and uses the combined stress intensity factor K of the mixed-mode mechanism as the basis for determining crack instability. It postulates that crack growth follows in the radial direction θ_c for which the circumferential strain factor (defined below) attains a maximum.

Employing the coordinate system of Figure 2.3(a), circumferential strain ε_θ for mixed-mode fracture in plane stress can be expressed in the form

$$\varepsilon_\theta = \frac{1}{4\sqrt{2\pi r}} \{ \frac{K_I}{E} \left[(3-5\upsilon) \cos\frac{\theta}{2} + (1+\upsilon) \cos\frac{3\theta}{2} \right] - \frac{K_{II}}{E} \left[(3-5\upsilon) \sin\frac{\theta}{2} + 3(1+\upsilon) \sin\frac{3\theta}{2} \right] \} \qquad (2.25)$$

The corresponding circumferential strain factor is defined as

$$\tilde{\varepsilon}_\theta(\theta) = 4\sqrt{2\pi r}\varepsilon_\theta$$

or

$$\tilde{\varepsilon}_\theta(\theta) = \frac{K_I}{E} \left[(3-5\upsilon) \cos\frac{\theta}{2} + (1+\upsilon) \cos\frac{3\theta}{2} \right] - \frac{K_{II}}{E} \left[(3-5\upsilon) \sin\frac{\vartheta}{2} + 3(1+\upsilon) \sin\frac{3\theta}{2} \right] \qquad (2.26)$$

which is noted to be independent of r. Crack extension angle θ_c is obtained by differentiating equation (2.26) with respect to θ and setting the result to zero. This leads to

$$2\upsilon K_I s^3 + 2(3+4\upsilon) K_{II} s^2 - (3+\upsilon) K_I s - (3+\upsilon) K_{II} = 0 \qquad (2.27)$$

where $s = \tan\theta_c/2$.

Equation (2.27) is solved to obtain the direction of crack extension when the crack is found to be unstable under applied loading, i.e. when the combined stress intensity factor K exceeds the dynamic fracture toughness of the material. It should be noted that,

for problems involving dynamic loading, the material dynamic fracture toughness K_{Id} should be employed for determining crack instability because of its significant variation from the static toughness (Kanninen and Popelar 1985). Thus the critical value of the circumferential strain factor, obtained for mode I fracture by substituting K_{II} and θ each equal to zero in equation (2.26), becomes

$$\tilde{\varepsilon}_{\theta cr} = \frac{4(1-\upsilon)}{E} K_{Id} \tag{2.28}$$

which, when used in conjunction with equation (2.26), yields the following crack instability criterion:

$$K = \frac{1}{4(1-\upsilon)} \{ K_I \left[(3-5\upsilon)\cos\frac{\theta_c}{2} + (1+\upsilon)\cos\frac{3\theta_c}{2} \right] - K_{II} \left[(3-5\upsilon)\sin\frac{\theta_c}{2} + 3(1+\upsilon)\sin\frac{3\theta_c}{2} \right] \} \geq K_{Id} \tag{2.29}$$

where θ_c is obtained from equation (2.27).

2.5 REDISCRETIZATION

As stated earlier, the multidomain boundary element method requires the crack surfaces to belong to two different subdomains. To achieve this in the analytical model, the domains on either side of the crack are separated by an arbitrary line drawn from the crack tip. Thus, each of the crack surfaces forms part of the boundary of a separate subdomain for which equation (2.6) is independently evaluated. Continuity of displacements and equilibrium of tractions are then enforced along this prolonged line to yield the governing boundary equations for the entire structure.

In the present step-by-step analysis the combined stress intensity factor K is continuously compared against the dynamic fracture toughness of the material. At the time

step when the crack is found to be unstable, the crack length is extended by moving the crack tip forward in the appropriate direction as determined from equation (2.27). Since none of the available fracture criteria explicitly defines the length of extension for effective crack arrest, it remains a limitation of all discrete crack propagation analyses irrespective of the modelling technique employed.

Indeed, a proper choice of the magnitude of the extension is critical in such analyses because, at each stage of crack propagation, energy is released which is directly proportional to the length of crack extension. In modelling a propagating crack using the finite element method, the most basic assumption is to extend the crack tip to the nearest node in the appropriate direction. In this approach the length of crack extension depends directly on the size of the element at the crack tip. Since the element size is generally limited by economic considerations, the fracture energy associated with each crack increment is significant and the analysis must necessarily be equipped with an energy release mechanism. One such mechanism is the application of holding back forces on portions of the crack faces suggested by Keegstra et al. (1976). However, in the present boundary element formulation this requirement does not arise because the magnitude of crack extension is independent of the size of the elements. Hence the amount of released energy is easily controlled by limiting the size of each increment in crack length.

Furthermore, the magnitude of the crack extension also influences the predicted crack path itself. While the use of too large a value can force the crack to grow in a certain direction, very small values become computationally inefficient. Based on these considerations a crack extension equal to approximately 10 per cent of the current crack length is a suitable compromise. In addition, this value needs to be continuously monitored, particularly for large structures such as dams. In the case of the latter, this ratio should either be modified or else the absolute value of the extension should be restricted to a predetermined length based on the physical characteristics of the problem.

After each crack extension, the interdomain boundary beyond the new crack tip is

redefined to analytically separate the domains on either side of the crack. Figure 2.4 depicts this process, where AB is the crack length before extension and ABC is the corresponding interdomain boundary. During one stage of crack extension, the crack tip B is moved to B' and the nodes on the line ABC are relocated to the line ABB'C. The rest of the boundary discretization remains unchanged.

To complete the rediscretization process, the nodal response values are required at the new nodes before proceeding with the next time step. In corresponding finite-element-based formulations (Graves and Derucher 1987), this problem does not arise because the crack tip is moved to the nearest existing node and thus no new nodes are defined. This may, however, introduce certain errors in the crack profile, particularly if a node does not already exist in the required direction, in which case the tip is generally moved to the nearest appropriate node.

The present analysis exploits additional features of the boundary element method to yield accurate estimates for the response parameters at the newly defined nodes. Pertinent observations related to this scheme are summarized as follows:

(a) Once the nodal values of boundary displacements and tractions are known, displacements and stresses at selected points within the domain can be computed by suitably modifying the integral equations.

(b) The Houbolt method, used herein for numerical integration of the equations of motion, requires displacements at times $n\Delta t$, $(n-1)\Delta t$ and $(n-2)\Delta t$ to obtain the response at time $(n+1)\Delta t$. In other words, the only response parameter needed at the new nodes is the displacement. If integration techniques such as the Newmark or Wilson-θ methods were used instead, additional information in the form of velocities and accelerations at these nodes would be required in order to proceed with the analysis. Numerical errors involved in the evaluation of velocities and accelerations are thus avoided in the present formulation.

(c) Static boundary element formulation can be employed for computing the

'internal' displacements at the new nodes because these displacements are needed at specific times and are only dependent on the dynamic values of boundary displacements and tractions at those times.

(d) During each stage of crack extension, the crack penetrates only one of the two adjoining subdomains and the new nodes therefore lie in that subdomain. Thus the displacements at these nodes are based on the boundary displacements and tractions for this subdomain only (e.g. Subdomain I of Figure 2.4).

(e) It is known that the displacement and stress calculations at internal points located close to the boundary are generally not reliable. Since the amount of crack extension at each stage of cracking is small, the new nodes invariably lie close to a boundary. The internal point calculations are therefore carried out for nodes located along another arbitrary line in the subdomain involved and the required displacements at the new nodes are obtained by suitable interpolation. The arbitrary line can be located at such a distance from the subdomain boundaries as to minimize numerical inaccuracies.

In order to arrive at an expression for internal displacements (which are required at two previous time-steps), boundary integral equation (2.1) is employed. Since only static deformation is involved in this process the effect of inertia is neglected, its influence already accounted for in the determination of boundary displacements and tractions. Also, the coefficients C_{ki} of equation (2.1) form a unit tensor for points lying inside the domain and not on the boundary. Thus, the governing equation for displacements at internal points ξ becomes

$$u_i(\xi) = \int_{\Gamma_s} u_{ki}^*(\xi, x)\, p_i(x)\, d\Gamma_s - \int_{\Gamma_s} p_{ki}^*(\xi, x)\, u_i(x)\, d\Gamma_s \qquad (2.30)$$

where Γ_s denotes the boundary of the subdomain.

Equation (2.30) can be solved numerically by utilizing the boundary discretization for the subdomain. The resulting discretized equation for displacements at internal points is

$$\{u(\xi)\} = [G_{si}]\{p_s\} - [H_{si}]\{u_s\} \tag{2.31}$$

where $[G_{si}]$ and $[H_{si}]$ are system matrices which are uniquely defined for each internal point; and $\{u_s\}$ and $\{p_s\}$ are, respectively, the displacement and traction vectors corresponding to the boundary nodes of the subdomain. It should be noted that the nodal displacements along the boundary of the subdomain are already known since the global solution for the system is available, whereas the corresponding tractions are obtained from equation (2.10). System matrices now correspond to the particular subdomain only and need not be generated again. In fact, since the global matrices are obtained by assembling the individual sub-matrices, no additional computations are needed if these submatrices are temporarily stored separately. Finally, in equation (2.10) the accelerations correspond to the total nodal accelerations, while for the displacement vector one can use relative displacements. This is explained by noting that, in problems where support movements comprise the external excitation, rigid support displacements do not contribute to the internal forces.

The use of equation (2.31) involves an approximation since the dynamic displacements at boundary nodes are used statically to obtain the displacements at the new nodes. This procedure is analogous to static back-substitution to obtain displacements at the condensed nodes in dynamic substructuring employing the Guyan reduction scheme (Guyan 1964). In the present case, the errors introduced in the displacements occur only at the times when the crack is extended and, due to the presence of damping, disappear after a few subsequent time steps.

2.6 COMPUTER IMPLEMENTATION

Based on the present formulation, a computer program was developed and checked for simple test problems involving crack extension under static loads. The crack extension and rediscretization algorithm was tested to ensure that at each stage of crack extension the ratio of the length of the traction singular quarter-point elements to the existing crack

length does not exceed 0.1, in order to obtain the best accuracy for the computed stress intensity factors (Blandford et al. 1981). The program also ensures that the ratio of the length of the crack tip elements to the other boundary elements in the mesh remains within a reasonable range to ensure the overall conditioning of the system matrices. With the satisfaction of these criteria, use of transition elements between the crack tip elements and the adjoining boundary elements was considered unnecessary. The transition elements do not, in any case, improve the accuracy significantly (Blandford et al. 1981).

Away from the crack tip, the boundary element mesh was coded to contain both linear and quadratic elements. Since the accuracy in computing boundary integrals is critical for the numerical stability of the solution, analytical expressions for these integrals are employed wherever possible. Numerical integration based on Gauss quadrature is used elsewhere. In order to further improve accuracy without sacrificing efficiency, a variable number of Gauss points is used, particularly in the vicinity of a singularity where the fundamental solutions possess a high gradient.

2.7 APPLICATIONS

The analytical procedure described above can be applied to solve a range of dynamic fracture problems. The formulation in its present form is directly applicable to study crack development in structures composed of brittle materials for which the tensile strain criterion for crack extension is ideally suited. Furthermore, within the realm of linear elastic fracture mechanics, other material behaviors can also be considered by suitably modifying this criterion and using an appropriate form of equation (2.29). The resulting modifications to the formulation and the computer code is thus minimal.

In the following, the procedure is applied to three test problems. The first two are presented to confirm the accuracy of the formulation in terms of available analytical alternatives, whereas the third compares the predicted crack propagation process with that observed for a gypsum model structure tested on a shaking table.

2.7.1 Free vibration of cantilever beam

Since the functions $f^j(x)$ of equation (2.2) only approximate the inertia effect within the domain, this example is presented to confirm that the accuracy to be expected is satisfactory for dynamic problems involving only the lower modes.

The test structure comprises a cantilever beam with dimensions 305x305x1981 mm. Sixteen quadratic boundary elements were employed to obtain the lower-mode frequencies of this beam. The material properties are: modulus of elasticity = 0.5×10^6 Pa, Poisson's ratio = 0.0, and mass density = 0.515 kg/m^3. The results for free-vibration analysis of this beam are also presented by Ahmad and Banerjee (1985) using the boundary element as well as the finite element method. As noted earlier, their boundary element formulation is based on a particular solution approach different from that of the present study for the transformation of the inertial integral.

Table 2.1 shows that, compared to the finite element method, the boundary element results of Ahmad and Banerjee (1985) for the first four bending modes differ by a maximum of 2.6 per cent. The corresponding maximum difference for the present formulation is 2.9 per cent. Additionally, the average difference for all four modes is 1.2 per cent for the formulation of Ahmad and Banerjee (1985) and 1.8 per cent for the present study. From this comparison it may be concluded that the treatment of inertia effect in the present formulation yields acceptable accuracy for the lower modes.

2.7.2 Dynamic analysis of centrally cracked plate

To confirm the accuracy of the computation of the dynamic stress intensity factor and also to serve as a further validation of the approximate treatment of the inertia effect, a stationary crack in a finite elastic plate subjected to transient loading is analyzed in this example.

This problem has been studied by several investigators using both the finite element and the finite difference methods. The problem consists of a centrally cracked

rectangular strip subjected to suddenly applied tensile loading. The resulting time-dependent stress intensity factor has been presented by Mall (1980) using quadratic finite elements and a J-integral approach.

Figure 2.5(a) shows one quarter of the 20x40 mm rectangular strip with a 4.8 mm long central crack. The loading comprises a uniform tension $\sigma H(t)$, where σ is the magnitude of the applied stress and H(t) is the Heaviside step function applied dynamically in the plane strain condition. The linear elastic material properties of the plate are: modulus of elasticity = 200×10^6 Pa, Poisson's ratio = 0.3, and mass density = 5×10^3 kg/m^3. The boundary element mesh used to model the quarter plate contains forty-six elements on each side of the crack tip, with 0.24 for the ratio of crack tip element to the half-crack length.

The time history of the normalized dynamic stress intensity factor from the present analysis is plotted in Figure 2.5(b), together with the finite element results of Mall. The normalizing factor is $\sigma\sqrt{a}\sqrt{\pi}$, where 'a' is the half-crack length, i.e. 2.4 mm. In the present analysis a time step of 0.2 μs is employed. The comparison of the results, presented in Figure 2.5(b), indicates that both sets are in good agreement, including the magnitudes of the predicted peak response which fall within 2.7 per cent.

2.7.3 Crack propagation in model cantilever structure

This example consists of a initially cracked model structure made of gypsum which was tested on shaking table under quasi-static harmonic excitation. The intensity was sufficient to cause propagation of the initial crack up to complete rupture of the structure. The results of this investigation, conducted at Tsinghua University (Beijing), are reported in Pekau et al. (1991) and are also employed herein to demonstrate the performance of the present formulation for dynamic crack propagation.

As shown in Figure 2.6, the model structure consists of a cantilever beam which is considered fixed at the base, has a 100 mm x 200 mm cross-section and is 800 mm long.

The following material properties for the gypsum were employed: modulus of elasticity E = 1,766 MPa, Poisson's ratio = 0.2 and unit weight = 7,644 N/m^3. Damping equal to 2 per cent of critical was assumed in the first two modes of vibration. An initial crack, 50 mm long, was assumed to exist 100 mm above the base. Since the principal objective of the present study is to provide an accurate and efficient methodology for analyzing the propagation process of cracks under dynamic loadings, the assumption of an existing crack provides a realistic starting condition. Standard dynamic stress computations leading to crack initiation can always precede the current analysis.

The boundary element discretization of the initially cracked beam is shown in Figure 2.7, together with its frequencies for the first six modes of vibration. Figure 2.8(a) shows the quasi-harmonic time history of the input acceleration applied at the fixed end of the beam. Resulting displacement and acceleration at the free end of the cantilever are plotted in Figures 2.8(b) and 2.8(c), respectively. Time histories of the stress intensity factors K_I and K are plotted in Figures 2.9(a) and 2.9(b). From these figures, good agreement between the analytical and the experimental results is evident. Minor differences can be attributed to the presence (or development) of micro cracks in the model.

The resulting crack profiles are shown in Figure 2.10. Depicted is the stage-wise development of the computed profile, as well as a comparison with the experimental curve. It is evident that the experimental and computed profiles are in good agreement. Since the propagation of the crack over the width of the beam was of short duration, its experimental stage-wise development was not recorded.

Figure 2.11 shows the eight analytical stages comprising the development of the crack profile in terms of the crack length plotted as a function of time. Whereas Figure 2.10 shows that eight stages are required to model propagation to rupture, Figure 2.11 indicates three corresponding physical crack extensions.

As evident in Figure 2.11, the computed crack first begins to propagate at 0.396

sec, the time at which the dynamic fracture toughness K_{Id}=40 kPa $m^{1/2}$ is first reached, but stabilizes when the crack length is suitably increased in 3 stages. This phenomenon is repeated at 0.537 and 0.671 secs corresponding to the times of subsequent peak input accelerations. At 0.671 sec the crack is predicted to penetrate the other side of the beam, although further numerical calculations could not be carried out. At this time only a small portion of the beam width remains intact for which rediscretization is not feasible. If the crack tip were moved further, the remaining common boundary between the subdomains of the uncracked portion is too small to accommodate reasonably sized boundary elements together with a crack tip element without adversely affecting the accuracy of the results. Thus, at 0.671 sec the beam is assumed to rupture (i.e. in stage 8). The crack profile during this final rupture stage is assumed to follow in the direction tangential to stage 7, the last computed extension.

For the experiment, however, Figure 2.9(a) shows that the beam ruptured at a later time. Following the input acceleration peak at 0.81 sec of Figure 2.8(a), the experimental stress intensity factor K_I began to exhibit unstable behaviour indicative of unstable crack growth. At the next peak in the input acceleration, which occurred at 0.96 sec (Figure 2.8(a)), the model ruptured as recorded by the final portion of the experimental K_I data of Figure 2.9(a). The difference in the times of incipient rupture of 0.671 sec as computed and 0.81 sec from the test can be attributed to the lack of accurate information for the dynamic fracture toughness of the gypsum material.

2.8 CONCLUDING REMARKS

The results obtained for the foregoing three examples and their good correlation with the available data demonstrate the validity of the proposed formulation for dynamic crack propagation. As shown in the next Chapter, the formulation is well suited to study seismic cracking of concrete gravity dams. Since the latter are mostly unreinforced over their cross-section, the tensile strain criterion employed in the present formulation

provides an accurate means to predict crack extension, provided linear elastic fracture mechanics theory is assumed applicable. At the present stage of research in concrete cracking, this assumption is believed realistic for such massive structures when considering the complicated nature of this dynamic problem.

In the next Chapter, the procedure is applied to a parametric investigation of the seismic cracking in concrete gravity dams. Although the formulation remains largely unchanged, a refinement in the representation of the inertial effects is presented, wherein additional collocation is performed in the interior of the domains. Furthermore, since static loads resulting from the self-weight and the hydrostatic pressure of the reservoir water constitute important loading on a gravity dam, the present boundary element formulation is also modified to include the effect of these forces.

Table 2.1 Comparison of frequencies for cantilever beam

MODE	FREQUENCY (Hz)		
	FEM (Ahmad and Banerjee 1985)	BEM	
		Ahmad and Banerjee (1985)	Present study
1	0.378	0.368	0.367
2	2.188	2.214	2.169
3	5.583	5.591	5.440
4	9.908	9.986	9.997

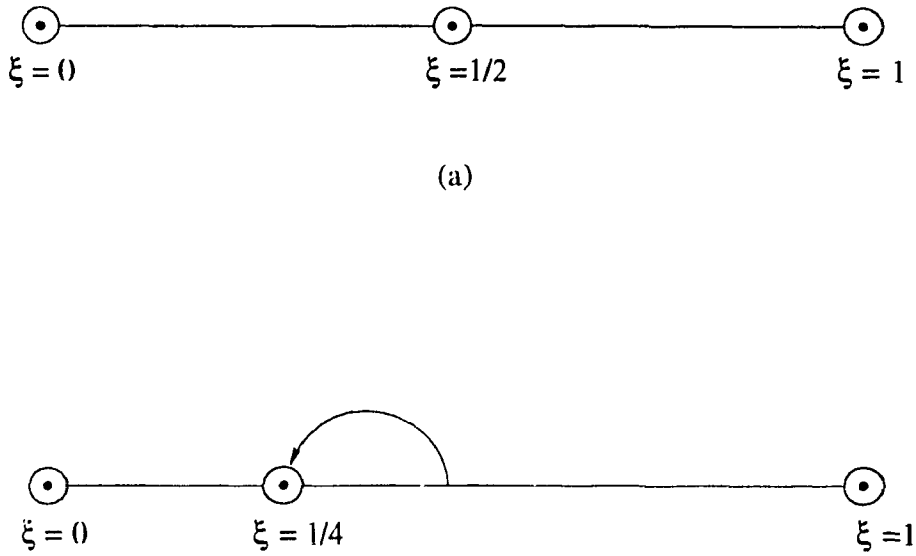

Figure 2.1 Boundary elements: (a) isoparametric quadratic element; (b) traction singular quarter-point element

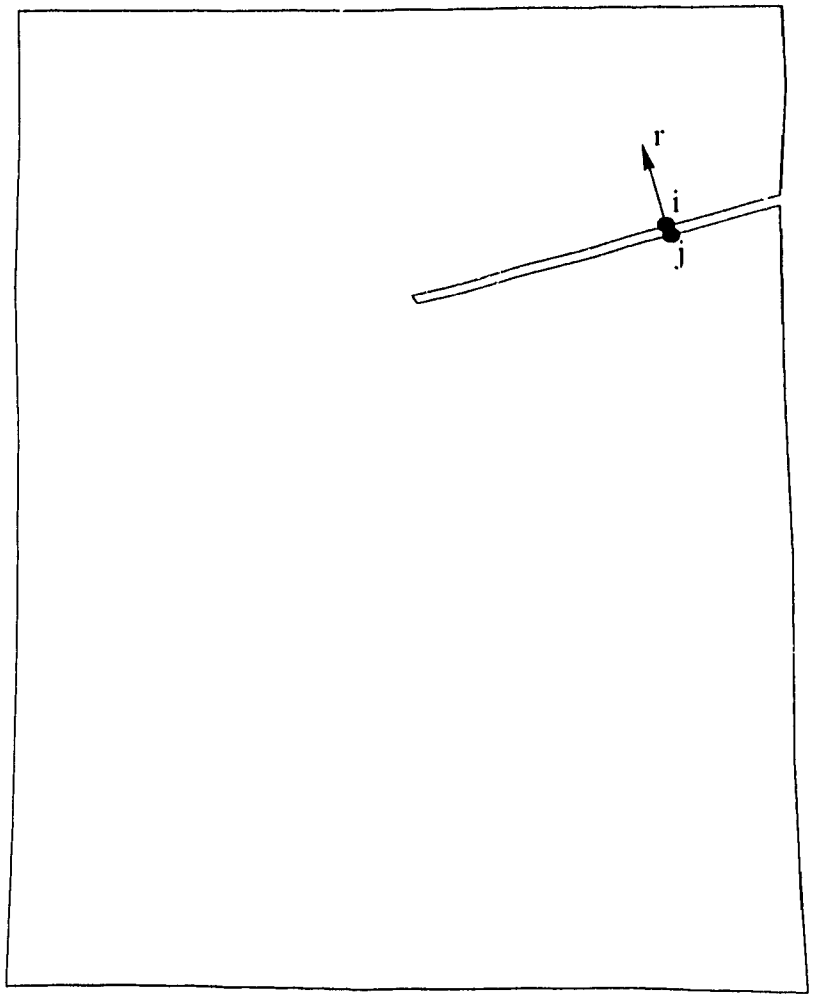

Figure 2.2 Typical nodal pair on crack flanks and the normal direction

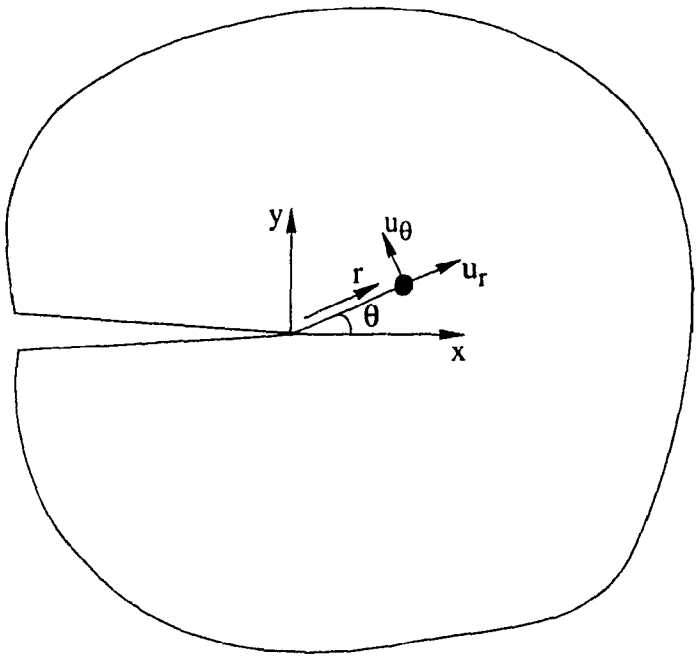

(a)

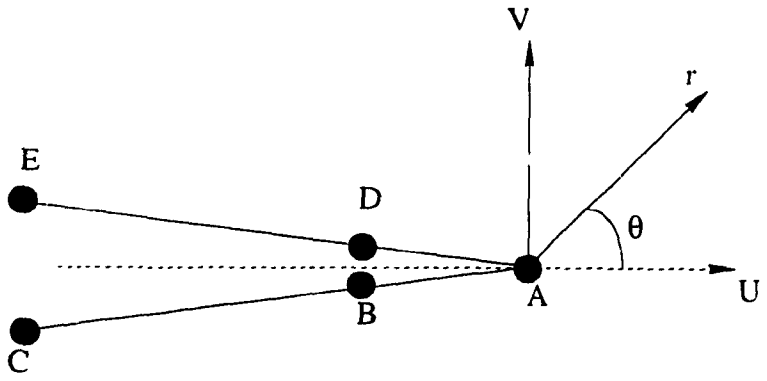

(b)

Figure 2.3 Crack tip coordinate system for: (a) displacement field; (b) calculation of stress intensity factor

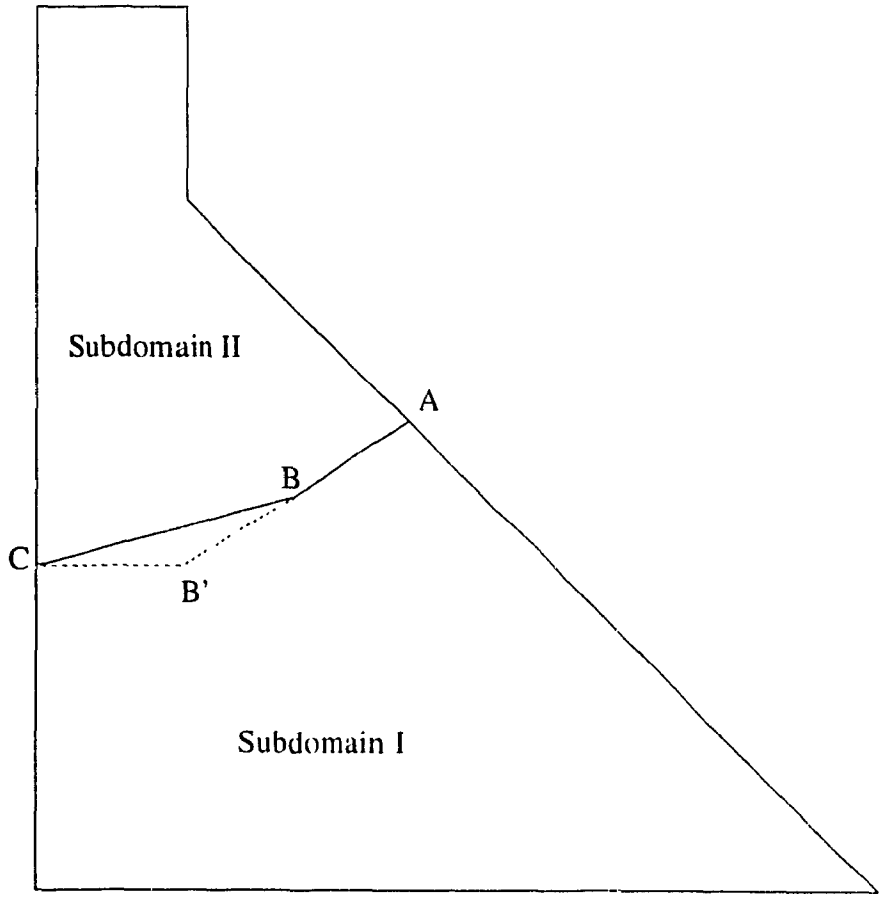

Figure 2.4 Rediscretization for movement of crack tip from B to B'

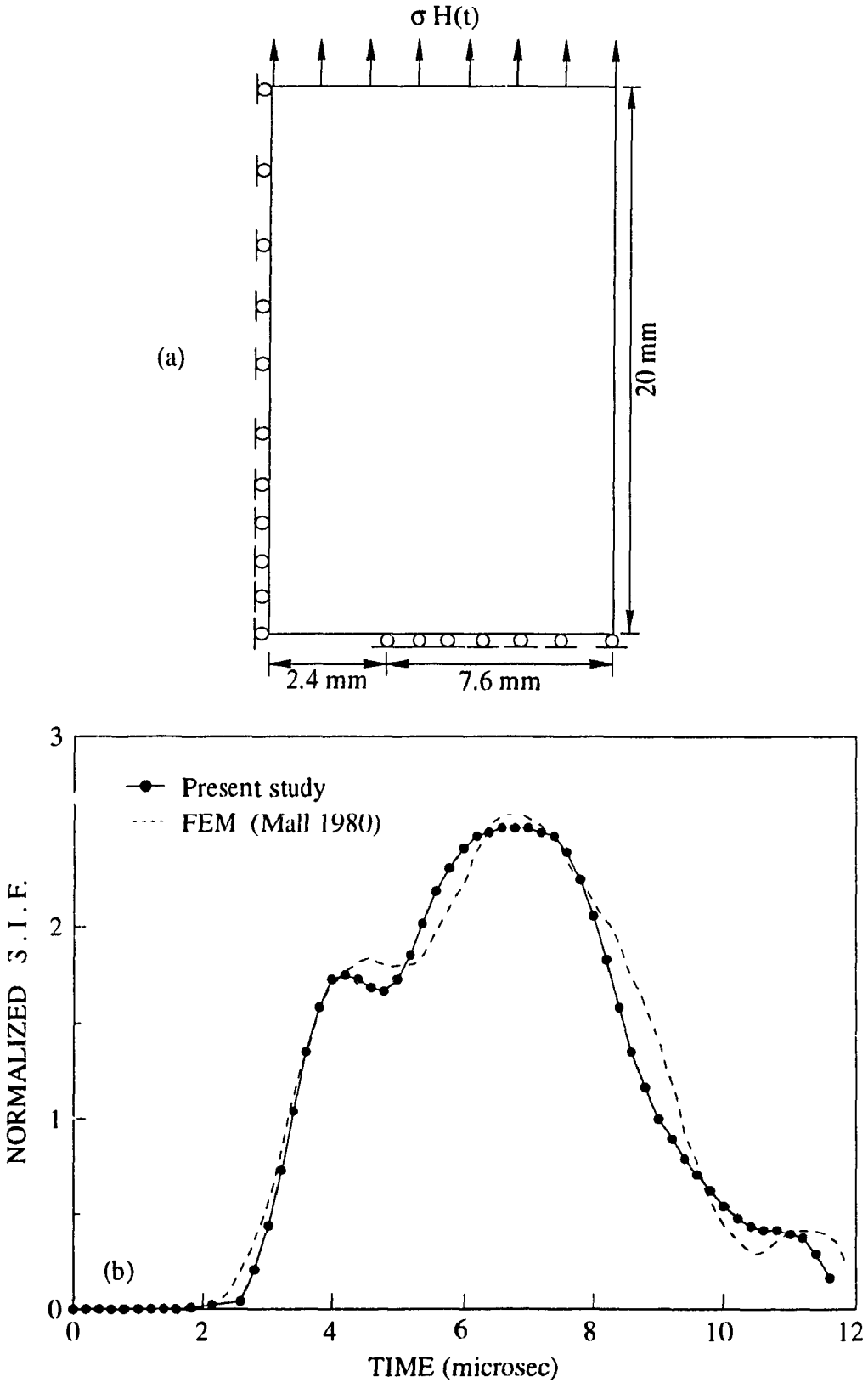

Figure 2.5 (a) One quarter of a plate with central crack; (b) time history of normalized S.I.F.

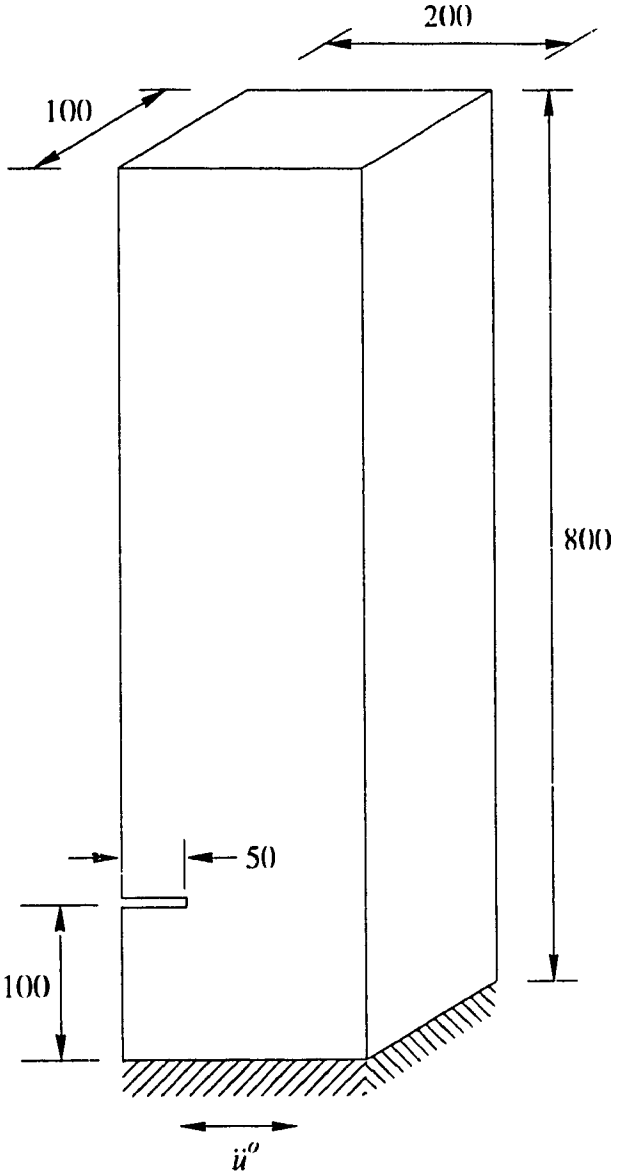

Figure 2.6 Model structure with initial crack
(dimensions in mm)

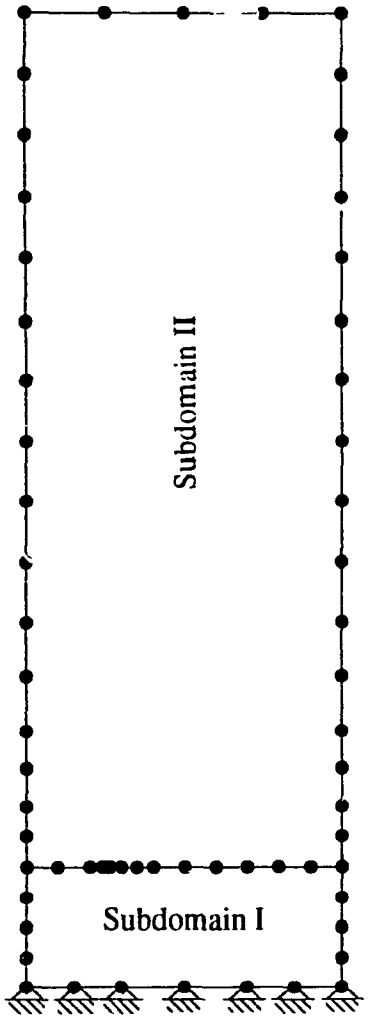

Dynamic characteristics of beam

Mode	Frequency (Hz)	Period (sec)
1	61.15	0.0163
2	369.40	0.0027
3	451.19	0.0022
4	903.84	0.0011
5	1390.36	0.0007
6	1494.80	0.0006

Mesh characteristics : 2 Subdomains
3 Nodes
63 Quadratic boundary elements
36 Traction singular quarter-point crack tip elements

Figure 2.7 Boundary element discretization of model structure and dynamic characteristics

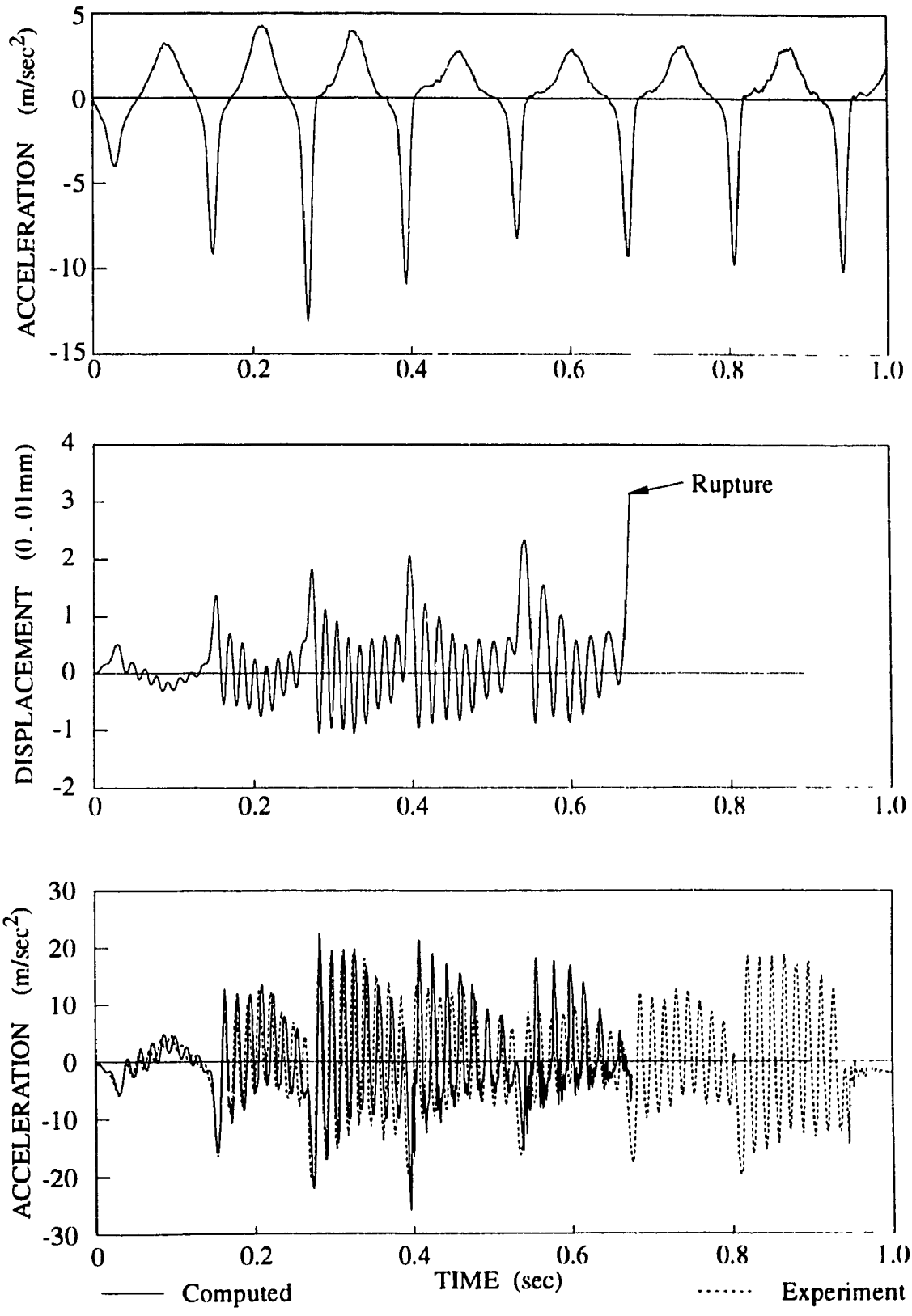

Figure 2.8 Time histories of response for model structure : (a) support excitation; (b) computed crest displacement; (c) comparison for crest acceleration

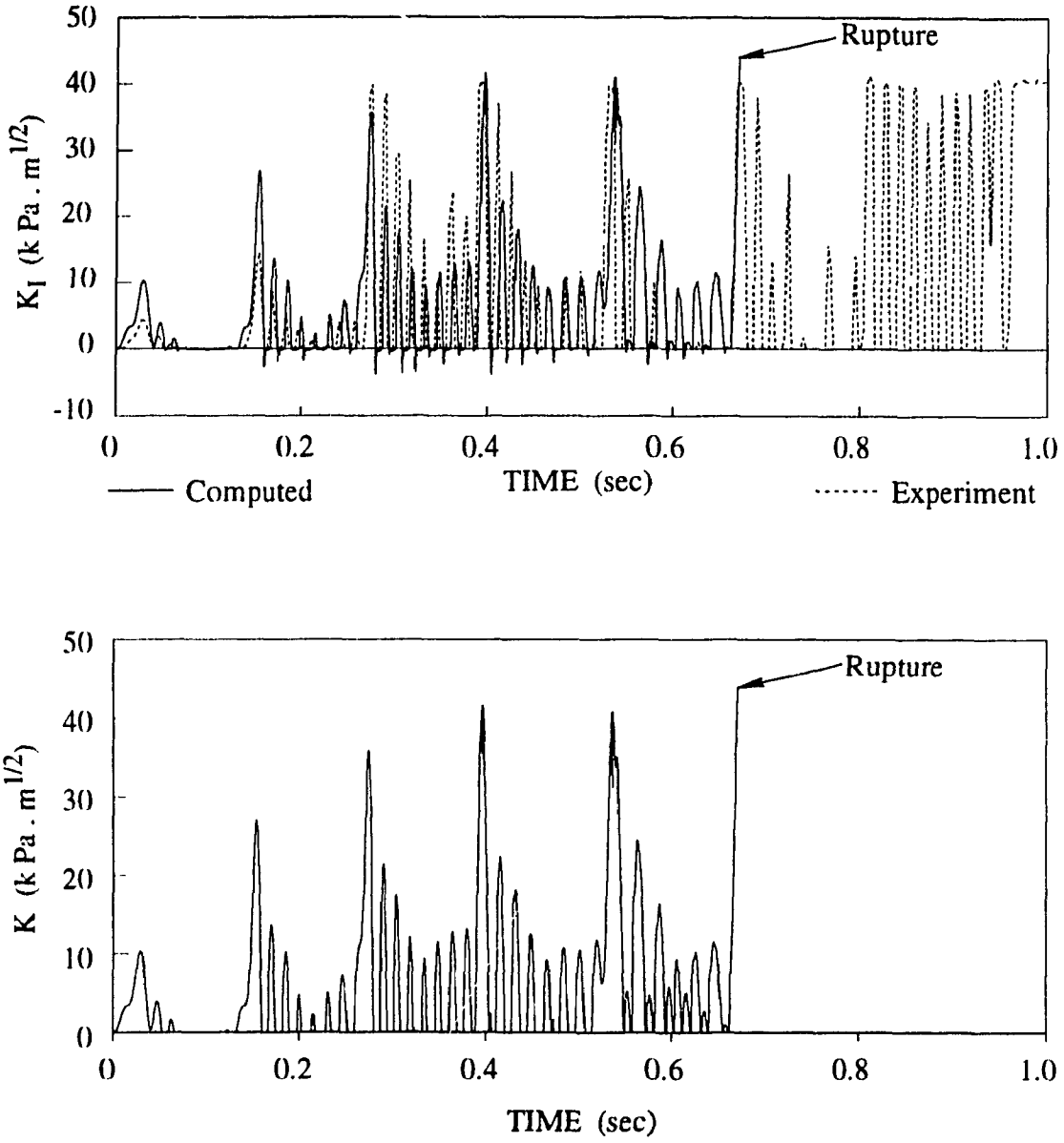

Figure 2.9 Time histories of stress intensity factors : (a) comparison of computed and experimental K_I; (b) computed K

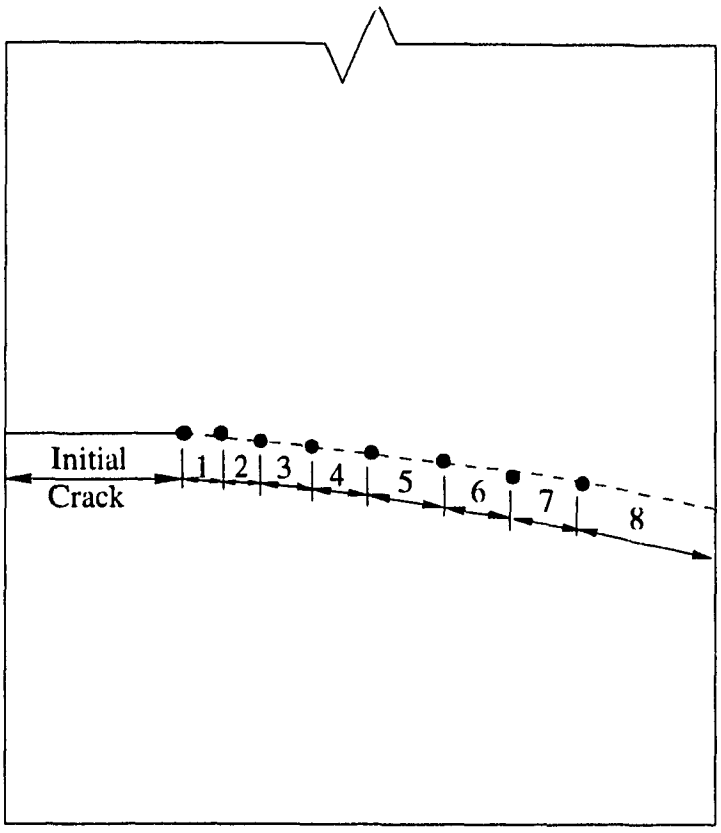

Figure 2.10 Comparison for stage-wise development of crack profile

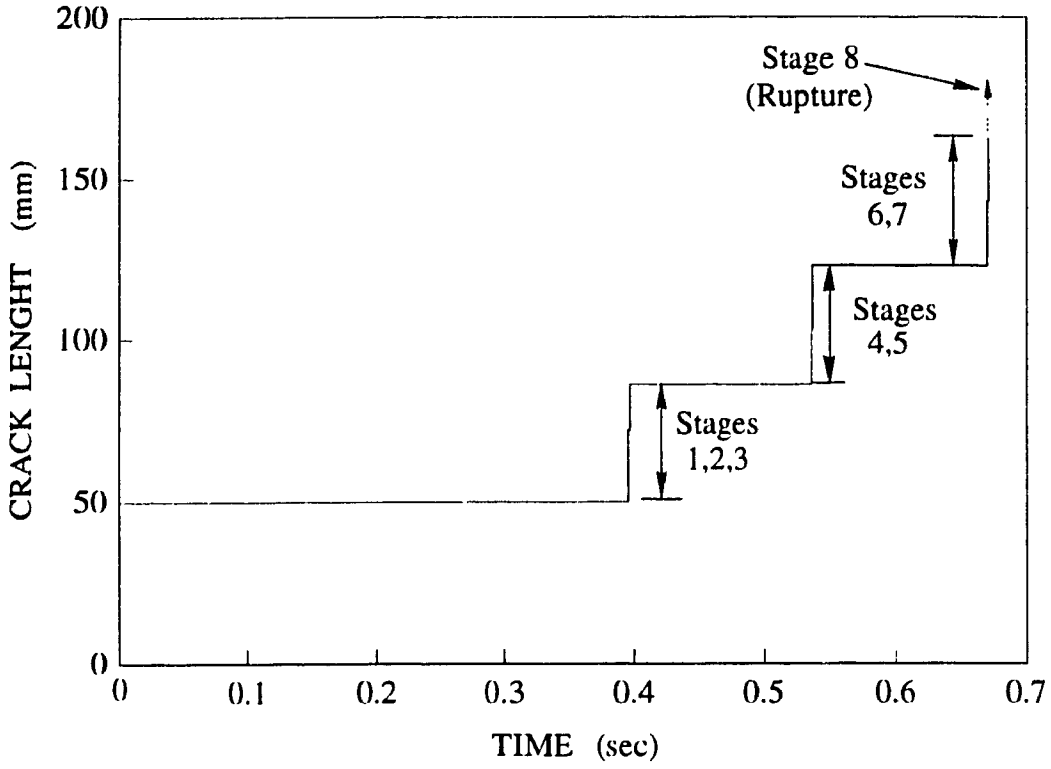

Figure 2.11 Computed crack length as a function of time

CHAPTER III

SEISMIC ANALYSIS OF SINGLE CRACK PROPAGATION IN CONCRETE GRAVITY DAMS

3.1 INTRODUCTION

The dynamic crack propagation analysis procedure presented in Chapter II is now applied to study earthquake induced cracking in a concrete gravity dam. As already noted, the dynamic boundary element formulation involves an approximation in the derivation of the mass matrix. Since the significance of this approximation in non-linear problems such as the present crack propagation analysis has not been addressed in the literature, convergence of the procedure is examined first with particular regard to the need for additional refinement in the boundary element discretization of the dam. To this end, a refinement in the representation of the inertia of the system is introduced into the formulation whereby the boundary-only integration is supplemented by also including internal collocation within the dam domain. Furthermore, the dynamic system governed by equation (2.17) included only time-dependent external influences and did not account for the static forces. In the fracture analysis of concrete gravity dams, however, such static loads as the weight of the concrete significantly affect the crack opening behavior during dynamic loading and should be accounted for continuously in the time history analysis. Simple superposition of static and dynamic responses is not logical in such situations because of the influence of static loads on crack opening displacements and, consequently, on stress intensity factors. A modelling procedure for static forces in the boundary element fracture analysis of dams is therefore also discussed in the present Chapter.

With the above modifications to the formulation presented in Chapter II, cracking of the Koyna dam under the 1967 Koyna earthquake is investigated in a parametric study, employing a single preassigned crack. Parameters which generally influence the seismic

behavior of concrete gravity dams comprise the presence of significant static loads, reservoir interaction, foundation interaction, reservoir bottom absorption and the direction in which earthquake loading is applied. In addition, the value of the dynamic fracture toughness for concrete and the length by which the discrete crack is extended at each stage of crack propagation also have a very significant influence on the resulting crack profile. In the present study, in order to keep the analysis of this complicated non-linear fracture problem simple, the interaction of the dam with the surrounding media is approximated in the case of the reservoir water and neglected in the case of the foundation rock/soil. The parametric investigation focuses instead on certain material and analytical parameters which have a more direct bearing on the propagation process of the crack as well as on the final profile attained by the crack. These comprise the static loads, the dynamic fracture toughness of concrete and the length of incremental crack extensions.

3.2 DYNAMIC BOUNDARY ELEMENT FORMULATION WITH INTERNAL COLLOCATION

In the dynamic boundary element formulation of Chapter II, the displacement within the domain was expressed by using a finite series of functions, which were assumed to act as body forces in the corresponding static problem. The resulting static displacement field and the corresponding stresses were used in conjunction with the divergence theorem to transform the inertial domain integral to a boundary integral. Since the inertia term does not involve any derivatives the choice of such functions is not very critical; their main requirement being that they should enable the desired integral transformation. However, since these functions are related only to a static problem, the inertia of the structure is, at best, approximated and consequently the representation of the higher modes becomes unreliable. Accuracy could, in general, be improved by either a refinement in the representation of the domain displacement (Ahmad and Banerjee 1985) or by employing internal nodes for domain collocation. The latter procedure is adopted for the present

study and is briefly described below.

Considering a boundary element discretization of a dam to contain m boundary elements and n_b boundary nodes, the governing equation in assembled matrix is given by equation (2.10) rewritten here as

$$[H]\ \{u\} - [G]\ \{p\}\ = -[M]\ \{\ddot{u}\} \tag{3.1}$$

in which the n_b x n_b global matrices [H] and [G] are derived from individual element matrices, which for the n^{th} node and the m^{th} element have the form

$$\begin{aligned} \left[h_{nm}\right] &= \int_{\Gamma_m} p_n^*(\xi, x)\, N(x)\, d\Gamma + \frac{1}{2}\delta_{nm} \\ \left[g_{nm}\right] &= \int_{\Gamma_m} u_n^*(\xi, x)\, N(x)\, d\Gamma \end{aligned} \tag{3.2}$$

where Γ_m is the boundary of the m^{th} element and the rest of the variables follow the notations of Chapter II.

In the case where internal collocation is also performed the total number of nodes in the system increases. If n_i is the number of internal nodes, then the total number of nodes $n_t = n_b + n_i$. In this case the function matrices $[\psi]$ and $[\eta]$, which are used in the computation of [M] (equation 2.(11)), can be directly computed at the internal nodes as the solution ψ_{li}^j and η_{li}^j are known at all points. The system submatrices $[h_{nm}]$ and $[g_{nm}]$ involving internal nodes, however, require careful evaluation depending upon whether the internal nodes coincide with source or field points.

When an internal node acts as a source point these submatrices can be computed from equation (3.2) for all field points lying on the boundary of the domain. In this case n refers to the internal node being considered. For the case when the internal nodes become field points with source points located on the boundary, the integrals in equation (3.2) vanish. For the remaining case where internal points represent both source and field points, equation (3.2) again yields null submatrices but the corresponding diagonal terms

in the global [H] matrix assume unit values. The resulting matrix equations can thus be written in partitioned form as

$$\begin{bmatrix} [M_{bb}] & [M_{bi}] \\ [M_{ib}] & [M_{ii}] \end{bmatrix} \begin{Bmatrix} \{\ddot{u}_b\} \\ \{\ddot{u}_i\} \end{Bmatrix} + \begin{bmatrix} [H_{bb}] & [0] \\ [H_{ib}] & [I] \end{bmatrix} \begin{Bmatrix} \{u_b\} \\ \{u_i\} \end{Bmatrix} = \begin{bmatrix} [G_{bb}] & [0] \\ [G_{ib}] & [0] \end{bmatrix} \begin{Bmatrix} \{p_b\} \\ \{p_i\} \end{Bmatrix} \quad (3.3)$$

where [I] is unit matrix of size n_i x n_i and subscripts b and i represent, respectively, the terms corresponding to boundary and internal nodes.

Either of equations (3.3) or (3.1) can be used to obtain the transient solution depending upon whether internal collocation is included or not. The traction vector {p} can be transformed to a nodal force vector and damping of the system can be included in equation (3.3) to yield equation (2.17) as the matrix equilibrium equation of the damped dynamic system representing a gravity dam. The rest of the formulation for crack propagation remains unchanged.

3.3 MODELLING OF STATIC LOADS

Static loads acting on a gravity dam generally comprise the gravity loads, the hydrostatic water pressure and the earthfill pressure of the upstream and the downstream fill, if any. While the gravity loads oppose crack opening in a dam, the influence of other static loads will depend upon their direction with respect to the location of the crack.

In dynamic fracture analysis the influence of those static loads which oppose crack opening can be simulated by letting the crack surfaces overlap and using this negative relative displacement, together with the dynamic contributions at each time step, to obtain the stress intensity factors. This procedure was used by Feng (1994), where the change in stiffness during crack closure was modelled by using impulses acting at the crack flank nodes. Since, in the present procedure, the crack surfaces are not permitted to overlap, the effect of the static loads is modelled by modifying the dynamic equation of motion itself.

Thus equation (2.17) is rewritten as

$$[m]\{\ddot{u}\} + [c]\{\dot{u}\} + [k]\{u\} = [m_o]\{\ddot{u}^o\} + \{Q\} + \{F_s\} \qquad (3.4)$$

where $\{F_s\}$ represents the static load vector. The static loads are applied as step loads and the initial conditions for the dynamic problem are revised accordingly, the static displacement of the structure being used as the initial displacement with initial velocity zero. Subsequent crack opening and closing occurs under the combined effect of static and dynamic loads, with the crack behavior modelled according to the procedure already outlined.

3.4 PARAMETRIC STUDY OF SEISMIC CRACKING IN KOYNA DAM

The Koyna dam in India is one of the rare examples of a major gravity dam significantly damaged during an earthquake. The dam is a 104 m long concrete gravity structure with maximum height of 103 m at non-overflow section. The cross-section of the tallest non-overflow monolith of the dam is shown in Figure 3.1 and, as can be seen, the dam has a non-typical cross-section resulting from a change made during construction when it was decided to build the dam to its full height in one stage rather than the planned two phases. The site of the dam was initially considered non-seismic but on December 11, 1967 - 5 years after the dam was commissioned - a severe earthquake caused significant distress to this dam. The earthquake registered 6.5 on the Richter scale and had its epicenter very close to the dam, resulting in ground motions with peak acceleration of 0.63 g in the longitudinal direction, 0.49 g in the transverse direction and 0.34 g in the vertical direction. Strong ground shaking lasted approximately 4 sec. Time histories of the transverse and vertical components of the ground acceleration are shown in Figure 3.2. The ground motion was recorded on a strong motion accelerograph located in a gallery close to the foundation of the dam. As a result of this earthquake, the non-overflow monoliths of the dam suffered severe cracking while the overflow sections escaped serious

damage As shown in Figure 3.3, cracking of the dam resulted in roughly horizontal cracks on the upstream, the downstream or on both faces at and around elevation 66.5 m, where the dam cross-section changes. The extent to which these cracks penetrated the body of the dam could not be determined, although the possibility that some of these extended through the width of the dam was not ruled out.

The cracking induced in this instrumented dam has become a classical problem in the seismic behavior of concrete gravity dams. In the following, the foregoing boundary element-discrete crack procedure is applied to this dam in order to demonstrate its performance and also to examine various parameters affecting the results.

3.4 ! Boundary element model

For crack propagation analysis a 1.0 m long initial crack is assumed on the downstream face at elevation 66.5 m, which corresponds to the point of slope change and where various previous studies have predicted the occurrence and time of first cracking in the dam. The analyzed structure and the corresponding boundary element discretization are shown in Figure 3.4. A typical pattern indicating the locations of interior collocation points (scheme 3/3/3) used in some of the analysis phases is also displayed. The mesh consists of 143 nodes and 89 quadratic boundary elements, with traction singular quarter-point elements situated at the crack tip. A relatively fine mesh is introduced to represent the zone near elevation 66.5 m, where the assumed initial crack is located and future cracking is anticipated. An additional subregion near this zone and extending roughly down to elevation 40.0 m is also introduced. Such subregioning improves accuracy by confining the integration domain and by providing additional degrees-of-freedom in the form of interface nodes.

The foundation rock is not included in the model and the dam base is assumed to be fixed, thus neglecting foundation interaction. This assumption is reasonable because the foundation rock at Koyna is relatively stiff with estimated modulus of 70 GPa.

3.4.2 Material characteristics and loading

The following linear elastic material properties, applied over the entire cross-section, are adopted for the Koyna dam concrete: modulus of elasticity E = 31.0 GPa, Poisson's ratio $\nu = 0.2$; mass density $\rho = 2640\ kg/m^3$; and compressive strength $f'_c = 30.0$ MPa. Damping equal to 5 percent is assumed for the first two modes of vibration.

The loading consists of the self-weight of the dam, hydrostatic as well as hydrodynamic effects of the reservoir, and transverse and vertical components of the Koyna earthquake applied directly at the base of the dam. Full reservoir with water level at 92.0 m is considered which corresponds to the level when the earthquake occurred. The hydrodynamic effects are approximated by added mass with water treated as incompressible.

The most important material property in seismic crack propagation analysis based on linear elastic fracture mechanics is, of course, the dynamic fracture toughness K_{Id}. For the static toughness, values of 1.0 to 1.5 $MPa.m^{1/2}$ have been used in previous studies (Chapuis et al. 1985; Zhou and Lin 1992; Bhattacharjee and Léger 1993). Higher values have, however, been obtained from tests on cores recovered from existing dams (Saouma et al. 1990). Specific fracture energy up to 270 N/m was determined in some of these tests, which corresponds to a static fracture toughness of approximately 2.8 $MPa.m^{1/2}$ (based on concrete modulus of 31.0 GPa). Moreover, the fracture toughness of concrete is also shown to be dependent upon the size of the specimen tested (Mindess 1984) as well as on the loading rate in a dynamic environment (Brühwiler and Wittman 1989). Increasing magnitudes of the latter two parameters increase the toughness. In view of the above and in the absence of any test data for the Koyna concrete, a baseline dynamic fracture toughness of 2.0 $MPa.m^{1/2}$ is assumed in the present study. However, as shown later, this magnitude of toughness results in complete penetration of the initial crack through the dam at an early stage in the time history analysis, much before the arrival of the large peaks in the Koyna earthquake record. In order to also examine the cracking

process under these peaks, a relatively high value of the dynamic fracture toughness is required, namely a minimum of $K_{Id} = 9.0$ MPa.m$^{1/2}$ is found necessary in order to permit the analysis to be continued over the entire time history of the earthquake.

3.4.3 Effect of internal collocation points

As previously noted, additional internal collocation, which improves the representation of structural mass, is required in dynamic boundary element analyses where higher modes contribute significantly to the response. In the seismic analysis of uncracked concrete gravity dams it has been amply demonstrated in the literature that the first few modes suffice in response calculations and, hence, the boundary element procedure without interior collocation should give acceptable results. To confirm the latter for dams undergoing seismic cracking, analyses are conducted using the boundary-only discretization as well as for two other cases where internal nodes are introduced in each subregion. In one case, each subdomain is provided with a single internal node (scheme 1/1/1) and, in the other, three interior nodes per subdomain are considered (scheme 3/3/3). The fracture toughness of concrete used in this phase of the analysis is 9.0 MPa.m$^{1/2}$.

The final crack profiles obtained with and without internal points are shown in Figure 3.5. In all three cases the crack penetrates almost the entire width of the dam. In each case the crack begins to propagate at 4.24 sec and extends by approximately 2.0 m before stabilizing for a few time steps. After 4.6 sec it again starts propagating but, this time, crack arrest does not occur until the upstream face is nearly reached. Although some differences exist in the crack trajectories, the overall pattern is similar in the three cases.

The first 6.0 sec of the time histories of the horizontal crest displacement and acceleration of the dam are plotted in Figure 3.6 for the case of boundary discretization only, as well as when three internal nodes are employed in each subregion (scheme 3/3/3). Positive values correspond to movement towards downstream. The results indicate that

the predicted response is in good agreement for the two cases, except at times corresponding to the later stages of cracking. The peak response is also not particularly altered by the introduction of the internal points.

Envelope values of the principal tensile stresses on the upstream and downstream faces of the dam are shown in Figure 3.7, from which it is apparent that the results are almost identical, with or without internal points. The envelopes also show that, at certain locations, the principal tensile stress exceeds the expected dynamic tensile strength of concrete, which is estimated to be 3.6 MPa. These locations correspond to the heel of the dam and an upstream face region close to elevation 66.5 m.

The good correlation between the results of the analyses with and without interior collocation confirms that the boundary-only representation of inertial mass is sufficient for the present application. The rest of the investigation therefore features the boundary-only discretization of the dam and no internal collocation is performed.

3.4.4 Effect of dynamic fracture toughness

Of the three values of the dynamic fracture toughness studied, namely 1.0, 2.0 and 9.0 MPa.m$^{1/2}$, the lowest represents the static fracture toughness of concrete and serves as a reference value in the design process, wherein the suggested limiting value for static toughness is zero, provided acceptable results are obtained (Saouma et al. 1990). The reason for the choice of the highest value (9.0 MPa.m$^{1/2}$) has already been discussed.

The predicted crack profiles corresponding to the three values of the fracture toughness are shown in Figure 3.8, from which it is evident that the pattern of cracking is not significantly influenced by the magnitude of this parameter. It is also noted that, irrespective of the magnitude of the fracture toughness employed, the initial crack propagates to penetrate, or nearly penetrate, the full width of the dam. Corresponding time histories of the crack length are presented in Figure 3.9. It can be seen that higher fracture toughness not only delays the start of crack propagation but also affects the total

time required for complete crack development. The elapsed times are 0.27, 0.31 and 0.45 sec, respectively, for the K_{Id} values of 1.0, 2.0 and 9.0 MPa.$m^{1/2}$. Evidently the cracking process occurs over a very short period of time regardless of the magnitude of the fracture toughness, once the initial crack becomes unstable. Similar observations have also been made by Chapuis et al. (1985) and Skrikerud and Bachmann (1986). It should be noted that, once the crack tip reached close to the upstream face, further analysis could not be pursued for K_{Id} = 1.0 and 2.0 MPa.$m^{1/2}$, because rediscretization using reasonably sized elements was not possible considering the small uncracked width remaining in front of the crack tip. For K_{Id} = 9.0 MPa.$m^{1/2}$, however, the crack stabilized by the time it approached close to the upstream face, due to decrease in the amplitude of ground acceleration by that time. As a result, the analysis could be continued for the rest of the ground motion, during which the portion of the dam above the crack continued to rock in a stable manner.

Time histories of horizontal displacement and acceleration at the dam crest for the two lower values of the fracture toughness are presented in Figure 3.10. It is noted that the crest responses begin to differ at 1.905 sec, at which time the initial crack starts propagating for K_{Id} = 1.0 MPa.$m^{1/2}$. As the crack grows, Figure 3.10(a) shows that the difference in the crest displacement becomes more pronounced but no instability is indicated. For both cases of the fracture toughness, the crest displacement does not diverge even when the crack penetrates the entire width of the dam. Furthermore, the magnitude of maximum displacement does not appear to be significantly affected by the cracking process (although reversal in sign occurs). The corresponding influence of cracking on crest acceleration is shown in Figure 3.10(b). Higher magnitudes of the acceleration are predicted after the initial crack starts propagating for K_{Id} = 1.0 MPa.$m^{1/2}$. The increase, however, does not appear to be related to the length of the crack. The maximum amplification occurs at 2.07 sec, at which time the crack is approximately 5.0 m long, and no further amplification is noticed with subsequent crack growth. For K_{Id} = 2.0

MPa.m$^{1/2}$, on the other hand, for which almost the entire crack propagation occurs at 2.45 sec, the acceleration amplitude is apparently unaffected by the rather abrupt cracking which occurs at this time.

Instantaneous dam deformations for K_{Id} = 2.0 and 9.0 MPa.m$^{1/2}$ are shown in Figure 3.11. It should be noted that these deformations correspond to similar crack lengths in the two cases but which do not occur at the same time. In order to distinguish clearly the deformed structure (dashed line) from its undeformed state, a magnification factor of 50 is used for the displacements. Clearly, the crack mouth opening is more pronounced for K_{Id} = 9.0 MPa.m$^{1/2}$, where the onset of crack propagation is delayed and the structure is subjected to the aforementioned large peaks of the acceleration in the ground motion. The magnitudes of the maximum crack mouth openings are 5.5 mm and 17.8 mm for K_{Id} = 2.0 and 9.0 MPa.m$^{1/2}$, respectively.

Time histories of principal tensile stresses computed at the centroids of selected boundary elements for K_{Id} = 9.0 MPa.m$^{1/2}$ are plotted in Figure 3.12. The selected elements are on the upstream face at the heel of the dam and at elevation 66.5 m. The influence of the magnitude of the fracture toughness on the potential development of multiple cracks in the dam can be noted from these data. Since the analysis is discontinued at 2.45 sec for K_{Id} = 2.0 MPa.m$^{1/2}$ because of complete penetration, the stress does not exceed the dynamic tensile strength for this value of the fracture toughness. Thus, no new cracks will initiate on the upstream face. In the case with K_{Id}=9.0 MPa.m$^{1/2}$ however, the propagation of the initial downstream crack is delayed and new cracks are predicted to form on this face. From Figure 3.12(a), it can be seen that a tensile crack will develop near the heel at 4.09 sec, when the dynamic tensile strength is first exceeded. Similarly, Figure 3.12(b) shows that another crack is predicted to start on the upstream face at elevation 66.5 m at almost the same time. It should be noted that, for K_{Id} = 9.0 MPa.m$^{1/2}$, the initial downstream crack assumed at the point of slope change starts propagating only at 4.24 sec. Thus, it appears that, for sufficiently high magnitudes of

the fracture toughness, cracking will become distributed in dams and a number of cracks will initiate and propagate simultaneously. In this regard, it is interesting to recall that cracking indeed occurred in the Koyna dam on both the upstream and the downstream faces near elevation 66.5 m.

3.4.5 Effect of crack length increment

At each stage of crack growth the available propagation criteria only give the direction in which the crack tip should be extended, while the magnitude of crack extension remains unknown. In the absence of any theoretical basis, an arbitrary value is employed. Since the computational efficiency is directly related to the magnitude and hence the number of extensions, larger values are preferred by an analyst. This, however, may distort the predicted crack path itself. For the results presented in the other sections of this Chapter, a piecewise extension of 10 percent of the current crack length has been used with the magnitude of the maximum increment taken as 1.0 m. To examine the effect of thus limiting the maximum piecewise increment, some of the analyses are also conducted using a reduced maximum of 0.5 m and comparing the results with those obtained with 1.0 m. Obviously the maximum value of the crack length increment governs at the later stages of crack propagation, whereas the percentage criterion applies during the initial stages of crack extension.

It is found that the predicted crack path, as well as the overall dam response, remains largely unaffected by the above reduction in maximum crack length increment. The verification was conducted for two different values of the fracture toughness, namely K_{Id} = 2.0 and 9.0 MPa.m$^{1/2}$, for which the final crack trajectories are shown in Figure 3.13. As seen in Figure 3.13(a), for K_{Id}= 2.0 MPa.m$^{1/2}$ the final crack profiles corresponding to maximum crack extensions of 1.0 and 0.5 m are almost identical. Some influence of the length of the crack extension on the profiles is apparent in Figure 3.13(b) for K_{Id}= 9.0 MPa.m$^{1/2}$. This influence is, however, noticeable only at later stages of crack

development. Of course, for the first 5 m the two crack profiles are identical since the percentage increase in the crack length governs, but the cracks are seen to continue to grow in similar fashion for the next 3 m before beginning to differ. For the data presented in Figure 3.13(b), the entire crack growth involves 35 stage-wise extensions when the maximum increment is limited to 0.5 m compared to 20 extensions when the maximum piecewise growth is limited to 1.0 m. The corresponding CPU times on a SUN-Sparc Station are 2980 and 1345 sec, respectively, for the selected maxima of 0.5 m and 1.0 m. Since the exact crack profile is rarely required in practice the present methodology, being not sensitive to crack extension length, appears well suited to exploit the preceding efficiency in computer time.

3.4.6 Effect of static loads

The static loads which oppose opening of the downstream crack are the self-weight of concrete above the crack and the hydrostatic pressure on the upstream face. In particular, since the Koyna dam profile differs from most other gravity dams because of the unusually high portion above the slope change elevation where initial cracking has been assumed, the crack propagation process may be expected to be affected by the weight of the crest block. To analyze the influence of these loads on cracking, two different loading cases are investigated. In Case 1, the self-weight of the dam is neglected and the reservoir is considered empty. Thus the only loadings considered are the horizontal and vertical components of the ground acceleration. In Case 2, the weight of concrete is included and the analysis is conducted for a full reservoir incorporating both the hydrostatic and the added mass effects of the impounded water. For this case also, the ground motion is applied in two directions. The dynamic fracture toughness of concrete is taken as 2.0 MPa.$m^{1/2}$.

Results are presented in Figures 3.14 and 3.15 and, as shown in Figure 3.14, the predicted crack profile is only slightly modified when static loads are introduced. In the

absence of static loads, Figure 3.14(a) shows that the crack tends to propagate more or less horizontally, whereas Figure 3.14(b) indicates that a small downward shift of the crack path occurs under the influence of the static loadings.

The effect of the static loads on crack opening is shown in Figure 3.15, where time histories of the mode I stress intensity factor K_I are plotted for the two load cases. Noting that K_I is positive whenever the crack is in the opening phase, Figure 3.15(b) reveals that, under the influence of the static loads of Case 2, the crack remains closed until approximately 1.95 sec, at which time the first major peak in ground acceleration arrives. Compared to this, and mainly due to the absence of the static loads in Case 1, cyclic opening and closing of the crack is much more evident in Figure 3.15(a) for the entire duration of the analysis.

Examination of the results of crack propagation as a function of time in the above two load cases indicates that the presence of the static forces also results in delaying the propagation of the initial crack. In Case 1, the initial crack starts propagating at 0.985 sec and grows by 2.5 m before stabilizing. In subsequent cycles of the ground motion, the crack remains mostly open and crack instability reappears at 1.88 sec. This time crack propagation continues until 1.95 sec, when the crack tip reaches close to the upstream face. In Case 2, however, due to the stability provided by the static forces, not only is the crack induced to grow at a much later time (2.18 sec), it also stabilizes rather quickly when the crack length is increased by only 0.29 m. Since the ground motion also intensifies around this time, crack growth resumes at 2.48 sec, with the crack now propagating almost instantaneously through the entire width of the dam.

3.5 CONCLUDING REMARKS

The foregoing results confirm the applicability of the proposed boundary element procedure for the dynamic crack propagation analysis of concrete gravity dams. The boundary-only representation of the inertial mass is found to be sufficient for seismic

fracture analysis and internal collocation is therefore not required. Among the parameters examined, the dynamic fracture toughness of concrete is found not to influence significantly the final rupture pattern of a single crack propagating within the dam, although it affects the time and duration of crack propagation. The magnitude of the toughness also influences the distribution of cracking in the dam and it appears that, for sufficiently high fracture toughness, multiple cracks will initiate and propagate simultaneously. Convergence of the employed boundary element procedure in terms of the final cracking pattern is found not to be sensitive to the assumed size of the crack length increment at each stage of crack propagation. Also found is that the stabilizing static loads affect primarily the time at which the crack is induced to propagate, their influence on the final pattern of cracking being not pronounced. Finally, motivated by the foregoing observation concerning the predicted occurrence of multiple rather than single crack propagation as studied herein, the current analytical procedure is modified, in the next Chapter, to account for the initiation and propagation of such simultaneous cracking and applied to the seismic fracture analysis of the Fongman and Koyna dams.

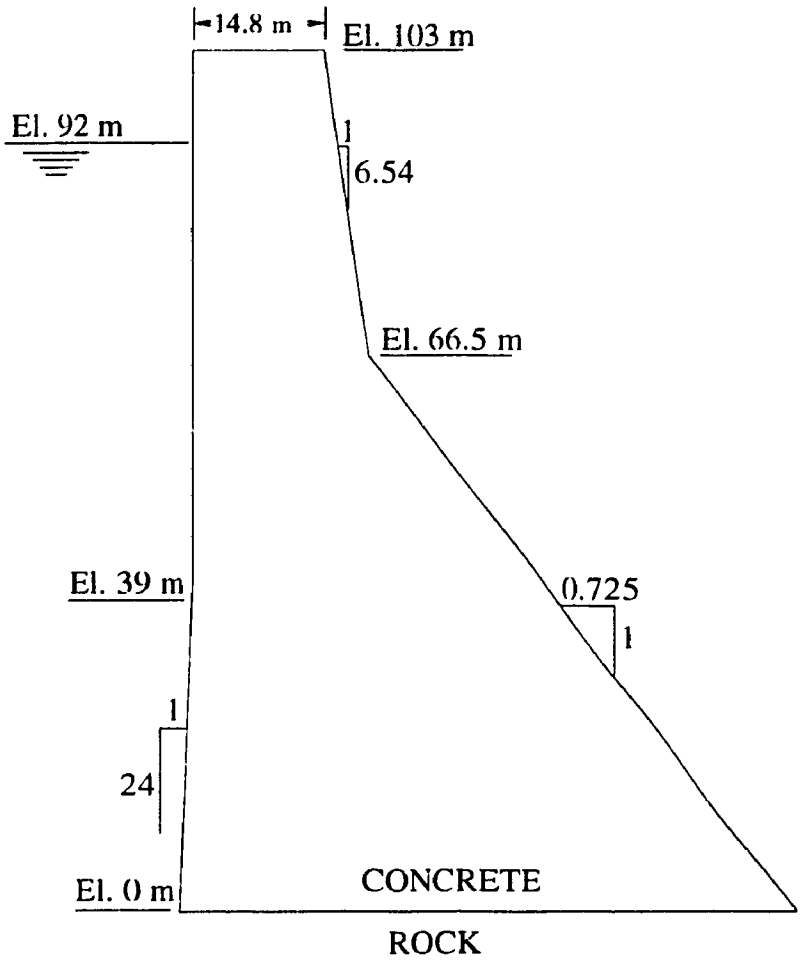

Figure 3.1 Tallest non-overflow monolith of Koyna dam

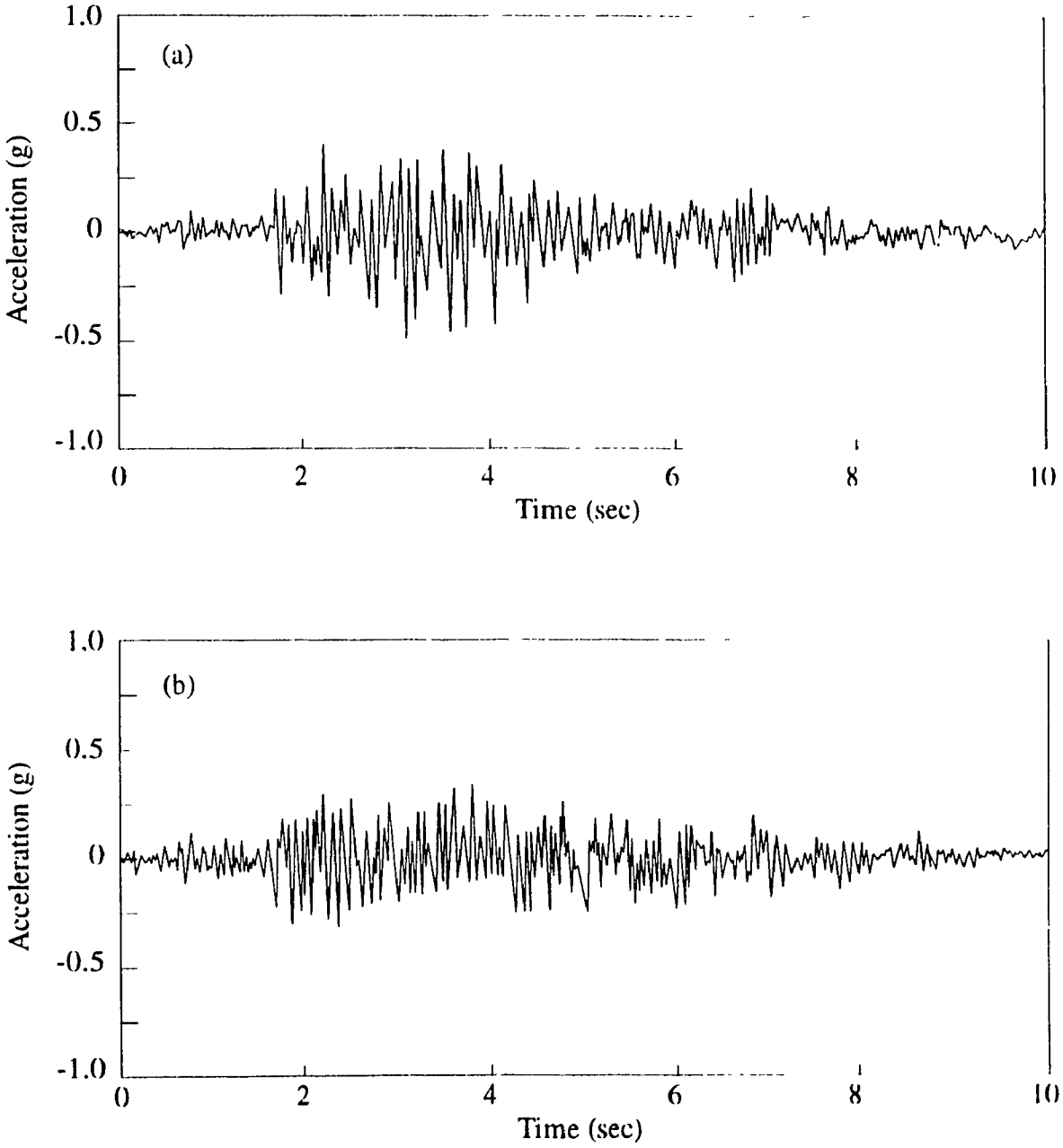

Figure 3.2 Time histories of ground acceleration for Koyna earthquake of Dec., 11, 1967 : (a) stream direction; (b) vertical

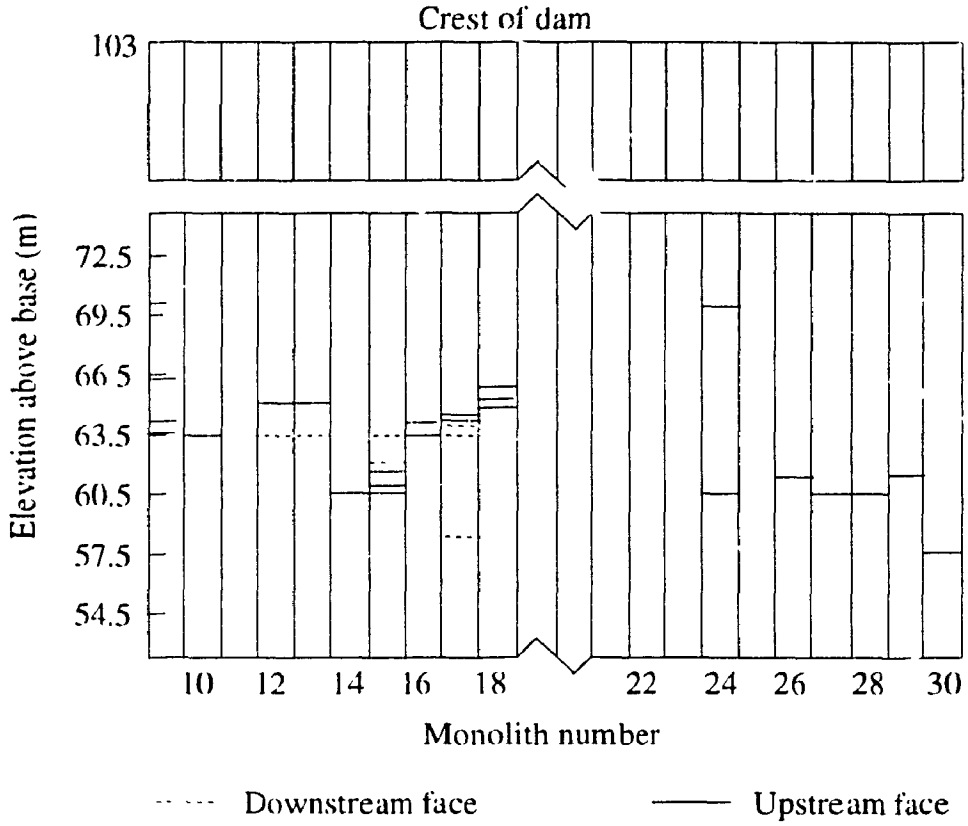

Figure 3.3 Observed pattern of cracking in Koyna dam

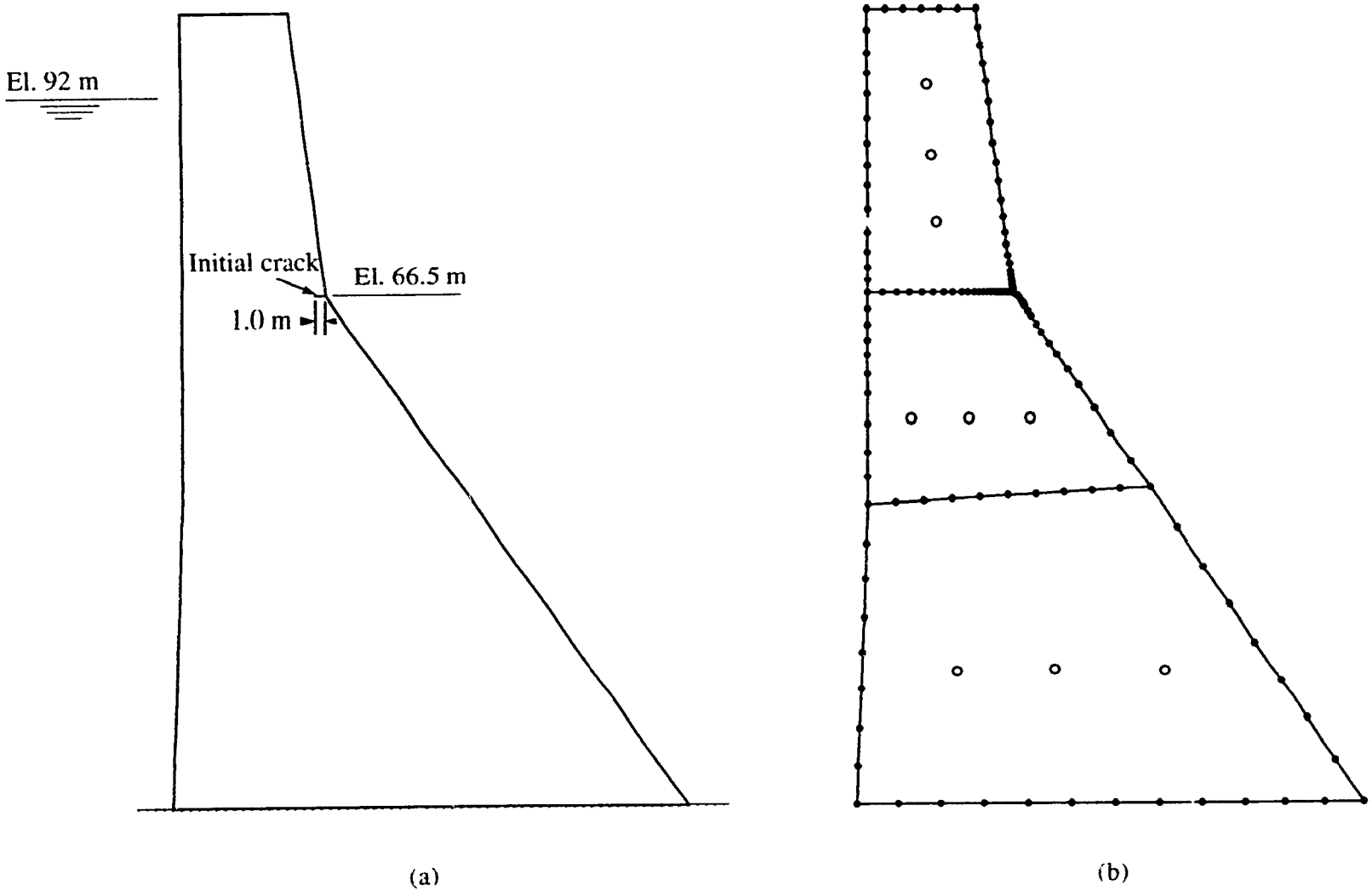

Figure 3.4 Koyna dam : (a) analyzed section with the pre-assigned single crack;
(b) BE discretization with internal points (scheme 3/3/3)

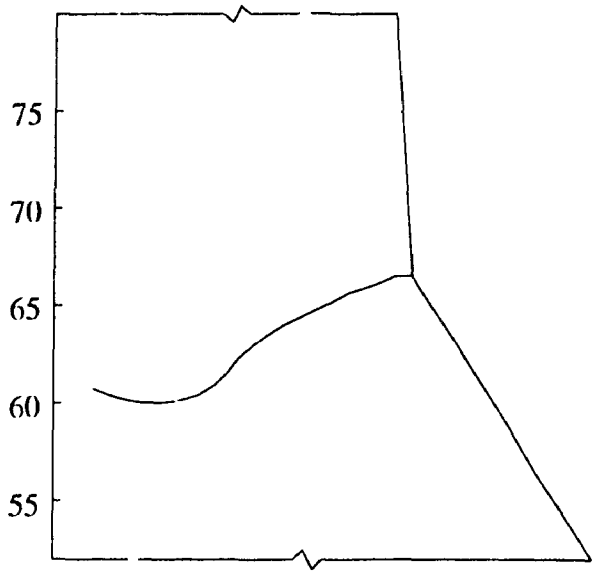

(a) No internal points

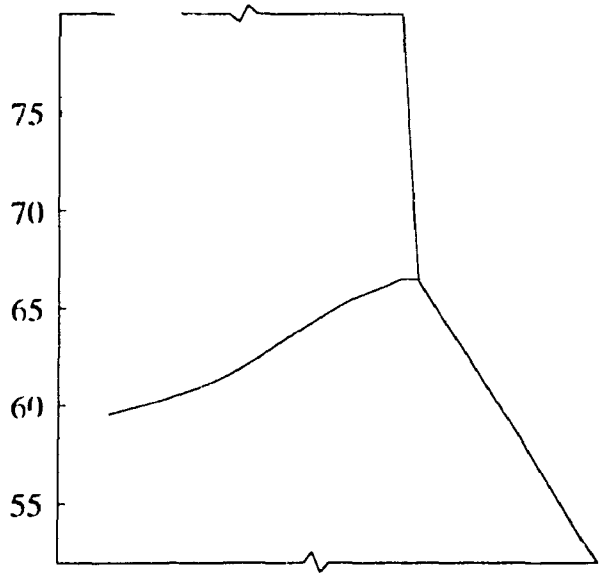

(b) Internal points (1/1/1)

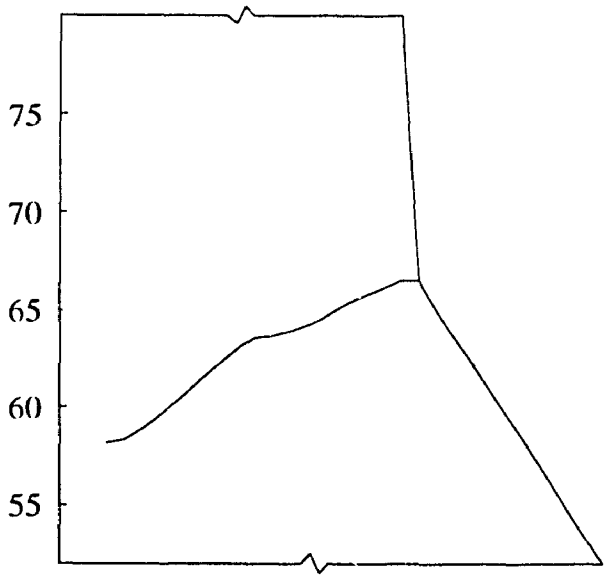

(c) Internal points (3/3/3)

Figure 3.5 Crack profiles with and without internal points for $K_{Id} = 9.0$ MPa.m$^{1/2}$

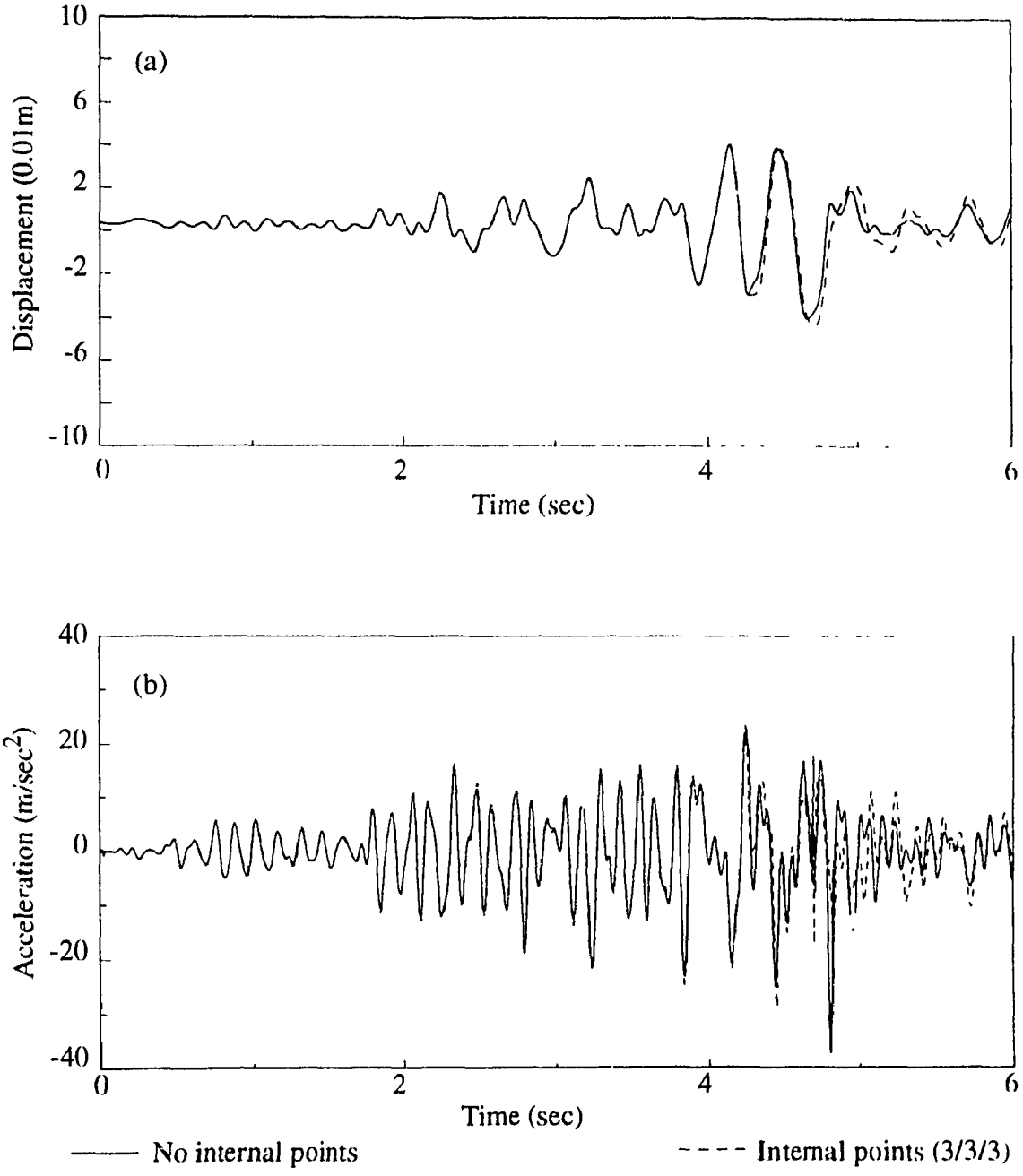

Figure 3.6 Time histories of crest response with and without internal points for K_{Id} = 9.0 MPa.m$^{1/2}$: (a) displacement; (b) acceleration.

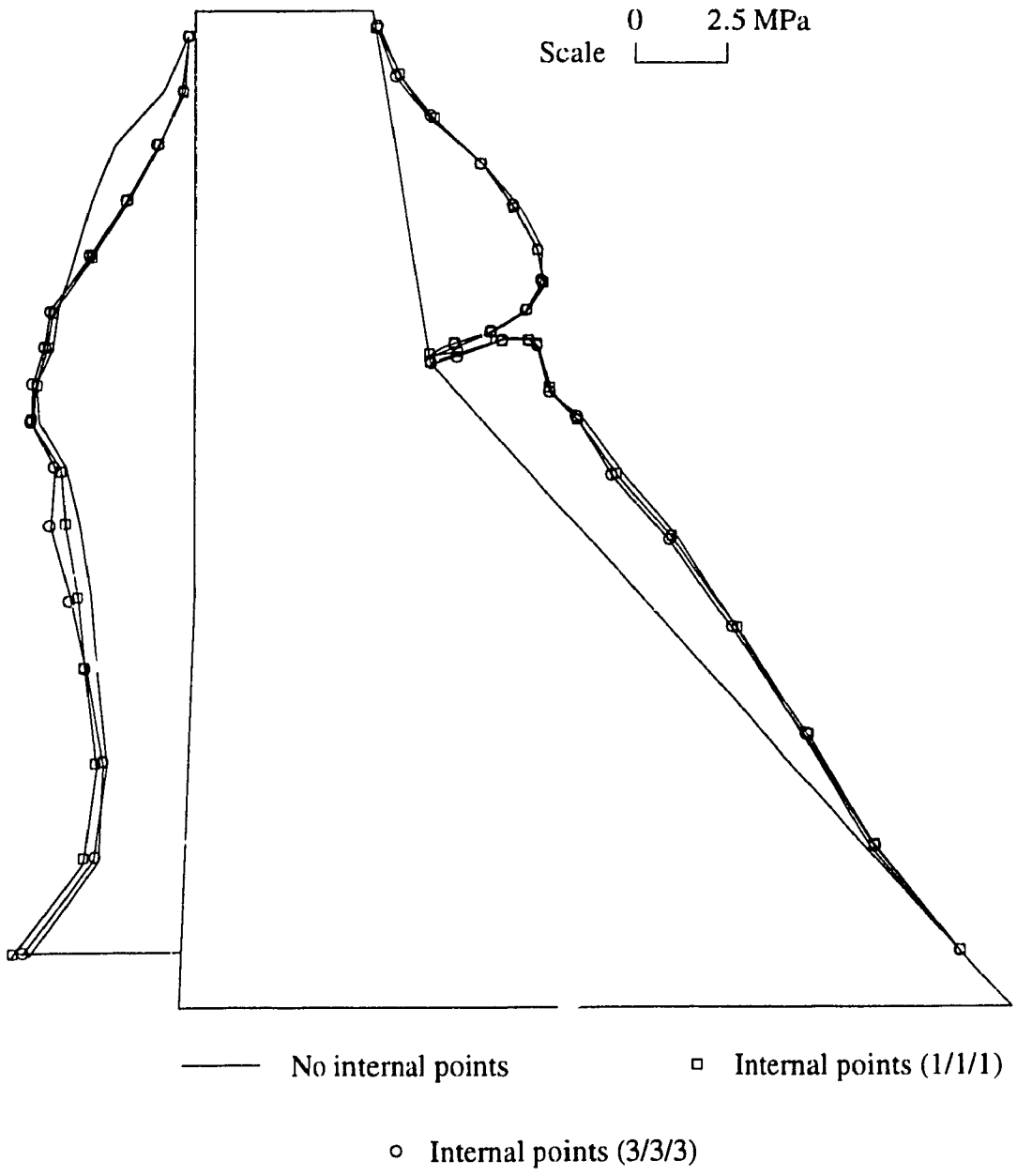

Figure 3.7 Envelopes of principal tensile stress (MPa) with and without internal points for $K_{Id} = 9.0$ MPa.m$^{1/2}$.

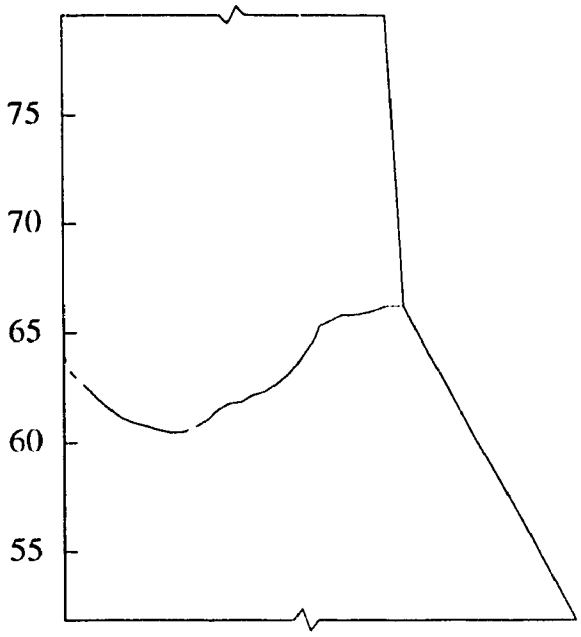

(a) K_{Id} = 1.0 MPa.m$^{1/2}$

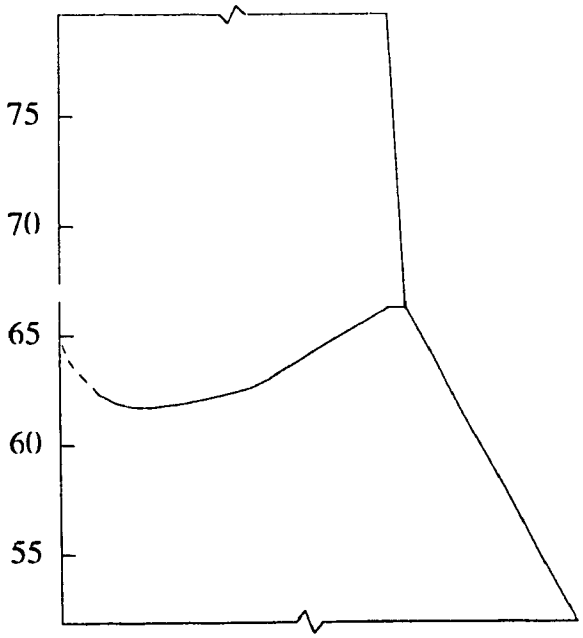

(b) K_{Id} =2.0 MPa.m$^{1/2}$

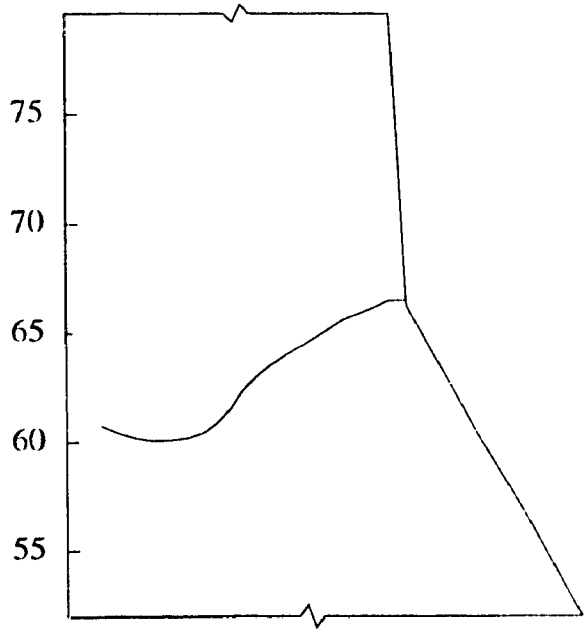

(c) K_{Id} = 9.0 MPa.m$^{1/2}$

Figure 3.8 Crack profiles for different fracture toughness

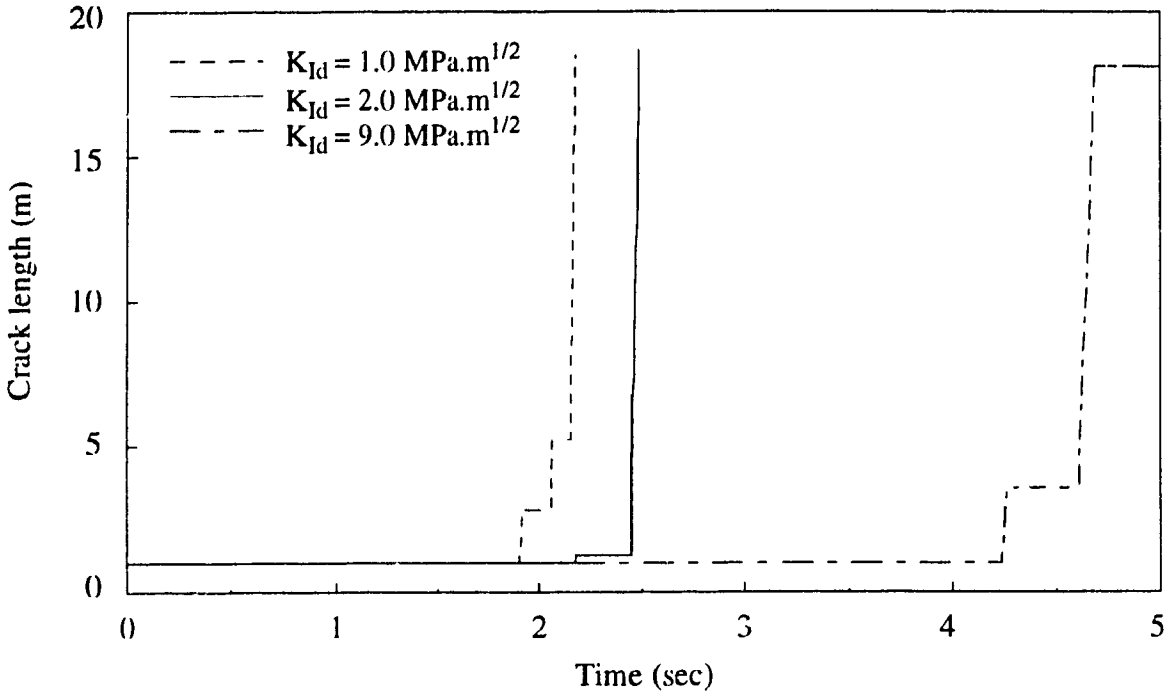

Figure 3.9 Time histories of horizontal projection of crack length for different fracture toughness K_{Id}.

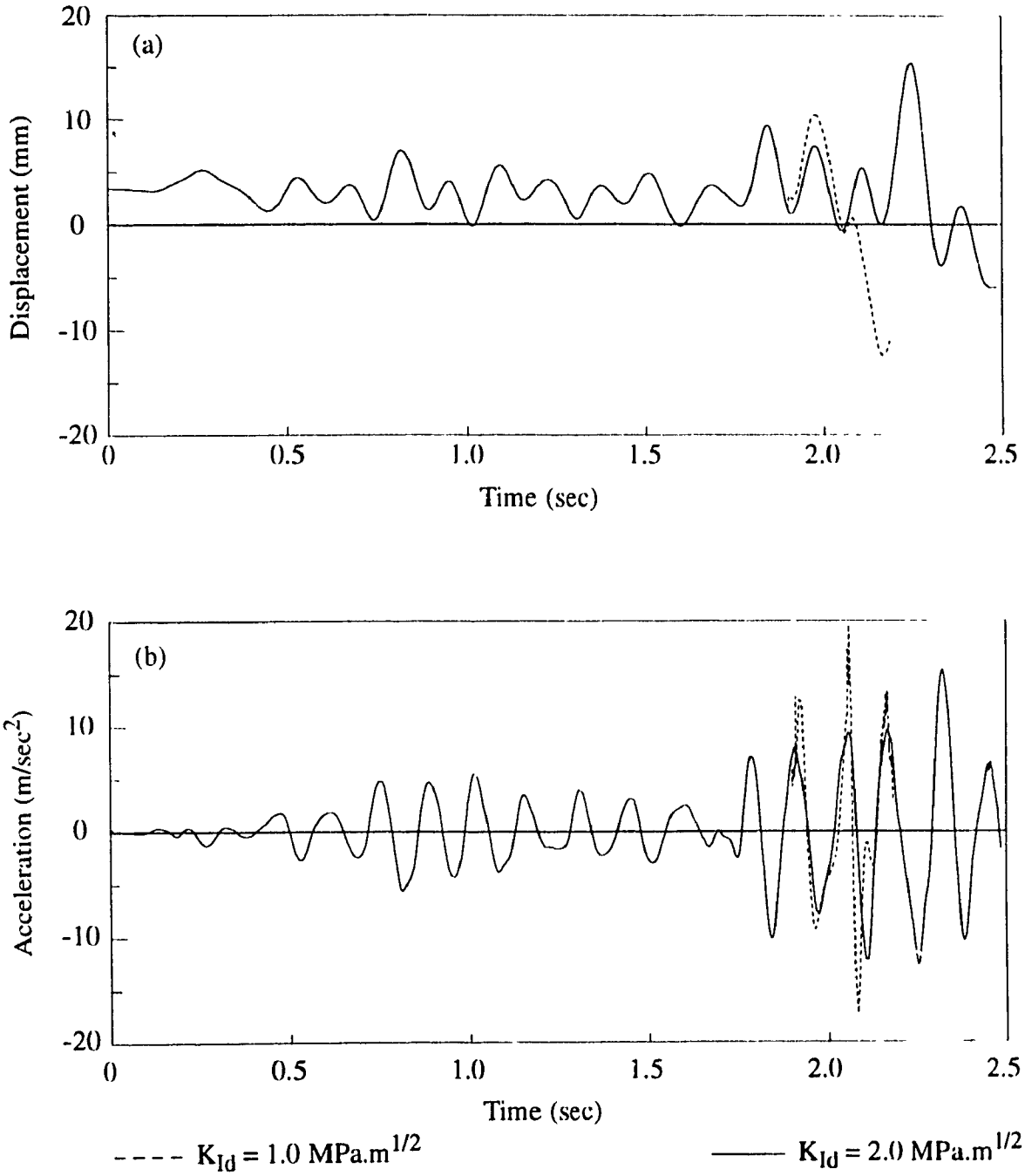

Figure 3.10 Time histories of crest response for different fracture toughness K_{Id}: (a) displacement; (b) acceleration.

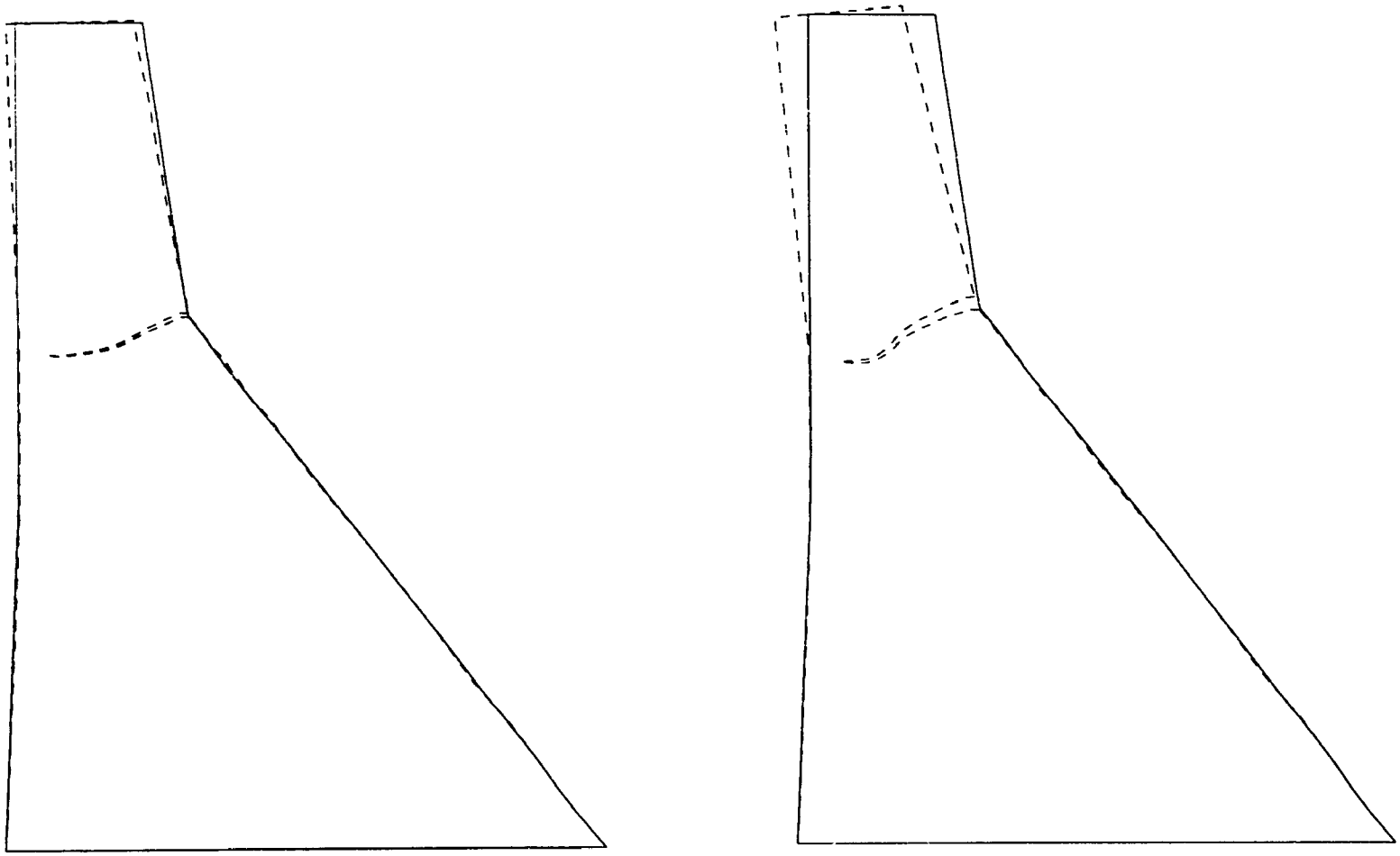

(a) $K_{Id} = 2.0$ MPa.m$^{1/2}$ (b) $K_{Id} = 9.0$ MPa.m$^{1/2}$

Figure 3.11 Instantaneous deformation of cracked dam for different fracture toughness K_{Id}

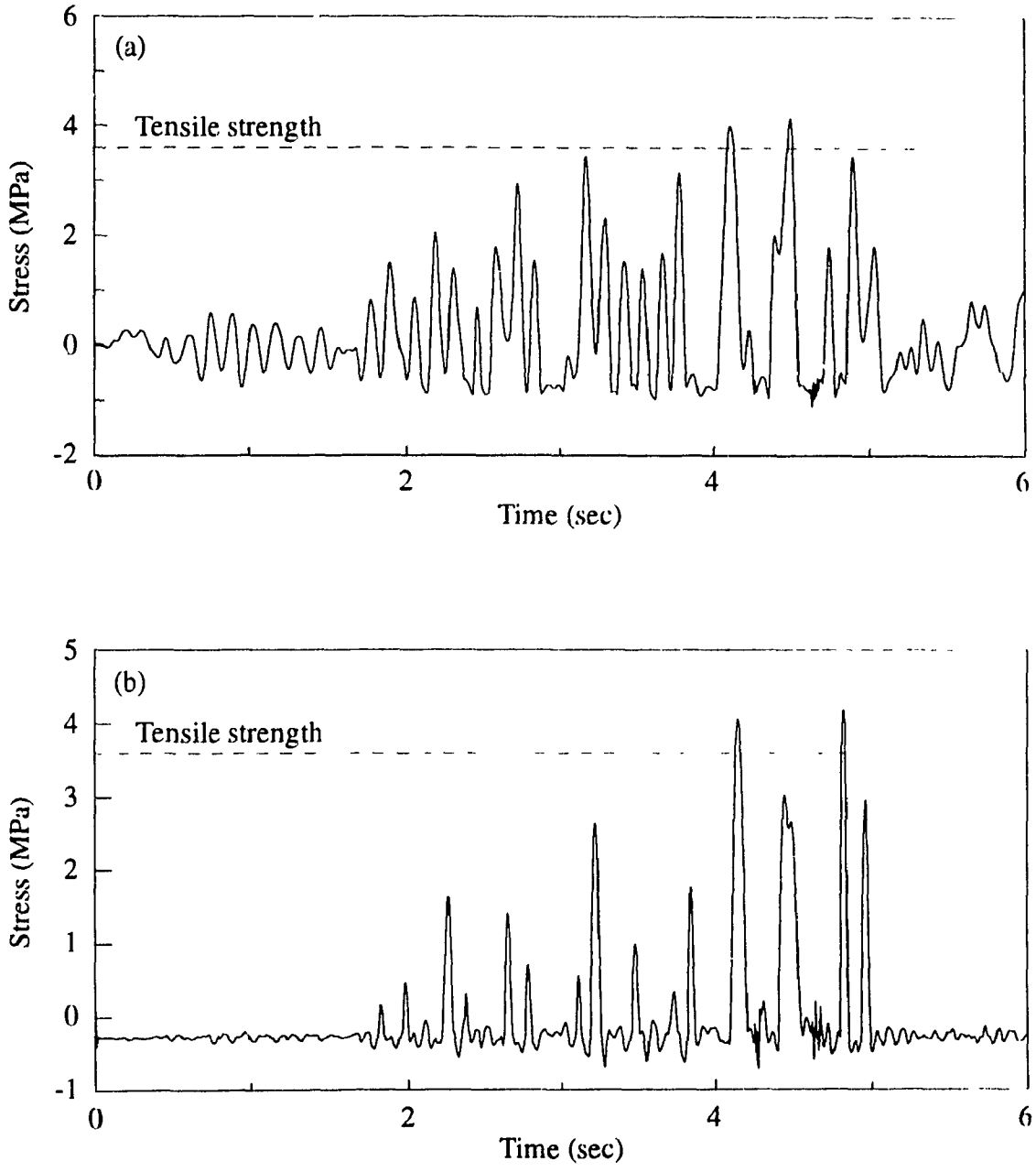

Figure 3.12 Time histories of principal tensile stresses at selected locations on upstream face of dam: (a) heel; (b) elevation 66.m.

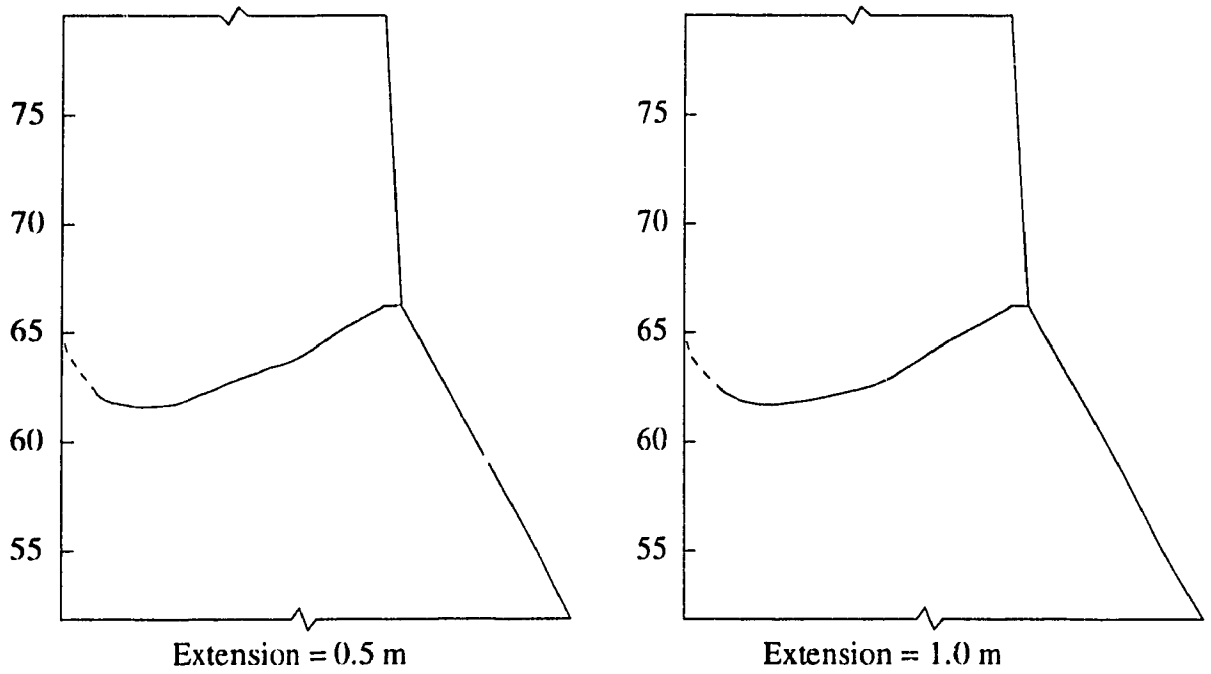

(a) $K_{Id} = 2.0$ MPa.m$^{1/2}$

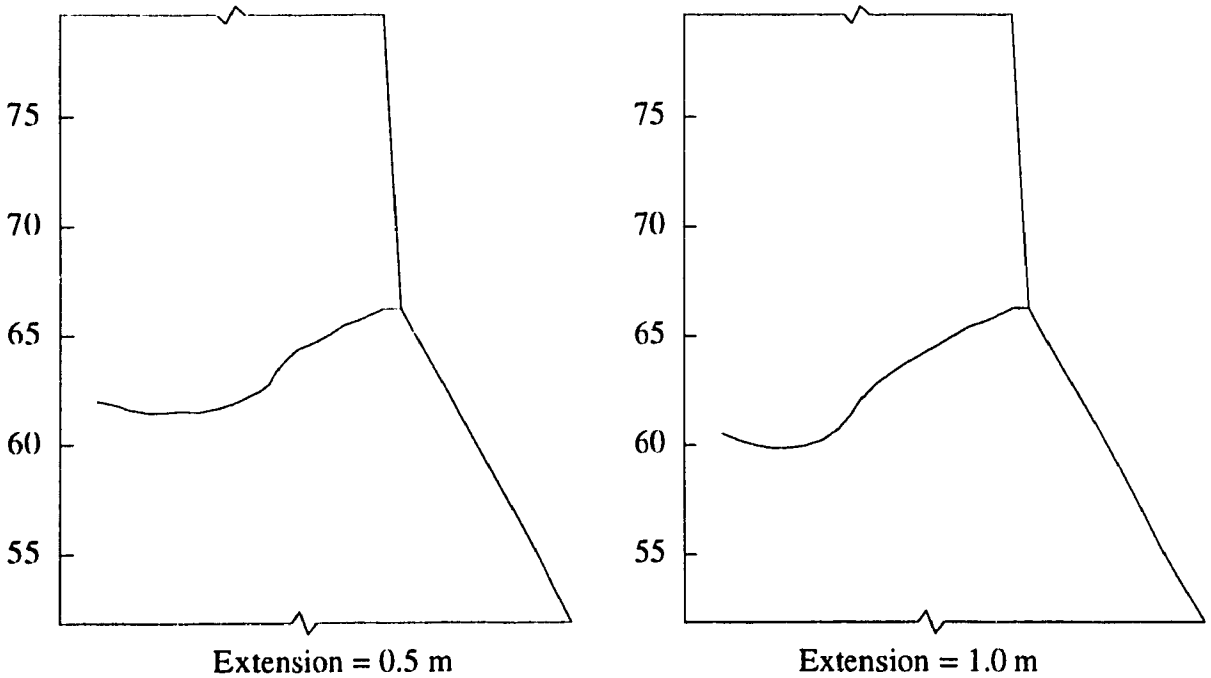

(b) $K_{Id} = 9.0$ MPa.m$^{1/2}$

Figure 3.13 Effect of maximum crack extension on crack profile.

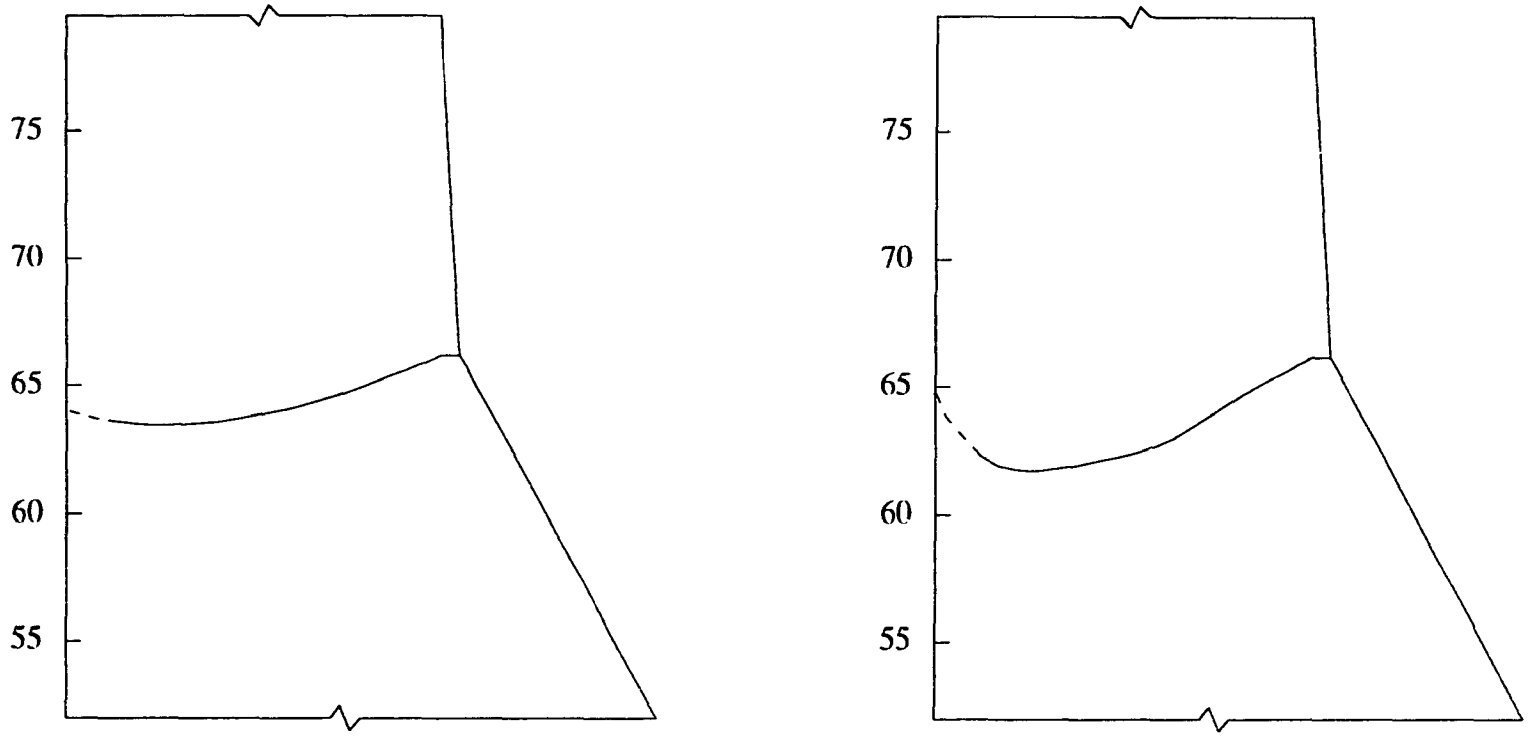

(a) Case 1

(b) Case 2

Figure 3.14 Effect of loading condition on crack profile for $K_{Id} = 2.0$ MPa.m$^{1/2}$: (a) dam self-weight and reservoir ignored: (b) all loads considered.

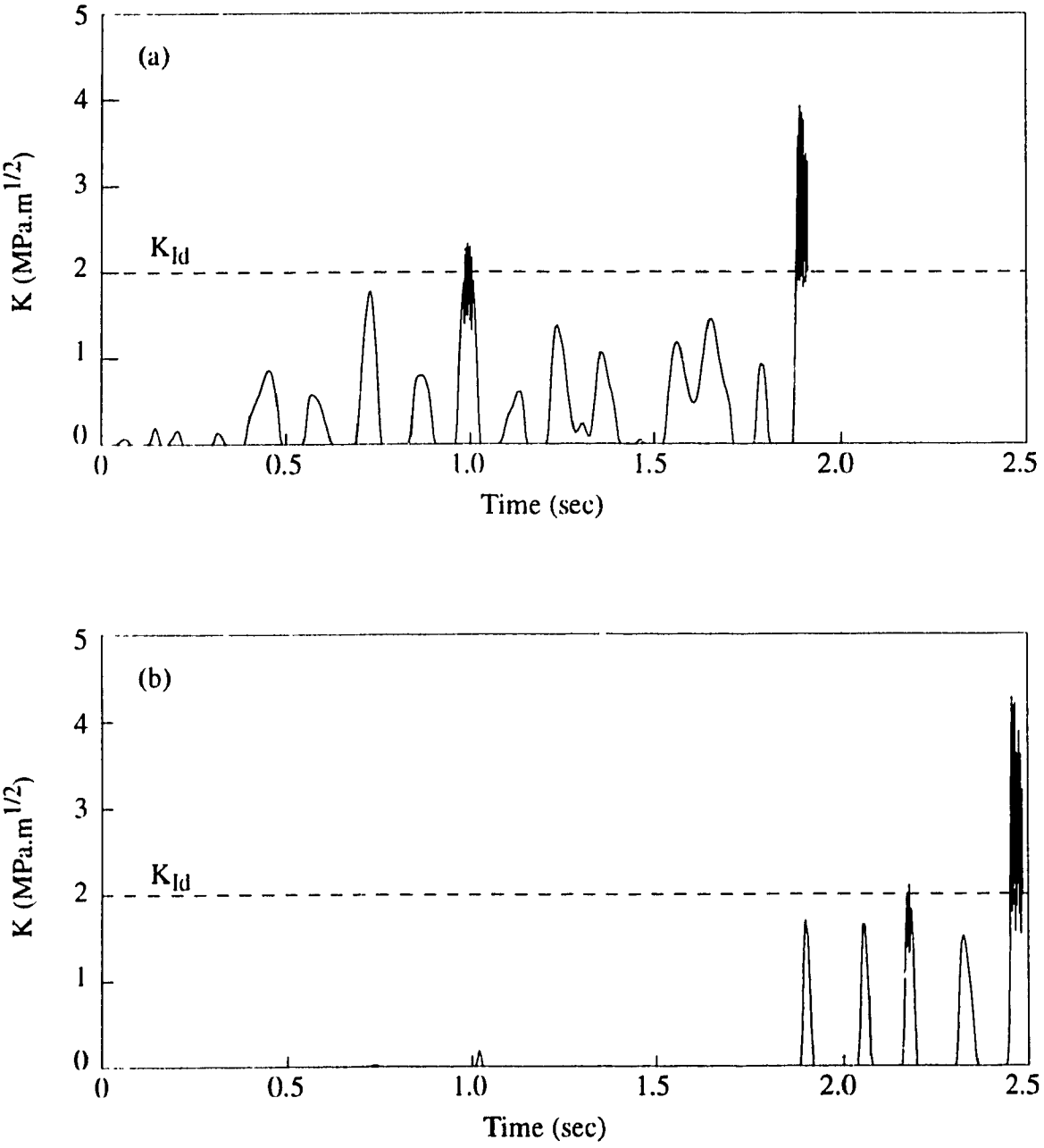

Figure 3.15 Time histories of combined mode stress intensity factor K for different loading conditions : (a) dam self-weight and reservoir ignored; (b) all loads considered

CHAPTER IV

ANALYSIS OF MULTIPLE SEISMIC CRACKING IN CONCRETE GRAVITY DAMS

4.1 INTRODUCTION

The analytical procedure presented in Chapter II and applied for the parametric evaluation of seismic cracking in Chapter III could account for only a single crack in the dam. In the present Chapter, the procedure is extended to the more general case where the occurrence and simultaneous propagation of multiple cracks can be simulated. The formulation together with the linear elastic fracture mechanics crack extension criterion is kept largely unchanged, although a more elaborate numerical procedure is employed to monitor opening/closing, stability and propagation of multiple cracks.

It should be noted that each new crack requires a subdivision of the dam domain along the crack profile; consequently, the presence of a large number of cracks makes the analysis increasingly complicated. Seismically induced cracking in concrete gravity dams is, however, limited to a few cracks which can be efficiently modelled using the present procedure. Although a large number of small cracks are usually present in a concrete dam (due to initial shrinkage, weathering, etc.) and others may initiate when the dam is subjected to an earthquake, during a strong seismic event only a few of these cracks actually propagate sufficiently deep into the body of the dam to endanger the safety of the structure. This has been observed both during the instances of seismic cracking in prototype dams as well as in available analytical (Ayari and Saouma 1990; Bhattacharjee and Léger 1993) and experimental investigations (Niwa and Clough 1980; Donolon and Hall 1991; Zhou and Lin 1992). Indeed, once a crack is formed, it is likely to release the tensile stresses over a considerable depth above and below preventing formation of other large cracks in nearby regions.

A brief discussion of the generalized methodology for multiple crack modelling is presented below. The extended numerical procedure is verified using the results of a model test conducted by Zhou and Lin (1992). This is followed by a detailed examination of the cracking process for the Koyna dam employing both single and multiple fracture models. Particular attention is focussed on the patterns of rupture predicted by these fracture models, as well as on the associated crack opening behaviors. The latter are of major interest in evaluating the possible development of hydrodynamic uplift pressure inside a propagating crack.

4.2 IMPLEMENTATION OF BEM FOR MULTIPLE CRACK PROPAGATION

4.2.1 Modelling and monitoring of multiple cracks

Modelling of a single crack in a domain has been discussed earlier and the same general principles apply when more cracks than one are present. For each crack, the surrounding domain is divided into sub-regions by extending a line from the crack tip to the opposite boundary. The direction of this line is completely arbitrary as it is only used to separate analytically the domains containing the crack flanks. Each additional crack thus increases the number of sub-domains by one. If any two cracks exist at nearly the same elevation but on opposite faces of the dam, the same arbitrary line could be employed as the dividing line, but in the present computer implementation separate lines are used to provide better control during rediscretization following crack propagation. During the time step-by-step analysis, opening and closing of each crack is monitored continuously. When a crack is detected to be unstable, the direction of crack propagation is computed and the boundary element mesh along the crack line is appropriately modified as discussed below.

If during the analysis multiple cracks lie close to each other, it is possible that one of the crack tips advances towards the interface line corresponding to an adjacent crack. In

such a case, the affected sub-domain boundary needs to be relocated to accommodate the extending crack. The problem can be more easily circumvented by judiciously choosing the initial orientations of the interface boundaries so that they are less likely to interfere with crack development. If in certain cases this is still found to be not sufficient, particularly when multiple cracks initiate at similar elevations on the two opposite faces, the analysis is stopped once the crack tip approaches an interface line. Modifications to the initial boundary element mesh become necessary at this stage.

4.2.2 Choice of analytical factors influencing fracture analysis

As noted earlier, in the present formulation for discrete crack propagation two other analytical factors should be considered, namely, the inclusion of interior domain collocation and the magnitude of incremental crack extension. Since, for seismic fracture analysis of concrete gravity dams boundary-only discretization has been shown to be sufficient, no interior nodes are defined in the analyses presented in the following section. Similarly, based on the results of the parametric investigation reported in the preceding Chapter, a piecewise extension of 10 percent of the instantaneous crack length, but limited to a maximum increment of 1.0 m, is employed in the following crack propagation analysis of the prototype Koyna dam. For the model dam application, the corresponding increment is 2 percent with a maximum permitted extension of 25 mm.

4.2.3 Applications

In the following, the multiple cracking responses of the Fongman and the Koyna concrete gravity dams are presented. The Fongman dam is employed in order to confirm the validity of the present numerical procedure to simulate multiple crack propagation. On the other hand, the earlier investigation of single crack propagation in the Koyna dam is extended to include multiple cracking response of the dam under the Koyna earthquake. As noted in Chapter III, the Koyna dam provides the only example of a gravity type

concrete dam where significant cracking occurred during a sesimic event soon after construction. Although the available information about the observed cracking of this dam is incomplete and certain analytical assumptions are made, it is believed that the results can still be realistically correlated with the actual cracking.

Since some of the geometric characteristics of the Koyna dam differ considerably from other gravity-type concrete dams, fracture response of the Pine Flat dam is investigated also. The dam represents a typical concrete gravity dam and the results for this case, which are discussed in the Appendix B, provide further insight into the fracture behavior of gravity dams under strong earthquakes.

4.3 MULTIPLE CRACKING OF FONGMAN DAM

Fongman dam is a 77.5 m high concrete gravity dam situated in northeast China and has previously been used as an example problem for studying earthquake induced cracking by Zhou and Lin (1992). In their investigation two initial horizontal cracks were considered starting from the upstream face of the dam. Seismic stability as well as unstable propagation of these cracks under ground shaking was studied. The analysis featured a finite element discrete crack model of the dam and employed a linearized solution procedure for the dynamic fracture analysis. Relative motion of crack surfaces was simulated by applying a series of normal and tangential impulses at contact points and the mode superposition method was used to obtain the dam response. A laboratory model of this dam, scaled at a dimensional ratio of 1:40 and made of gypsum, was also tested on shaking table.

The present analysis of this laboratory model of the dam with two initial cracks is based on the boundary element discretization depicted in Figure 4.1(a). The lower crack, at a distance 0.775 m from the base, is designated as C1 and the upper crack, at 0.49 m from the crest is designated as C2. Initial lengths of these cracks are, respectively, 0.275 m and 0.25 m. The model is considered fixed at the base and with no reservoir in order to

match the boundary conditions of the test.

The boundary element mesh consists of 129 nodes and 70 quadratic boundary elements. Three traction singular quarter-point elements are employed at each crack tip, two on the crack flanks and one ahead of the tip. The following material properties of the gypsum, consistent with those reported by Zhou and Lin (1992), are used in the analysis: dynamic modulus of elasticity E_d = 1650 MPa; Poisson's ratio ν = 0.2; mass density, γ = 665 kg/m^3; and damping equal to 1.5 per cent of critical for the first mode.

The dynamic fracture toughness of the gypsum is not mentioned in that reference and is computed from similitude relations to be 25 kPa.m$^{1/2}$, corresponding to fracture toughness of 1.5 MPa.m$^{1/2}$ for the dam concrete. The computed modal frequencies of the model dam are compared against those obtained from the laboratory test. For the first two modes the computed natural frequencies are 59.6 and 125.0 Hz, in good agreement (average difference 6.5 per cent) with the corresponding test frequencies of 62.05 and 138.05 Hz. As in the test, harmonic excitation at the natural frequency of the fundamental mode is assumed at the base.

The predicted final crack profiles are presented in Figure 4.1(b), together with the laboratory test results from Zhou and Lin (1992). Good agreement is evident. In the analysis, the lower crack C1 propagates first, but stabilizes after extending in two stages by a total of only 94 mm. Immediately thereafter, upper crack C2 becomes unstable and propagates quickly to approach the downstream face. Once the tip of this crack is sufficiently close to the downstream face, further propagation cannot be modelled and complete separation along crack C2 is predicted. Such complete rupture in the upper part of the dam is not likely to influence significantly the response of the lower portion, as long as the separated crest block remains in place. Since this was indeed the case during the laboratory test, the continuation of the analysis with almost complete separation along crack C2 can be expected to predict adequately the response of lower crack C1. With crack C2 artificially arrested near the downstream face, in the continued analysis crack C1

begins to propagate further and also penetrates through the dam. As in the case for C2, once the tip of crack C1 reaches close to the downstream face further remeshing is not possible and rupture is assumed. In the laboratory test, the two initial cracks also propagated to penetrate completely through the dam, after which the separated upper portions continued to rock after rupture. The computed times of crack propagations indicate that both cracks grow very quickly to reach the opposite face, a feature also noticed in the model test.

4.4 SINGLE AND MULTIPLE CRACKING OF KOYNA DAM

Seismic crack propagation analysis of the Koyna dam was presented Chapter III considering a single initial crack originating from the downstream face. In the present single and multiple fracture investigation, the same material properties are employed. For the case of simultaneous multiple cracking in the dam, influence of increasing the concrete fracture toughness from 2.0 to 5.5 and 9.0 MPa.m$^{1/2}$ is also examined. Furthermore, since the multiple fracture model involves cracking on the water retaining upstream face of the dam, opening/closing behavior of these cracks is also monitored in order to obtain an insight into the phenomenon of hydrodynamic uplift pressure build-up in such cracks.

Water pressure effect in the cracks is, however, not included in the analysis, since no model for hydrodynamic interaction in cracks propagating under seismic action exists to the authors' knowledge and opinions also differ concerning the importance of this phenomenon. The recent study by Tinawi and Guizani (1994) comprises the first attempt at examining the problem analytically. Although it does demonstrate the significance of hydrodynamic pressure inside cracks, the procedure is applicable only for short pre-existing open cracks and does not address the question of pressure development within a propagating crack. In engineering practice, the commonly used agency guidelines include those of the U.S. Bureau of Reclamation (USBR 1976) and U.S. Federal Energy Regulatory Commission (FERC 1991). The FERC guidelines assume that the initial uplift

pressure in a crack remains unchanged during an earthquake, whereas the Bureau guidelines assume that the internal water pressure is relieved completely when a crack opens during an earthquake. The justification given for these assumptions is that a crack will open and close cyclically in quick succession during strong ground shaking, thus inhibiting the water pressure to react. The opening/closing behavior of the cracks is therefore monitored closely in the results presented herein in an attempt to obtain appropriate data associated with this phenomenon.

4.4.1 Potential cracking models

In order to predict the locations of potential multiple cracking, stress analysis of the intact dam subjected to 6 sec of vertical and horizontal accelerations of the recorded Koyna earthquake is first performed. Envelopes of the resulting principal tensile stresses are presented in Figure 4.2, where it is seen that the tensile stresses exceed the tensile strength of concrete near elevation 66.5 m on both the downstream and the upstream faces (zones 1 and 2, respectively). On the downstream face, due to the change in slope at this elevation, the stress singularity results in a computed maximum tensile stress almost three times the tensile strength of concrete. Another zone of high tensile stress is obtained on the upstream face near the base (zone 3). However, since the observed cracking in the Koyna dam is limited to zones 1 and 2 only, in the present study cracking of the dam is investigated in these regions. Fracture in zone 3 was also considered but an initial crack modelled at this location did not propagate during seismic analysis.

Based on the above, three different sets of small cracks are pre-assigned on the faces of the dam and the fracture response of the dam is investigated for each of these three models of cracking. In the first two, a single 1 m long initial crack is introduced separately on the downstream and the upstream faces of the dam, cracks C1 and C2 at elevations 66.5 and 70.0 m respectively, whereas in the third case a multiple cracking model is assumed with cracks C1 and C2 originating simultaneously on both faces of the

dam. The corresponding boundary element discretizations for these cracking models are depicted in Figure 4.3. As shown, the initial crack(s) and the arbitrary line(s) emanating from the crack tip(s) are used to divide the dam domain into appropriate subregions. For the fracture models involving single cracks, an additional subdomain is defined to provide more degrees-of- freedom and to reduce the domain integration area below the crack. In the multiple cracking model, the presence of additional nodes along the second crack line supplies the additional degrees-of-freedom and further sub-zoning is therefore not adopted.

Envelopes of the principal tensile stresses on the faces of the dam are presented in Figure 4.4 for the three cracking models. For the models with a single crack propagating from either the downstream or the upstream face, Figures 4.4(a) and 4.4(b) show that the tensile stresses on both faces of the dam are reduced to levels below the strength of concrete. Thus it appears that, if the initial cracking originates on either face, other cracking will not develop before the initial crack has broken through to the opposite face. Similar behavior is observed in Figure 4.4(c) for cracks C1 and C2 propagating from both faces. Unlike the preceding two fracture models, however, this analysis was able to be continued for a substantially longer period of time prior to rupture, allowing the dam to be subjected to the more intense portion of the Koyna earthquake. In spite of this increase in ground shaking, the stress release caused by cracking is seen still to reduce the maximum tensile stress to below the strength of the concrete. Simultaneous other cracking is therefore not predicted to occur in the dam for this fracture model also.

It is therefore evident that the model for the actual cracking of the dam is most likely to be associated only with zone 1. Not only does the change in slope provide a singular point for first crack formation, this crack also breaks through the dam before cracking can be initiated at other locations. However, because initial cracks are not solely stress-induced but may also arise due to a variety of other causes including shrinkage, temperature effects, etc., the additional two fracture models are included in the following

examination of the fracture process of the Koyna dam. Moreover, for dams of other geometries involving more typical cross-sections, all the above three cracking models become possible candidates for the critical fracture process. Even for the Koyna dam, a previous finite element analysis based on the discrete crack approach (Wepf et al. 1984) as herein, as well as laboratory rupture testing (Niwa and Clough 1980), have indicated fracture behavior corresponding to the current single C1 cracking model, whereas other studies which employed either smeared crack modelling (Bhattacharjee and Léger 1993) or a quite high concrete fracture toughness (Ayari and Saouma 1990) have predicted final fracture patterns similar to the present multiple cracking model.

4.4.2 Assessment of static stability of cracks

Static analysis of the dam is first conducted in each case which indicates that, under the influence of the self-weight and the hydrostatic water pressure, the dam deflects toward the downstream, keeping crack C1 closed. In the two models where the upstream crack C2 is present, the possibility of the opening and consequent instability of this crack under the effect of static loads is examined by performing a classical stability analysis (USBR 1976) of the portion of the dam above the crack. Full uplift pressure is considered in the crack and a linear variation of uplift, full uplift at the crack tip to zero on the downstream face, is assumed in the uncracked length. Computed static stresses on the plane of the crack are all compressive, indicating a stable crack.

4.4.3 Comparison of fracture processes for single and multiple cracking models

Results for seismic crack propagation with initial cracks C1 and C2 considered separately are presented in Figures 4.5 and 4.6, respectively, whereas Figure 4.7 depicts the results for the multiple fracture model wherein C1 and C2 are treated simultaneously. As shown in Figures 4.5(a) and 4.6(a), the final rupture profiles for the single fracture models are more or less similar, with the initial crack breaking through to the opposite

face of the dam to cause complete rupture. Analogous final behavior is predicted from the multiple fracture analysis, in which cracks C1 and C2 merge within the body of the dam and also result in full separation of the crest block as seen in Figure 4.7(a). However, the final rupture pattern for this model differs markedly from the above profiles of the single crack models.

In the absence of other cracking, crack C1 of Figure 4.5(a) propagates smoothly and emerges close to El. 64 m on the upstream face. Similarly, when only upstream initial crack C2 is considered [Figure4. 6(a)], the crack travels toward the zone of high compression occurring at the point of slope change on the downstream face. For the multiple cracking model, however, it is apparent from Figure4.7(a) that the presence of crack C2 alters the profile of downstream crack C1 during its final stages of propagation. In this fracture model crack C1 completes its propagation while upstream crack C2 is still short; consequently the influence of C2 on crack C1 is only evident toward the end of the propagation of the latter. On the other hand, the final trajectories of crack C2 are noticeably different in Figures 4.7(a) and 4.6(a). With crack C1 already developed in Figure 4.7(a) for the multiple cracking model, a change in the orientation of the stress field in front of the crack tip causes C2 to bend downwards. This change in stress field orientation is due to the increase in shear stress which occurs in the intact concrete ahead of the crack tip when the crest deflects in the downstream direction.

Time histories of crack propagation data for the single fracture models shown in Figures 4.5 (b) and 4.6(b) indicate that these cracks propagate almost instantaneously to penetrate through the entire width of the dam. Instability of crack C1 of Figure 4.5(a) is first detected at 2.46 sec and the crack propagation is completed in the next few times steps, with a total elapsed time of 0.03 sec. The single upstream crack C2 of Figure 4.6(a) begins to propagate even earlier, at 2.27 sec, and penetrates the dam in 0.015 sec without arresting. Unlike this abrupt fracture behavior, the propagation of cracks C1 and C2 of multiple cracking model each comprises two distinct phases as shown in Figure 4.7(b). It is seen

that the downstream crack C1 is the first to grow, becoming unstable at 2.46 sec and propagating in two stages. In the first, this crack extends rapidly by about 15 m in 0.03 sec. As the crest movement reverses, the crack temporarily stabilizes but begins again to propagate when the dam crest deflects toward the upstream in the next cycle. This second stage of growth comprises a crack extension of about 4 m in 0.01 sec. At 3.8 sec, upstream crack C2 extends also in two phases. In this process, the tip of C2 approaches sufficiently close to crack C1 so that further propagation analysis would cause the sub-domain boundaries emanating from the two crack tips to intersect. It is therefore assumed that the upstream crack merges into the downstream crack at this time, resulting in complete rupture along the dashed line in Figure 4.7(a).

Time histories of the horizontal displacement of the dam crest for the single cracking models involving cracks C1 and C2 separately are plotted, respectively, in Figures 4.5(c) and 4.6(c).The crest oscillates about its static displaced position for approximately the first 2 sec while the earthquake acceleration magnitudes are relatively small and, in each case, rupture is associated with the first major peak of crest displacement in the appropriate direction. It is noteworthy that crack propagation is not necessarily in phase with the displacement of the crest. This is evident in Figure 4.6(c) where the crest displacement attains its peak value of 15.15 mm at 2.26 sec, whereas instability of the crack occurs only two time steps later, at 2.27 sec when the crest has already begun to move toward the upstream. Flexibility of the structure is the explanation for this phase difference, as a result of which the relative displacements along crack flanks are not directly related to the crest displacement.

In order to examine the possible development of hydrodynamic uplift pressure in cracks, the opening responses of the crack mouth are examined in Figures 4.5(d), 4.6(d) and 4.7(d) for the three fracture models. Although only the opening/closing behavior of crack C2 on the water retaining face of the dam is relevant for this phenomenon, results are also presented for downstream crack C1 as an indication of seismic damage on this

face of the dam. From the time histories of the crack mouth opening displacements of Figures 4.5(d) and 4.6(d) for the single fracture models, it is evident that the cracks remain more or less closed for almost the entire time. Noting that the critical openings to initiate propagation of C1 and C2 are 0.760 and 0.304 mm, respectively, it is also evident that the first major crack mouth opening coincides with rupture. For propagation of single crack C1 the crack mouth opening at rupture is 4.27 mm, with a corresponding magnitude of 3.9 mm for crack C2.

In comparison, Figure 4.7(d) shows that the crack opening behavior predicted by the multiple fracture model is very different. Downstream crack C1 is first to propagate (at mouth opening of 0.348 mm for this model) and experiences dramatic increases in the magnitude of opening compared to the corresponding single crack model. While the two stages of propagation of this crack are associated with relatively large crack mouth openings at approximately 2.5 and 3.0 sec, these or even larger openings do not necessarily induce instability at the crack tip, due also to the forementioned flexibility of crack flanks with increasing crack length. During the opening at 3.0 sec, the crack extends in length until the magnitude of the opening is 5.5mm, after which the crack does not propagate, although the crack mouth opening continues to increase to almost double this magnitude. The effect is even more strongly reflected during the subsequent opening of this crack at 4.0 sec, when the crack mouth opens by 43.7 mm but with crack instability not incurred.

Figure 4.7(d) also shows that crack C2 of this fracture model experiences a similar dramatic, but opposite, change in mouth opening behavior compared to the corresponding single cracking results of Figure 4.6(d). Unlike the above behavior of crack C1, the openings of upstream crack C2 appear insignificant, with maximum predicted opening of 1.8 mm just prior to rupture and an even smaller magnitude of the opening of 1.1 mm at the time of final rupture. Moreover, the elapsed time from the initiation of growth of this crack to rupture is very short, a feature also evident in Figure 4.6(d) for the single fracture

model.

4.4.4 Behavior with higher concrete fracture toughness

As mentioned before, the cracking behavior of the dam is also investigated for two higher values of the concrete fracture toughness, namely 5.5 and 9.0 MPa.m$^{1/2}$. Since multiple cracking has been predicted for higher magnitude of concrete fracture toughness, the analysis is performed only for the multiple fracture model. As for the case with K_{Id}=2.0 MPa.m$^{1/2}$, an initial crack in zone 3 on the upstream face near the base of the dam was also considered but found not to propagate.

The final crack trajectories for these two toughness values are presented in Figure 4.8. It is evident that substantially different cracking patterns are obtained for K_{Id}= 5.5 and 9.0 MPa.m$^{1/2}$. For K_{Id}= 5.5 MPa.m$^{1/2}$ the two cracks propagate into the dam and merge with each other, resulting in complete separation of the crest block. On the other hand, for K_{Id}= 9.0 MPa.m$^{1/2}$ downstream crack C1 also propagates deep into (but not through) the dam, whereas the upstream crack is arrested after only about a meter of propagation. Comparison of Figures 4.8(a) and 4.7(a) indicates that the final rupture patterns are very similar for K_{Id}= 2.0 and 5.5 MPa.m$^{1/2}$, although the details of the associated crack propagation processes discussed below differ considerably.

Corresponding time histories of crack mouth opening are presented in Figure 4.9. For K_{Id}= 5.5 MPa.m$^{1/2}$, the maximum opening of upstream crack C2 is 4.31 mm during the growth phase and 4.28 mm at rupture. Since this crack does not propagate significantly for K_{Id}=9.0 MPa.m$^{1/2}$, the crack mouth openings for this toughness are reduced to less than 1.0 mm. Growth phase magnitudes of the opening of downstream crack C1 are much larger and almost identical for the two values of toughness, although the corresponding final crack profiles have been noted to be considerably different. On the other hand, in spite of the very similar final crack trajectories for K_{Id}= 2.0 and 5.5 MPa.m$^{1/2}$, it is also interesting to note that the opening magnitudes for crack C1 are much smaller for the

increased toughness (7.8 vs 43.7). Due to the delayed beginning of crack growth for K_{Id}= 5.5 MPa.m$^{1/2}$, crack C1 is still at its initial length when the intense shaking of the earthquake acts on the dam, whereas for K_{Id}= 2.0 MPa.m$^{1/2}$ the crack is already extended to its final length before the large peaks of the earthquake arrive.

In the absence of any significant upstream cracking for K_{Id}=9.0 MPa.m$^{1/2}$, the principal tensile stress envelope for this case is examined in Figure 4.10. The delayed propagation of the downstream crack combined with the short final length of the upstream crack results in keeping the tensile stresses high throughout the dam faces. Comparing this envelope with that of the uncracked dam [Figure 4.2] reveals that they are almost identical. This is because the high values in the present case are reached before the downstream crack even begins to propagate. Thus, it appears that higher magnitude of concrete fracture toughness indeed result in distributing the surface cracking in the dam as noted previously, but these surface cracks do not necessarily propagate if the concrete toughness is sufficiently high.

4.4.5 Approximate post-cracking behavior based on multiple cracking model

Although the maximum opening of upstream crack C2, for which hydrodynamic pressure is under question, has been observed to be small during the growth phase of the crack, the rocking of the separated crest block may still lead to the development of significant uplift pressure during the post-rupture phase. In order to estimate both the magnitudes and durations of these openings, the time history analyses for the multiple cracking model corresponding to the two lower values of the concrete fracture toughness are continued even though the cracks are predicted to have merged. For K_{Id} = 9.0 MPa.m$^{1/2}$, where the crest block remains attached to the dam, it is found that the upstream crack openings remain very small for the entire duration of the applied excitation.

In order to undertake this approximate post-rupture analysis, the boundary element

discretization is not updated for the last stage of extension of upstream crack C2 and the small portion of concrete between the two crack tips is left intact. The results can be viewed as realistic for the post-cracking behavior based on the consideration that the intact portion is small and near the neutral axis of the cross-section. The imposed discontinuity in an otherwise through crack will therefore not significantly constrain the opening of the crack during further earthquake excitation. Furthermore, it can easily be demonstrated that sliding of the ruptured crest block is not likely to occur under the less intense base acceleration during the remaining time history of ground excitation.

The resulting complete time histories of crack mouth openings for K_{Id}=2.0 and 5.5 MPa.m$^{1/2}$ are plotted in Figure 4.11. For K_{Id}=2.0 MPa.m$^{1/2}$ Figure 4.11(a) shows that the magnitudes of opening of the upstream crack C2 are much more pronounced during the post-rupture response compared to the pre-rupture phase. The crack remains more or less closed during almost the entire time prior to predicted rupture. As noted previously, the maximum opening of this crack is .8 mm immediately preceding rupture, with a corresponding magnitude at rupture of 1.1 mm. Compared to these, the post-rupture maximum opening increases to 5.9 mm. The associated duration is, however, only 0.1 sec and the durations of other less prominent openings are also short. For downstream crack C1 on the other hand, the post-rupture openings are found to be reduced to a maximum of 7.7 mm from the aforementioned 43.7 mm immediately prior to rupture. Similar magnitudes of opening at the base of the ruptured crest block have also been reported by Saini and Krishna (1974), who performed a simplified seismic stability analysis of the separated top profile of the dam. When subjected only to the streamwise component of the Koyna earthquake, they obtained a maximum opening of approximately 33 mm at the face of the rocking block, in reasonable agreement with the 43.7 mm predicted herein since crack C1 is nearly fully developed across the dam cross-section at the time of this opening.

Post-rupture crack mouth behavior generally similar to the above is predicted for K_{Id}=5.5 MPa.m$^{1/2}$ in Figure 4.11(b), although the difference between the pre- and post-

rupture magnitudes are not as dramatic as for K_{Id}=2.0 MPa.m$^{1/2}$. The maximum opening of upstream crack C2 is 7.6 mm in the post-rupture phase compared to 4.31 mm shortly before rupture. The corresponding magnitudes for crack C1 are 3.8 mm and 7.8 mm. The time during which the critical crack C2 remains open is small for this fracture toughness also, generally less than 0.1 sec.

4.4.6 Summary of observations concerning hydrodynamic pressure build-up in crack C2

Since the development of dynamic uplift pressure in upstream cracks is directly related to their opening/closing behavior, the mouth opening data for crack C2 on the water retaining face of the dam are summarized in Table 4.1 for the practical case of K_{Id}=2.0 MPa.m$^{1/2}$. The data are compiled for the three phases of the fracture response of the dam, namely prior to rupture, at the time of predicted rupture and during the post-rupture response. It is evident that the opening response of the crack in the pre-rupture phase is more or less independent of the fracture model used and both the maximum magnitude and corresponding duration are very small. The largest opening is 0.8 mm with duration of 0.07 sec. Thus, it appears that the opening of the crack is not expected to be sufficient to allow the hydrodynamic pressure to build up prior to the time of rupture and hence unlikely to influence the pre-rupture response. Furthermore, as demonstrated by Tinawi and Guizani (1994), for crack openings smaller than 1.0 mm the effect of viscosity of the water inside a crack becomes important. For the above small pre-rupture openings, the resulting additional damping is therefore likely to further reduce the opening response of the crack.

In comparison to the above pre-rupture observations, considerably larger magnitudes of opening are predicted at rupture itself, as well as in the analysis following rupture. As indicated in Table 4.1, the maximum opening is 3.9 mm at the time when the crack breaks through the dam and 5.9 mm during the response following rupture. Although, the associated durations of these openings are still small (also less than 0.1 sec),

it appears that the opening magnitudes of this order could result in the dynamic uplift pressure penetrating the crack and affecting the post-fracture response of the dam.

It is noteworthy that a comparable magnitude of the opening of the upstream crack mouth has been reported by Bhattacharjee and Léger (1993). In their study which included also the post-rupture response, the crack opens by a maximum of 6.8 mm on the upstream face of the dam, although the cracking develops at a lower elevation and a slightly smaller magnitude of concrete fracture toughness K_{Id} = 1.5 MPa.$m^{1/2}$ was employed. The corresponding magnitude predicted in the present investigation is 5.9 mm in Table 4.1.

4.5 CONCLUDING REMARKS

The performance of the boundary element procedure for the analysis of multiple cracking in concrete gravity dams has been demonstrated in this Chapter. For the Koyna dam, the critical cracking is found to be associated with fracture originating at the point of downstream slope change and penetrating the dam almost instantaneously, as studied in Chapter III. However, complete rupture along the base of the crest block is predicted for the other two fracture models also. Increasing the concrete fracture toughness is found to influence the fracture process and for higher magnitudes of toughness cracking in the dam becomes distributed but with most of the cracks confined to the surface. Concerning the upstream crack opening and the possible development of hydrodynamic pressure, it is observed that the opening is fairly small during the pre-rupture response but increases considerably at rupture and in the post-rupture phase. The latter could be sufficient for the build-up of dynamic uplift pressure.

From the above it is evident that the boundary element fracture analysis procedure presented in this study is well suited to model a cracked dam and simulate crack propagation under dynamic loadings. However, the emphasis hitherto has been on an accurate and efficient modelling of the fracture process itself, whereas simplified assumptions have been made in the treatment of some other aspects of the problem. In

particular, interaction of the dam with the surrounding media is not modelled rigorously. It is, however, well recognized that the interaction of a dam with the foundation medium as well as with the reservoir water influences its dynamic response under seismic loading (Chopra 1987). Although a number of formulations are available in the literature for the treatment of dam-reservoir-foundation interaction (Chopra et al. 1980; Chandrashaker and Humar 1994), most of them work in the frequency domain and cannot therefore be employed in non-linear analysis involving cracking of the dam. In view of this, a boundary element formulation is presented in the next Chapter for the modelling of the semi-infinite foundation medium in the time-domain. Successful application of the procedure to the analysis of two-dimensional rigid foundations is demonstrated and its future implementation to account for foundation interaction in the fracture analysis of dams is discussed.

Table 4.1 Crack mouth opening data for C2

K_{Id} (MPa.m$^{1/2}$)	Mouth opening data	Pre-rupture		Rupture		Post-rupture
		Single fracture model	Multiple fracture model	Single fracture model	Multiple fracture model	Multiple fracture model
2.0	Magnitude (mm)	0.21	0.80	3.90	1.80	5.90
	Duration (sec)	0.05	0.07	0.03	0.06	0.09
	Time (sec)	1.85	3.23	2.28	4.21	4.34

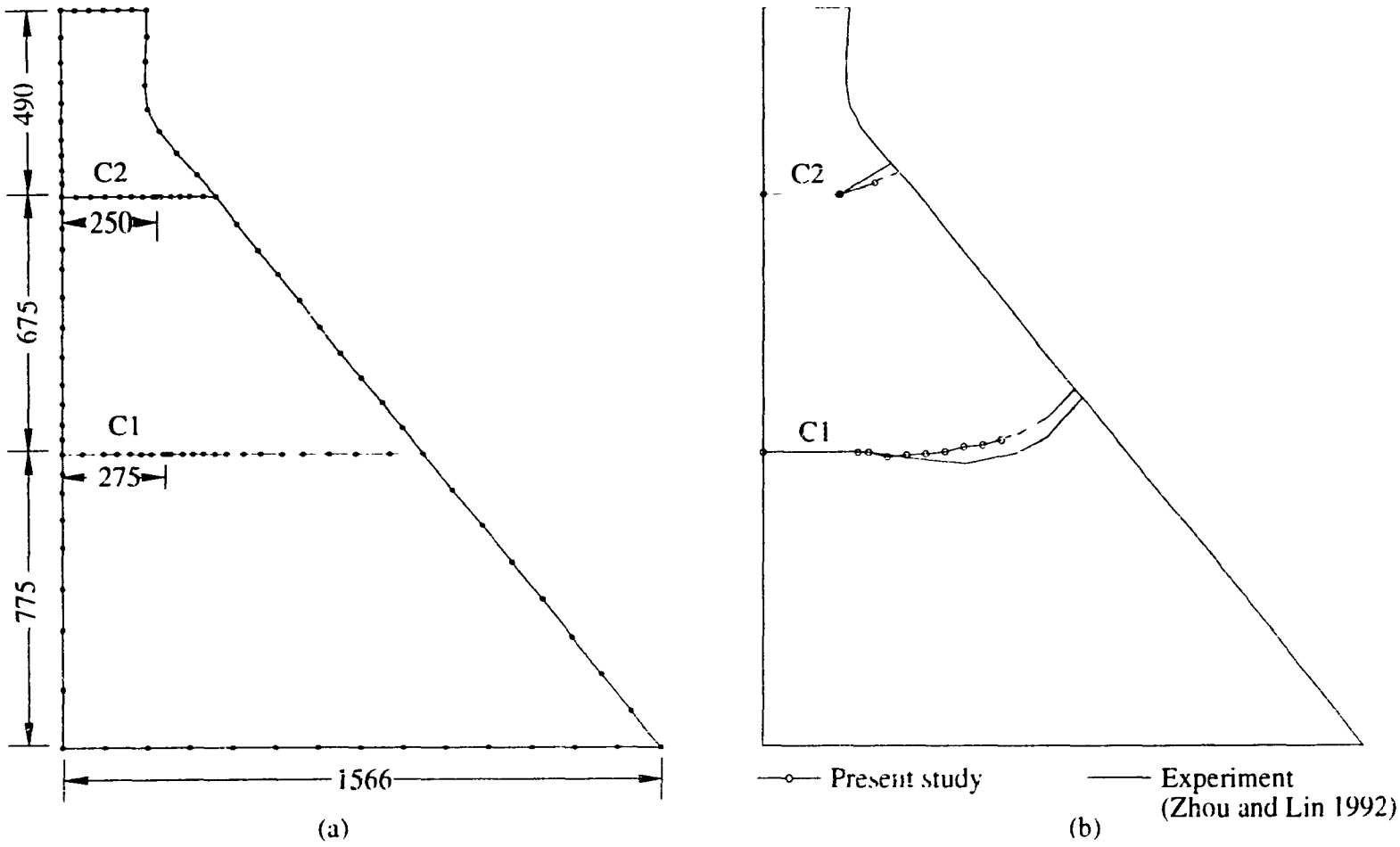

Figure 4.1 Fongman dam model with initial cracks: (a) boundary element discretization; (b) final cracking profiles

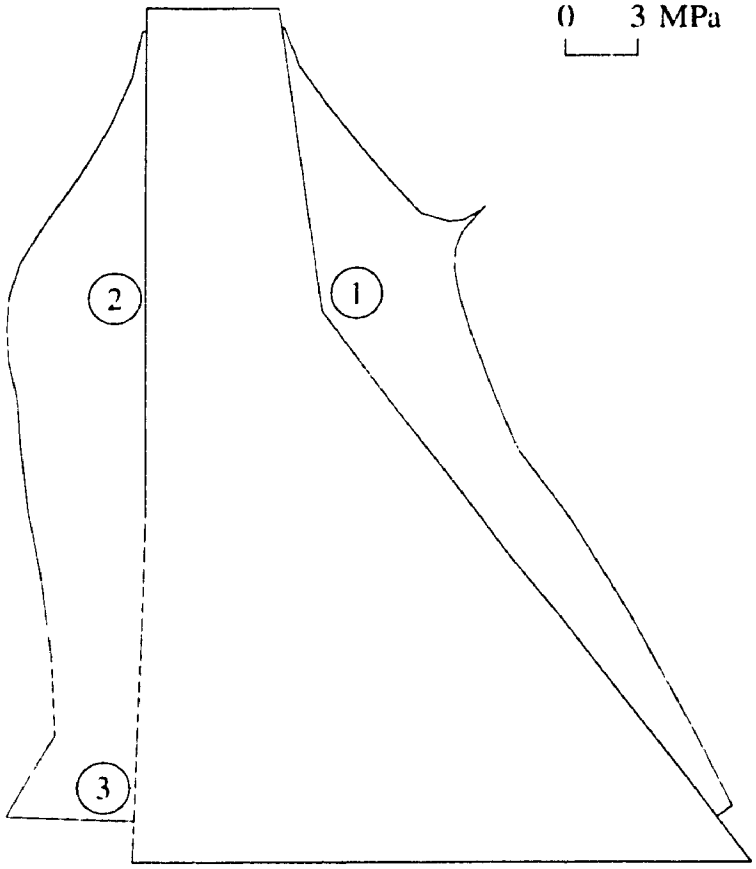

Figure 4.2 Envelope of principal tensile stresses for seismic analysis of Koyna dam without cracks

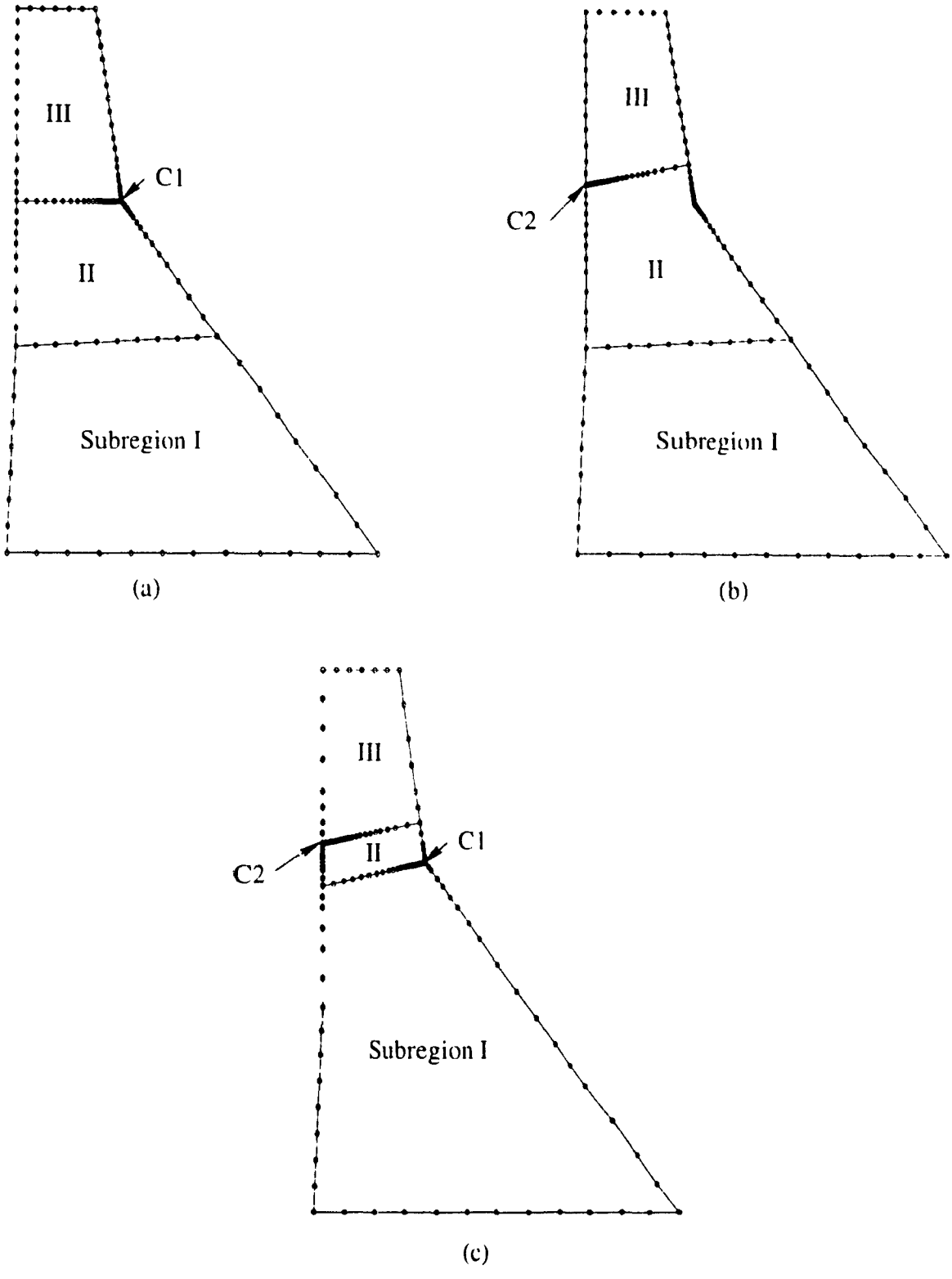

Figure 4.3 Boundary element discretizations of Koyna dam for different fracture models: (a) single downstream crack C1; (b) single upstream crack C2; (c) multiple cracking

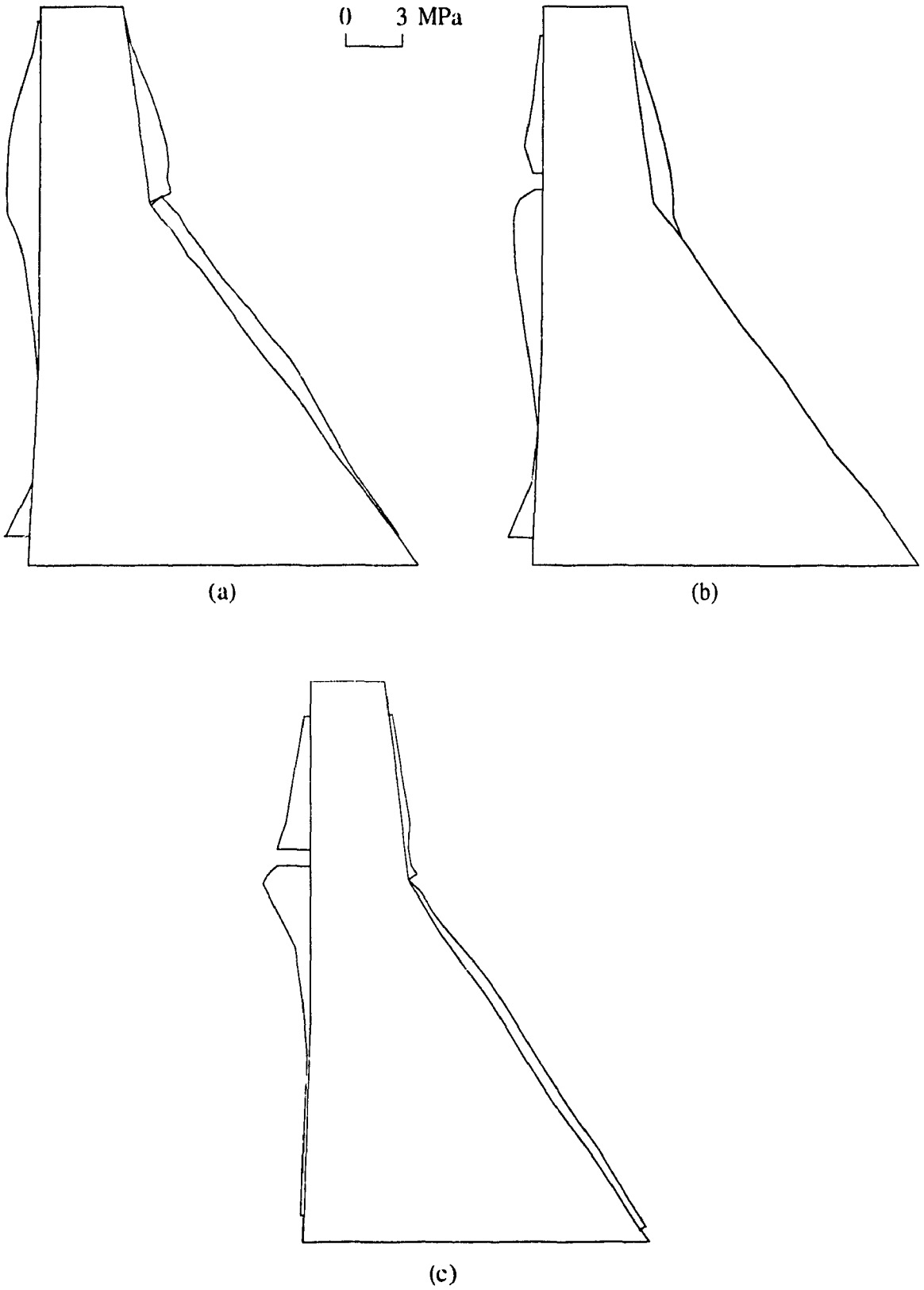

Figure 4.4 Envelopes of principal tensile stresses for different fracture models: (a) single downstream crack C1; (b) single upstream crack C2; (c) multiple cracking

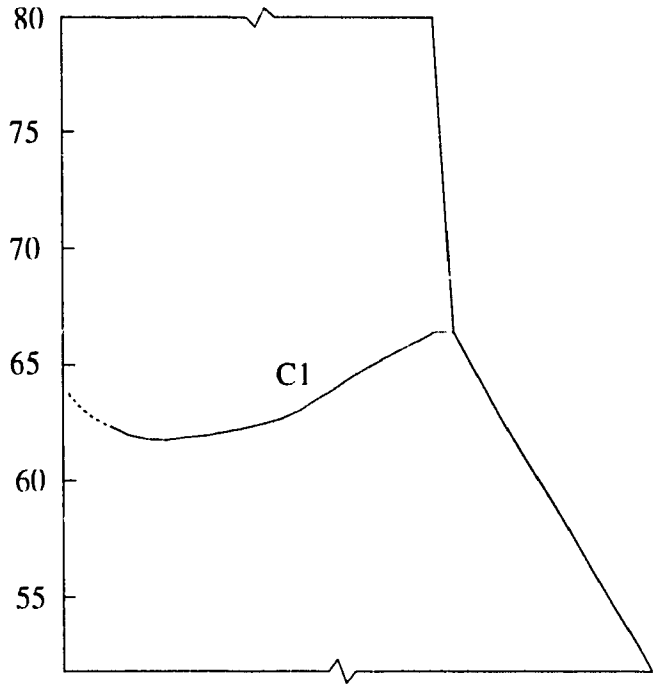

(a)

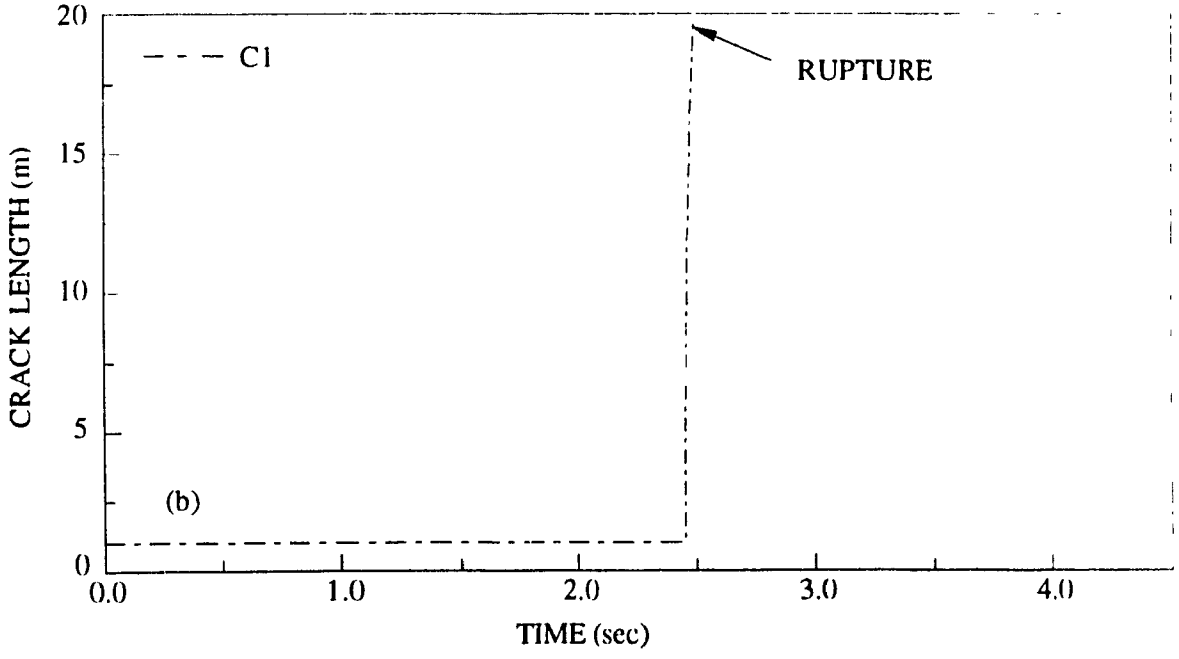

Figure 4.5 Fracture process for single downstream crack C1: (a) final cracking profile; (b) time history of crack length

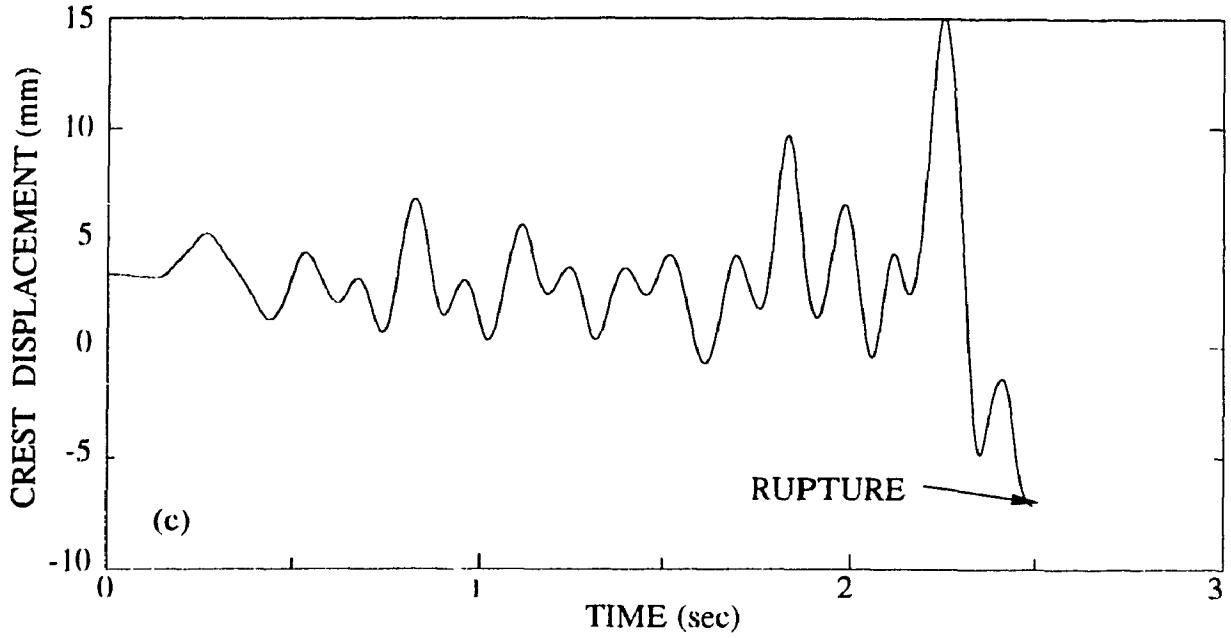

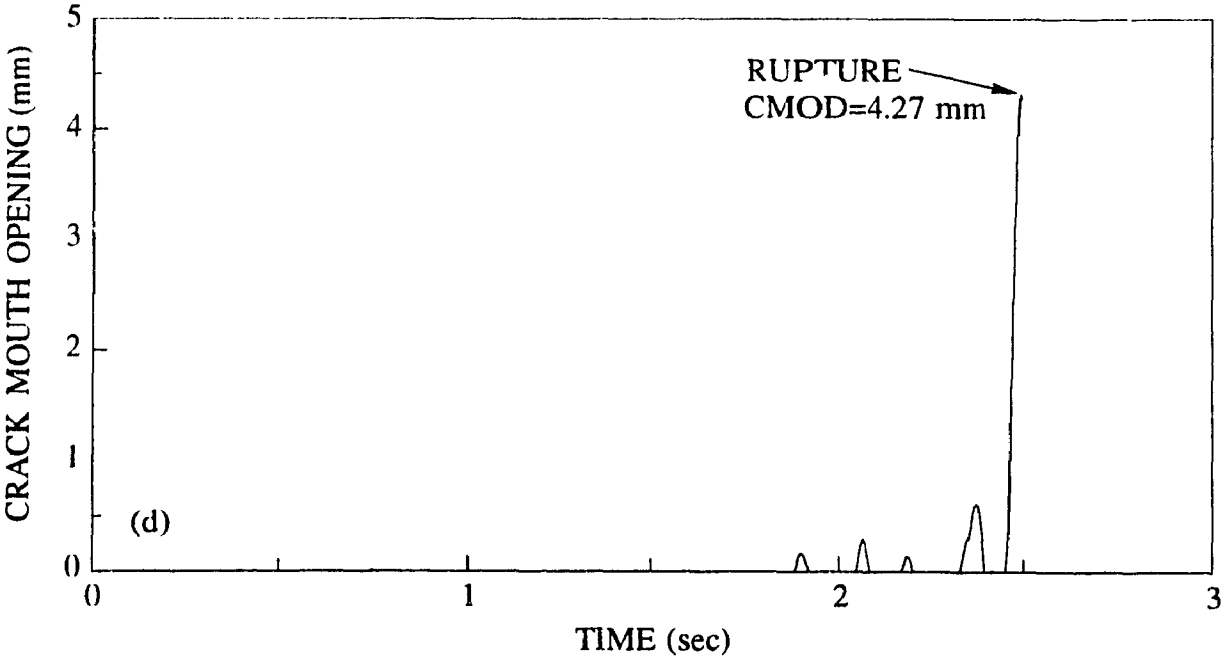

Figure 4.5 Continued: (c) time history of crest displacement; (d) time history of crack mouth opening

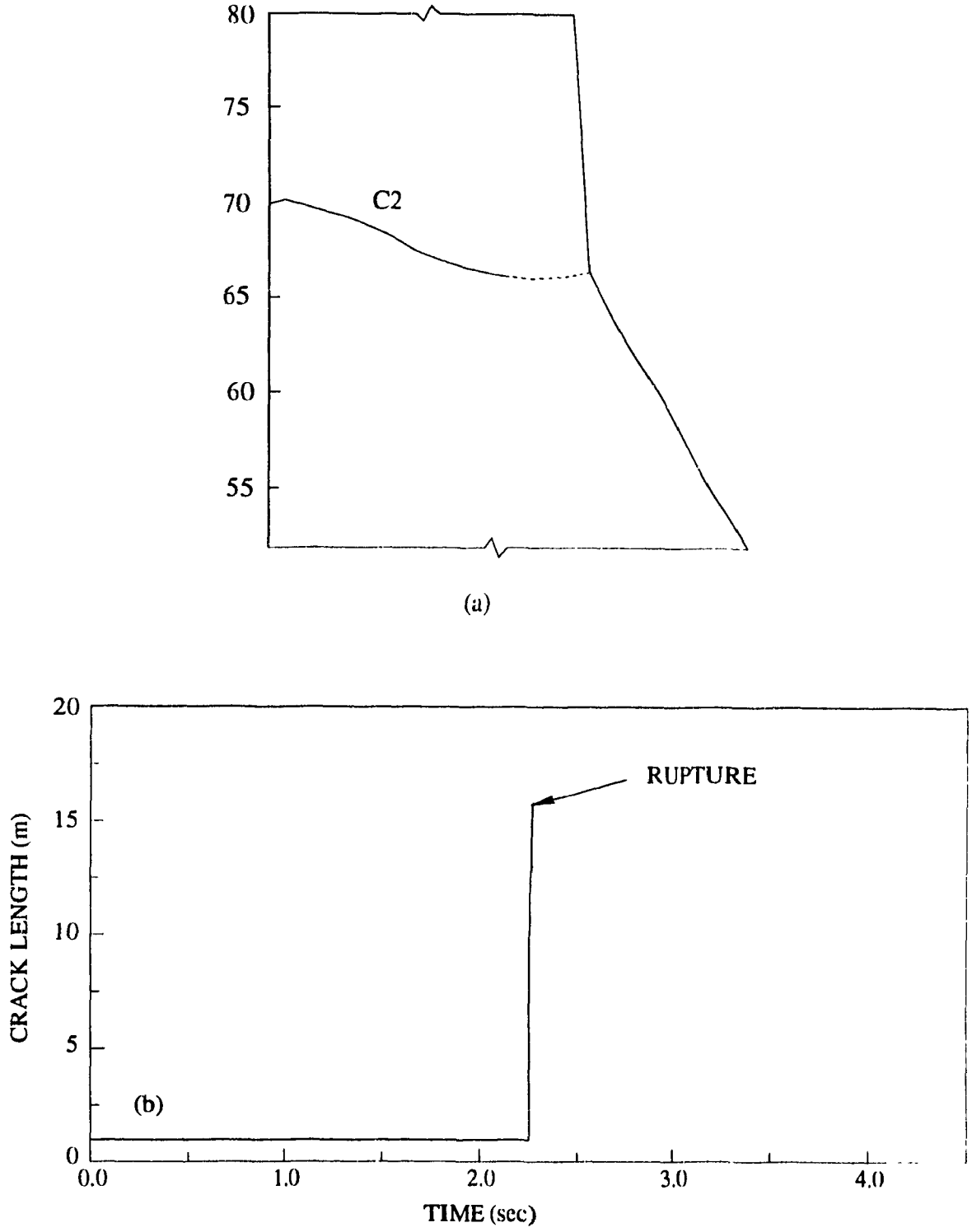

Figure 4.6 Fracture process for single upstream crack C2: (a) final cracking profile; (b) time history of crack length

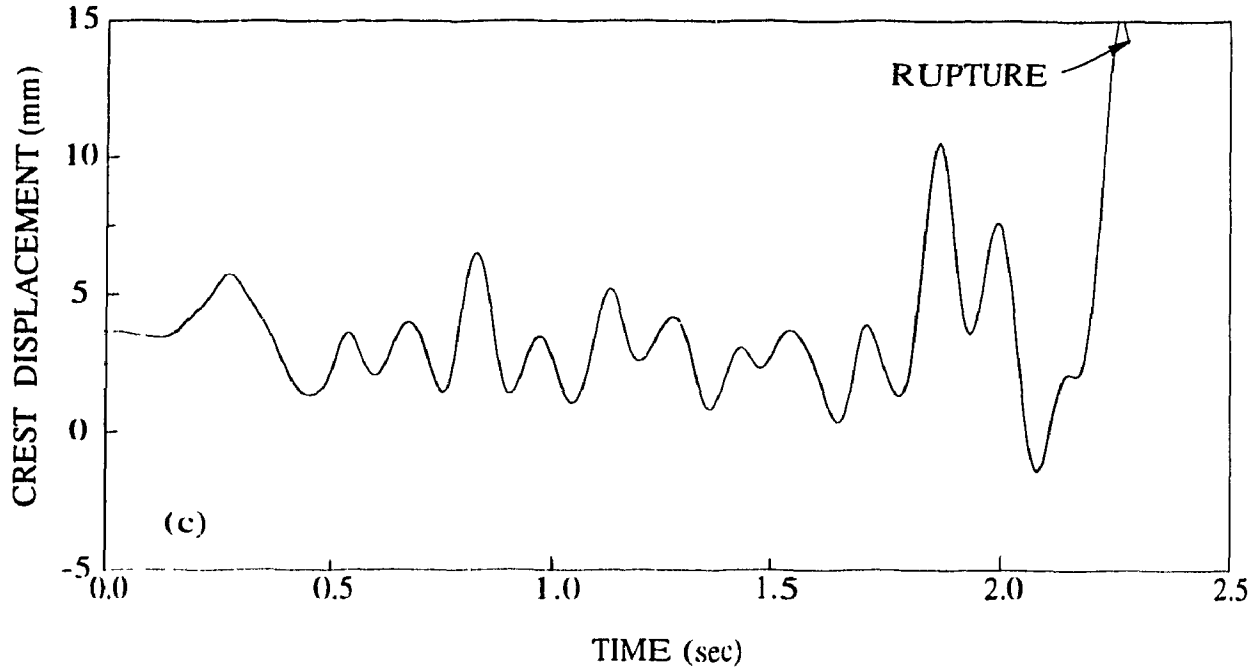

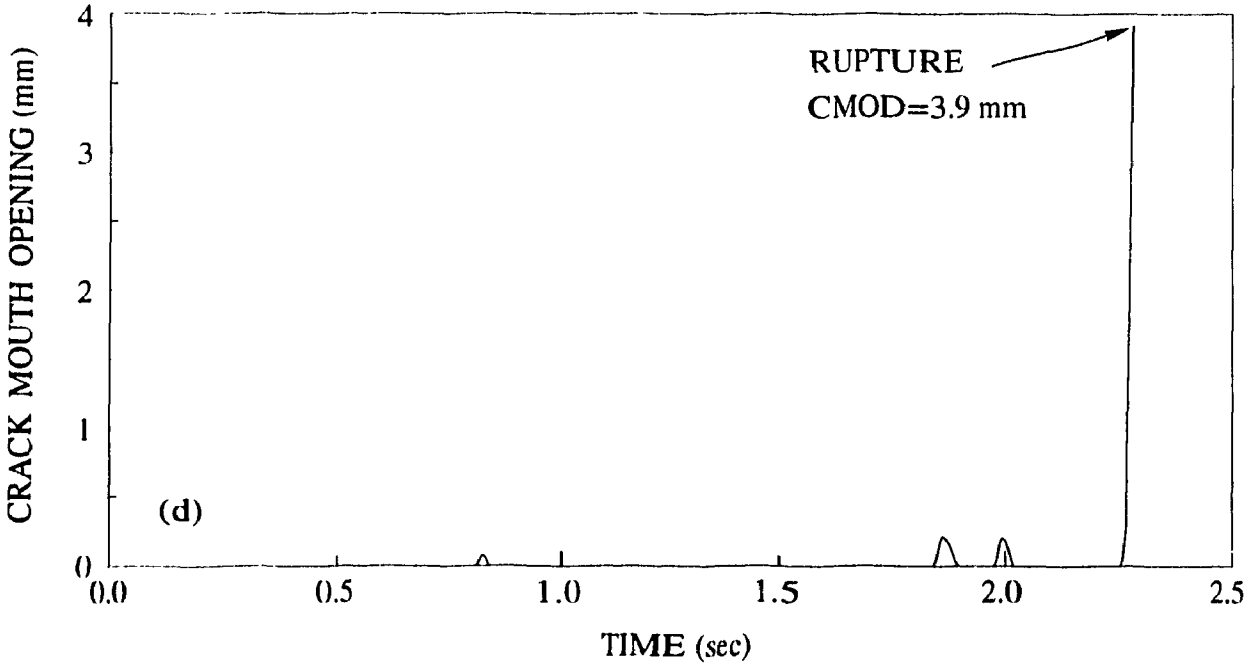

Figure 4.6 Continued: (c) time history of crest displacement; (d) time history of crack mouth opening

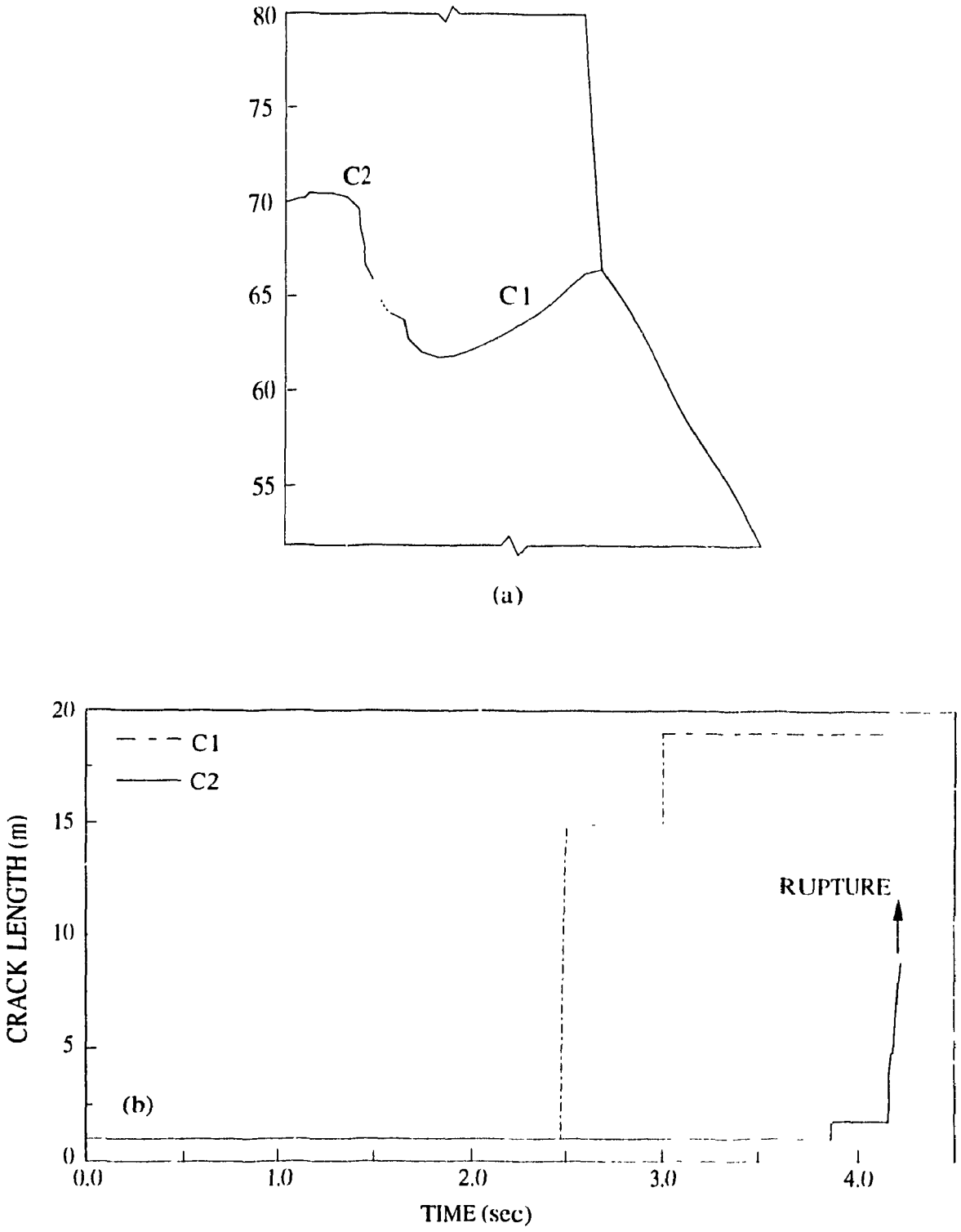

Figure 4.7 Fracture process for multiple cracking model: (a) final cracking profile; (b) time histories of crack length

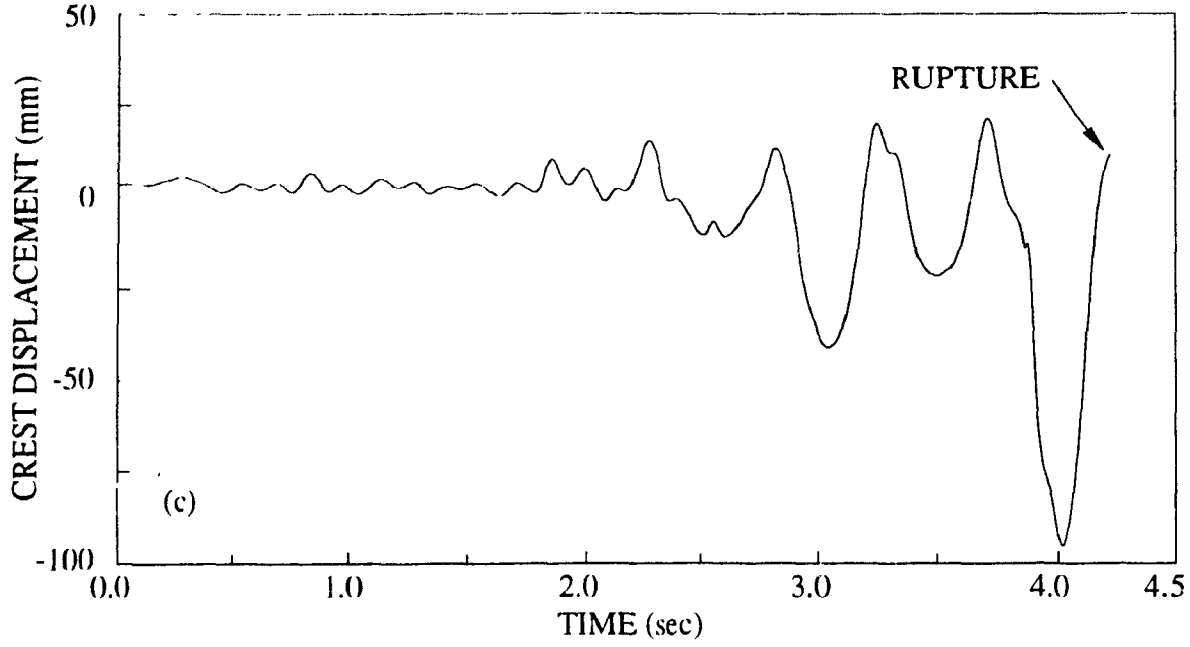

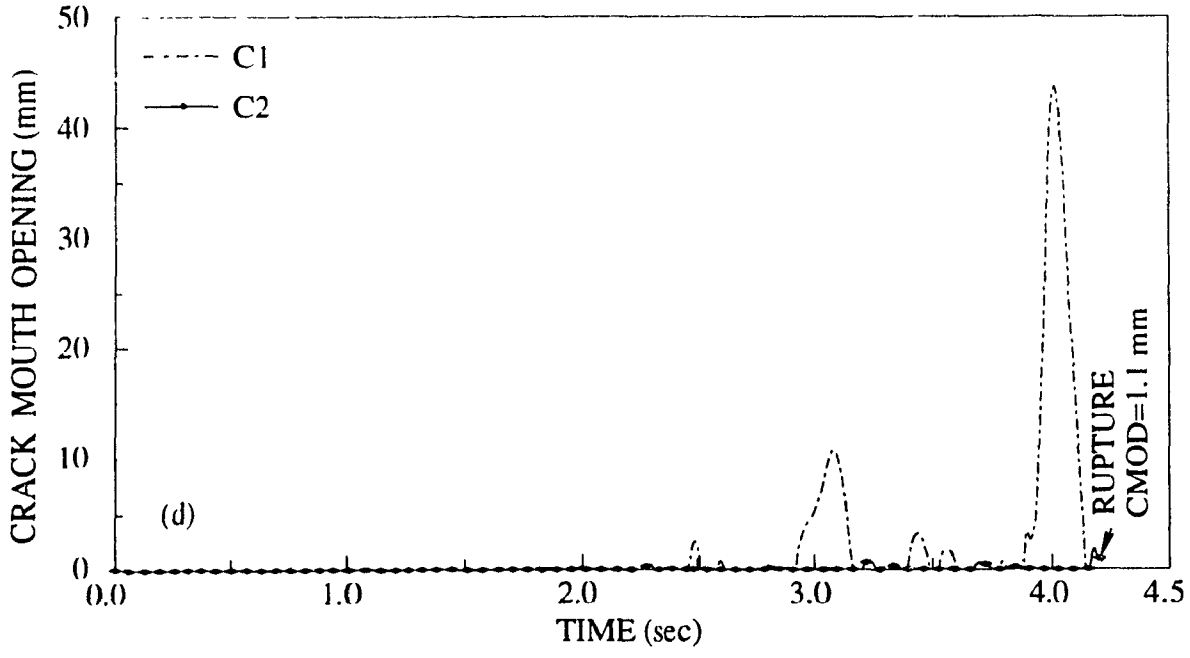

Figure 4.7 Continued: (c) time history of crest displacement; (d) time histories of crack mouth openings

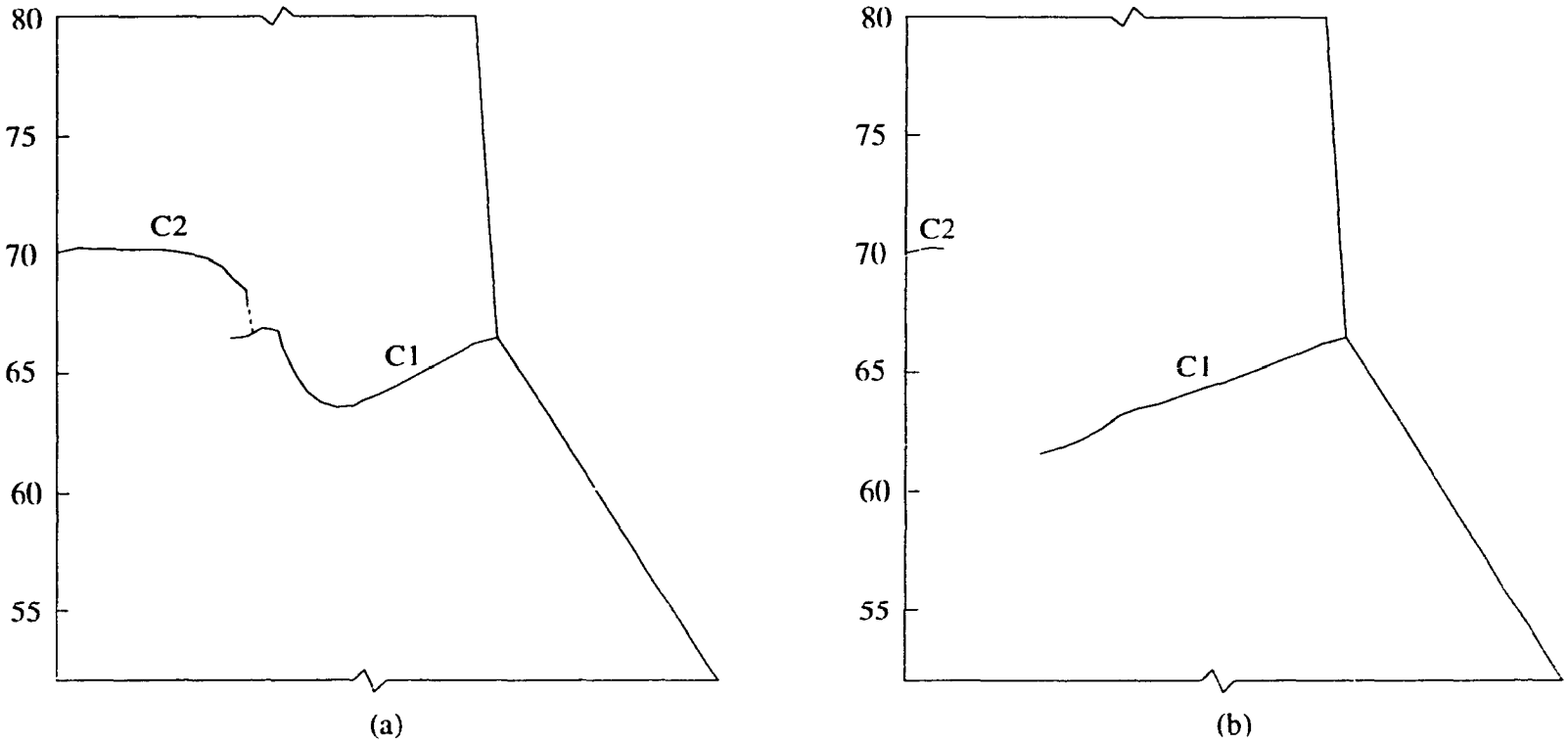

Figure 4.8 Final cracking profiles for multiple fracture model and higher magnitudes of dynamic fracture toughness : (a) K_{Id} = 5.5 MPa.m$^{1/2}$; (b) K_{Id} = 9.0 MPa.m$^{1/2}$

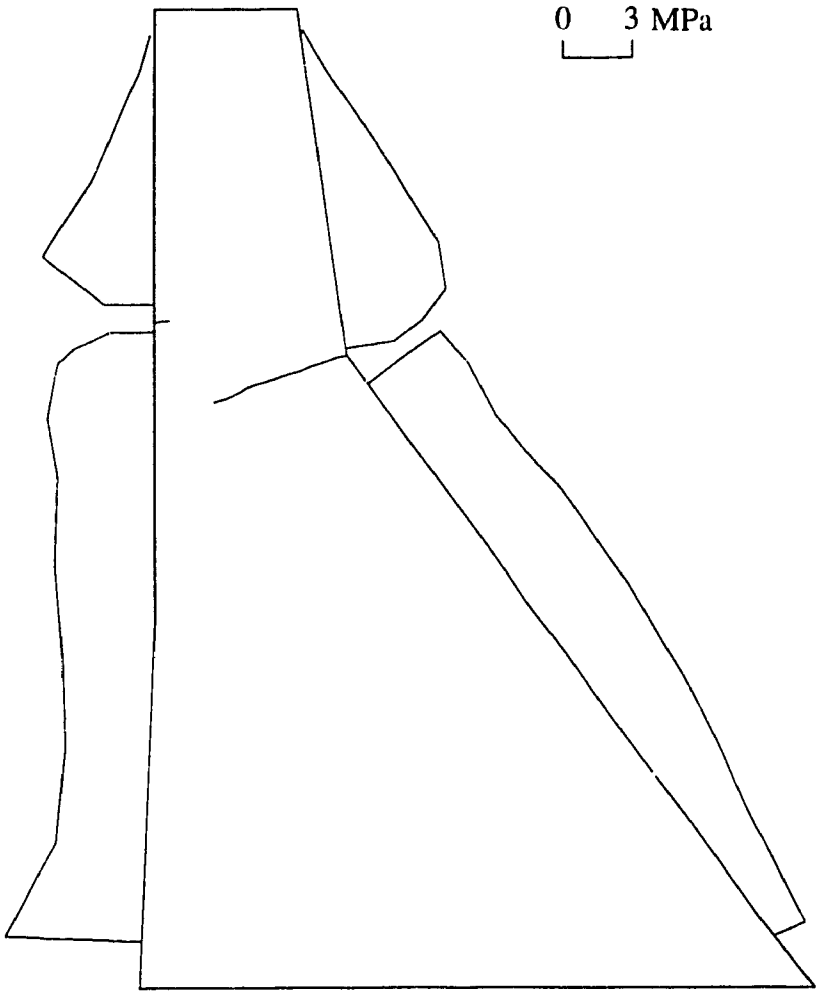

Figure 4.9 Envelope of principal tensile stresses for multiple cracking model and $K_{Id} = 9.0$ MPa.m$^{1/2}$

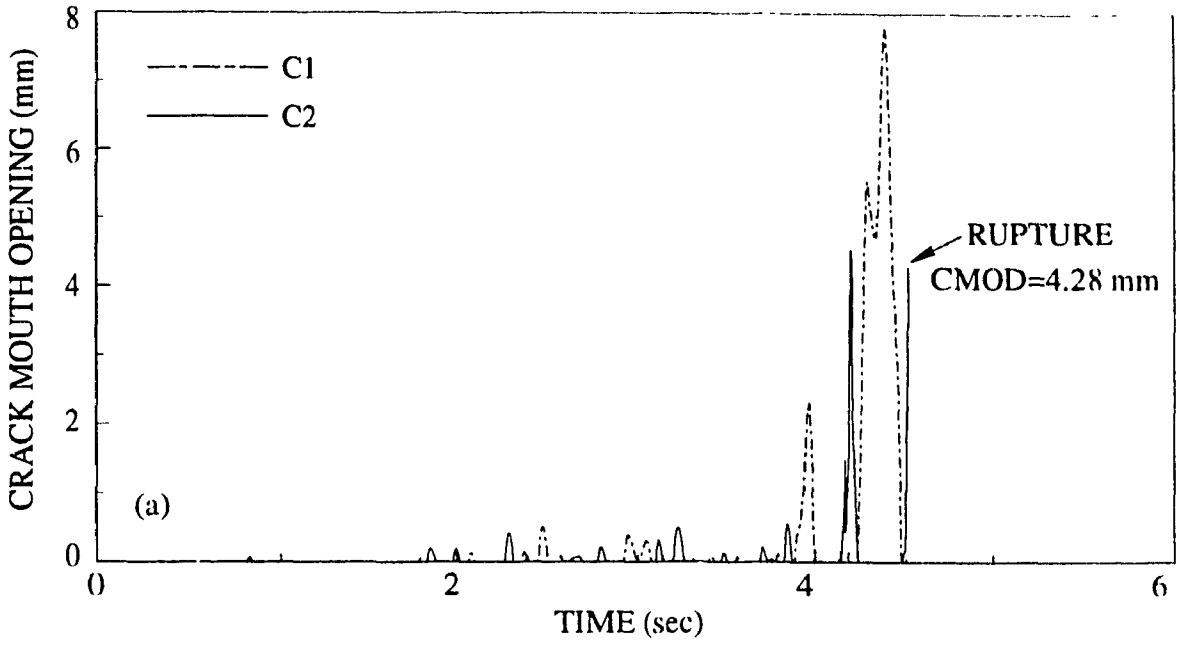

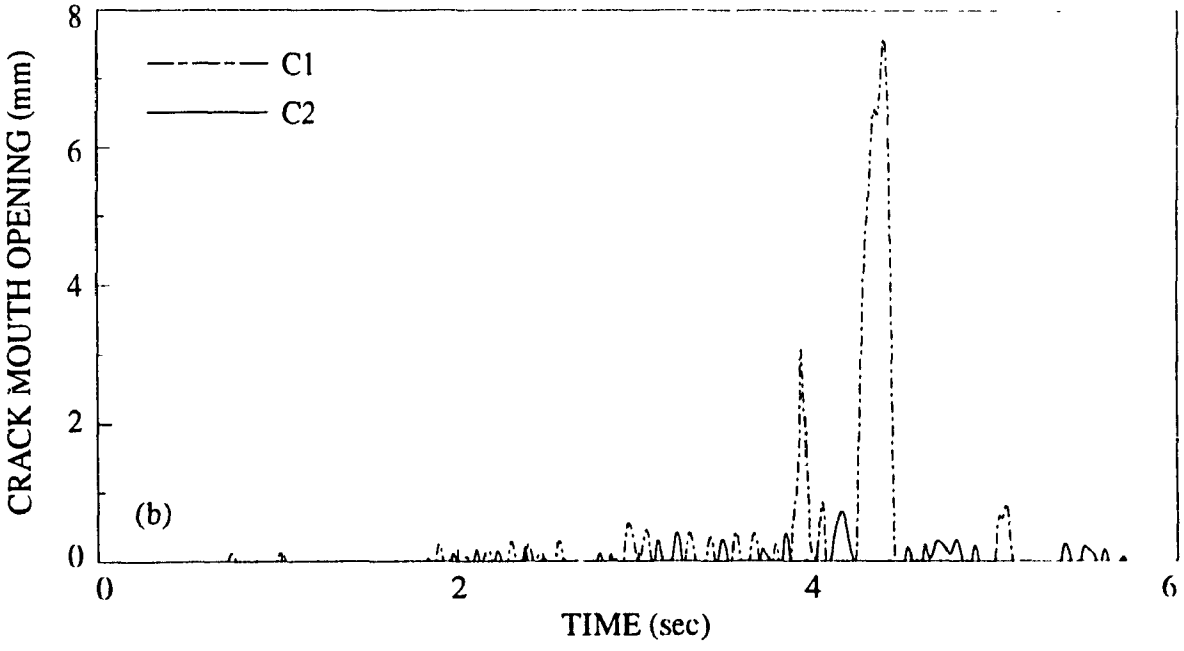

Figure 4.10 Time histories of crack mouth openings multiple cracking model: (a) K_{Id} = 5.5 MPa.m$^{1/2}$; (b) K_{Id} = 9.0 MPa.m$^{1/2}$

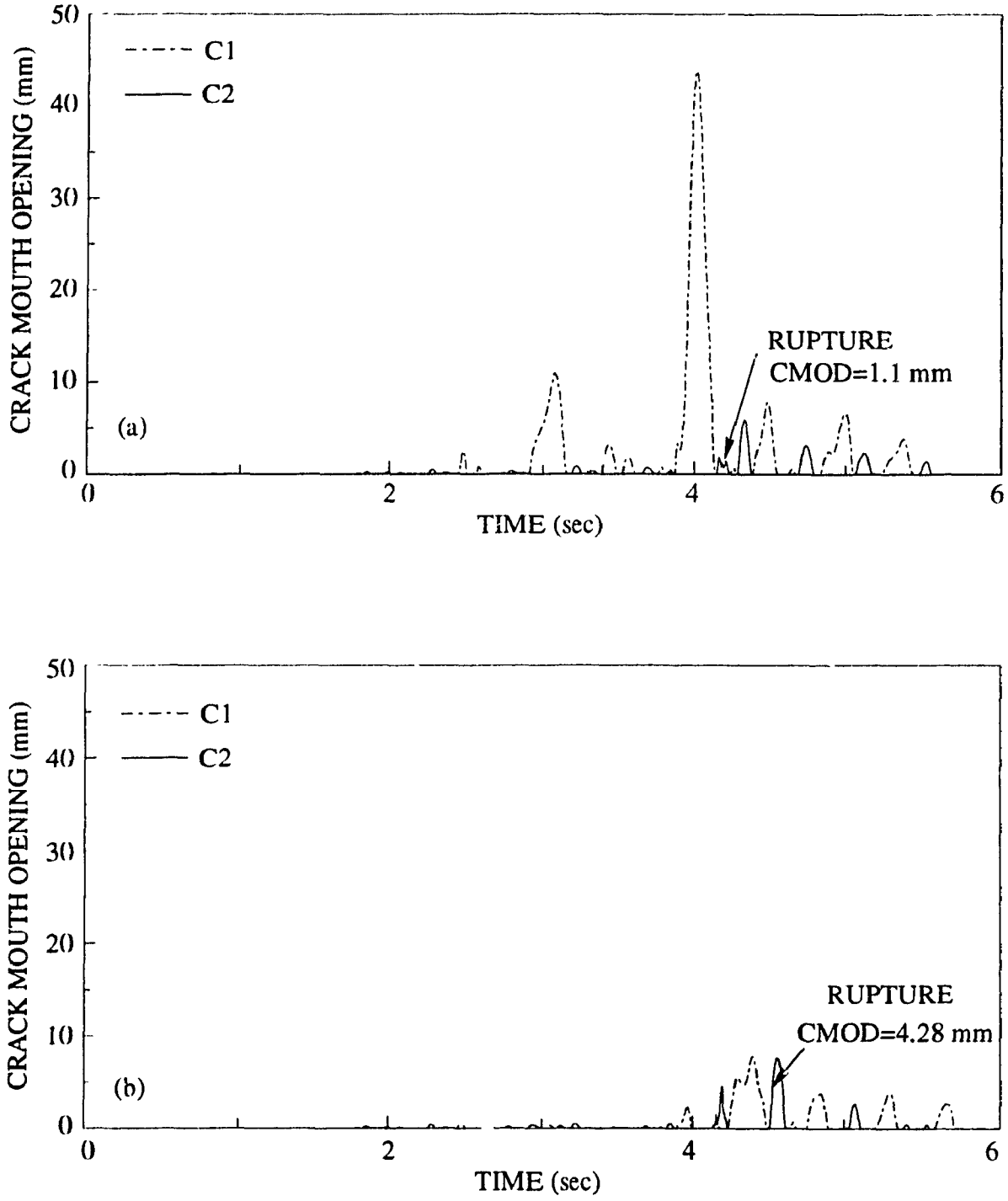

Figure 4.11 Post-rupture behaviour for multiple cracking model : (a) K_{Id} = 2.0 MPa.m$^{1/2}$; (b) K_{Id} = 5.5 MPa.m$^{1/2}$

CHAPTER V

ELASTODYNAMIC BOUNDARY INTEGRAL FORMULATION FOR FUTURE DAM-FOUNDATION INTERACTION ANALYSIS

5.1 INTRODUCTION

In earthquake response analysis of concrete gravity dams, it has been demonstrated (Vaish and Chopra 1974; Abdalla 1984) that the interaction of the dam with its foundation is an important consideration which should be included in a rational analysis. Not only does the flexibility of the foundation material bear on the natural periods of the dam, it also influences the magnitude of the dynamic loading induced by an earthquake. Furthermore, the semi-infinite extent of the foundation half-space also provides significant additional damping by radiating energy away from the structure.

In fracture analysis of dams, the foundation interaction effects have been neglected generally in the past because of the additional computational requirements and because, until recently, the emphasis had been on the proper modelling of the concrete cracking itself. The available formulations for analyzing dam-foundation interaction therefore feature a linear-elastic dam together with a linear-elastic or visco-elastic foundation medium. As a result, most of the analytical procedures have been developed in the frequency domain, which facilitates considerably the representation of the semi-infinite characteristics of the foundation rock/soil. Both finite element (Vaish and Chopra 1974; Chopra and Gupta 1982; Hall 1986) and boundary element techniques (Abdalla 1984; Medina et al. 1990; Chandrashaker and Humar 1994) have been used for modelling of the foundation medium, while the dam itself has generally been represented as an assemblage of finite elements.

The frequency domain modelling of the foundation cannot, however, be employed in analysis of dams where concrete cracking, and consequent non-linear behavior, are to

be included. In such cases, a time-domain formulation is required in order to obtain the foundation stiffness/flexibility coefficients in a time-varying manner to be used directly in crack propagation analysis under earthquakes.

To the author's knowledge, the seismic fracture analysis of concrete gravity dams by El-Aidi and Hall (1989a; 1989b) constitutes the only study where the rock foundation of the dam was included, albeit approximately, in the formulation. A rigid massless plate was assumed attached to the base of the dam and available frequency independent stiffness and damping functions for a rigid plate attached to the surface of three-dimensional half-space were utilized. The procedure restricts the foundation degrees-of-freedom to the three rigid body motions and, consequently, cannot account for the flexibility of the dam base.

In the following, a boundary integral formulation for two-dimensional elastodynamic response of the foundation medium of a dam is presented in the time-domain. The developed procedure can thus be employed directly to include foundation interaction effects in the fracture analysis of gravity dams subjected to earthquake excitation. The boundary element representation of the half-space is validated by obtaining its response to applied surface stresses and comparing the results with those available in the literature. Since the basic problem in dam-foundation interaction analysis is the determination of the dynamic contact stresses between the dam base and the underlying rock or soil, the procedure is also applied to obtain the dynamic response of two-dimensional footings and the results are compared with the available analytical solutions. In order to simplify the boundary conditions, rigid footings are considered at present but the formulation is equally applicable to flexible footings, as offered at the base of a concrete gravity dam. Both surface and embedded rigid strip footings are considered and good correlation with available results is demonstrated in each case. Future implementation of this time-domain formulation in modelling the foundation interaction effects in seismic crack propagation analysis of concrete gravity dams is discussed also.

5.2 MODELLING OF THE FOUNDATION MEDIUM

5.2.1 Literature review

In formulating a procedure for analyzing dynamic interaction between a dam and its foundation medium, proper representation of the underlying semi-infinite rock or soil poses a significant analytical challenge. Various techniques have been used in the past for accurate and efficient modelling of the dynamic characteristics of this half-space. Use of inhomogeneous Fredholm equations by Karasudhi et al. (1968) and Green's function by Luco and Westmann (1972) constitute the early attempts to obtain a closed form solution for dynamic contact stresses between an elastic half-space and a rigid footing. In recent years numerical techniques comprising lumped parameters, finite differences, finite elements, and boundary elements have often been used to represent the semi-infinite foundation medium in soil-structure interaction problems.

Of the above methods, the finite difference technique with its inability to handle complicated boundary conditions and the lumped parameter model requiring prior knowledge of exact impedance functions found only limited application. On the other hand, the finite element technique, which was until recently considered the most versatile, has been widely used for soil-structure interaction analysis. In spite of its ability to easily handle complex foundation geometries, embedment and material nonhomogeneities, it is realized that the method cannot properly model a soil medium with infinite boundaries. Various corrective measures have been proposed (Lysmer and Khulemyer 1969; Waas 1972; Liang 1974) which partially improved upon the approximation (Mansur 1984). Subsequently, however, the method was effectively employed by Vaish and Chopra (1974) for linear elastic structure-foundation interaction problems by utilizing the concept of sub-structuring. The flexibility of the foundation medium, which constitutes one of the sub-structures, was obtained in a frequency domain formulation and the mode-superposition technique was used to obtain the earthquake response of the dam-foundation system.

Although this procedure has the merits of simplicity and economy its frequency domain formulation precludes extension to non-linear problems such as the present dam fracture analysis. Moreover, the procedure still requires a sufficient length of the foundation to be included in order to account for the energy lost due to radiation; also the need for a relatively fine finite element mesh to model the higher frequencies results in a fairly large system. A subsequent formulation by Dasgupta and Chopra (1979) for the dynamic stiffness of the visco-elastic half-plane avoided these modelling limitations, but the foundation stiffness was still derived in the frequency domain.

In modelling the dynamic characteristics of the semi-infinite foundation medium, the present boundary element method offers many advantages over the finite element technique. Reduction of problem size and accurate representation of radiation damping are inherent characteristics of the method which have been exploited to obtain the dynamic stiffness of two- and three-dimensional surface and embedded foundations. Alarcon and Dominquez (1980) were the first to apply the boundary element method to the analysis of rigid strip footings, but the formulation was developed in the frequency domain. Other frequency domain boundary formulations are those by Abdalla (1984) and Damisah (1981) in two dimensions and by Ottenstreuer and Schmid (1981) in three dimensions.

Application of the method in the time-domain has been presented by Veletsos and Verbic (1974) who analyzed a circular foundation employing a convolution approach and by Karabalis (1984), who examined three-dimensional foundations of arbitrary shapes and also developed a better solution procedure based on impulse response. For two-dimensional elastodynamics, the available time-domain formulations are however neither efficient nor applicable to general problems. For example, the two-dimensional wave-propagation formulation by Mansur (1984) relies on the use of half-plane fundamental solution and thus introduces singularities at every time step. On the other hand, the studies conducted by Wolf and Darbre (1984a; 1984b) employ the indirect boundary element method which requires the development of appropriate Green's functions and thus lack

generality.

5.2.2 Present approach

The present Chapter derives a two-dimensional boundary element procedure for modelling a linear elastic foundation half-space in time-domain in order to combine the advantages of the direct boundary element method with those of a time-domain solution. The approach, apart from being straightforward, provides the response in a more natural way. It also constitutes a firm basis for extension to non-linear problems and can thus be implemented easily to represent foundation interaction in the fracture response analysis of dams. The analytical formulation, together with the numerical implementation, is described in the following section.

5.3 ELASTODYNAMIC BOUNDARY INTEGRAL FORMULATION

Considering a homogenous, isotropic and linear elastic soil medium occupying a region Ω in space with boundary Γ, the governing equations of motion are

$$(c_1^2 - c_2^2)\, u_{k,jk} + c_2^2 u_{j,kk} + f_j = \ddot{u}_j \tag{5.1}$$

where $u_j = u_j(x,t)$ is the displacement vector associated with each point $x \in \Omega + \Gamma$; f_j is the body force vector at a point in Ω; c_1 and c_2 are propagation velocities of compression and shear waves in the unbounded domain expressed, respectively, as

$$c_1^2 = \frac{\lambda + 2\mu}{\rho}, \quad and \quad c_2^2 = \frac{\mu}{\rho}$$

where λ and μ are Lame's constants and ρ is the mass density of the medium contained in the domain. Standard tensor notation is employed in equation (5.1), where a repeated subscript implies summation, a comma denotes spatial differentiation, and temporal differentiation is indicated by an overhead dot.

In order to formulate an integral identity corresponding to equation (5.1), the boundary element technique relies on the existence of a fundamental solution for the governing equations and employes Betti-Rayleigh reciprocal theorem to transform these equations to an integral form. The dynamic boundary element analysis procedure based on the dual reciprocity approach discussed in Chapter II utilizes the static (frequency-independent) fundamental solution of the governing problem to perform this transformation. One of the main advantages of this procedure is that, unlike other dynamic boundary formulations, the mass matrix of the system is derived corresponding to the boundary degrees-of-freedom and integration over the domain is not required. The procedure can be applied to any elastodynamic problem, including those involving infinite domains, although it should be noted that the employed fundamental solution satisfies only the regularity conditions of elastostatics (i.e. the solution correctly vanishes at points sufficiently distant from the source) and not the elastodynamic radiation conditions. The latter are required to ensure that the waves reflected from the base of the structure are transmitted away into the infinite foundation medium, to simulate the geometric damping in a soil-structure interaction problem. As a result, significant approximations will be introduced if the procedure is directly employed for modelling the dynamic behavior of foundation media. Indeed, for low frequency excitations, the procedure will adequately approximate the dynamic response of the soil-medium, albeit in an asymptotic sense only. However, since ground motions induced by earthquakes involve a wide spectrum of frequencies, additional corrections will be required for higher frequencies. One of the approaches could be the doubly-asymptotic procedure (Underwood and Geers 1981), wherein an asymptotic approximation is introduced for high frequencies. Errors will, however, still remain for intermediate frequency ranges.

It is, thus, evident that an accurate formulation for the dynamic response of half-space requires a fundamental solution from elastodynamics itself. The adopted solution should inherently satisfy both regularity and radiation conditions for infinite domains, so

that the geometric damping in the soil-medium is accurately represented. The available elastodynamic solutions comprise the fundamental singular solution corresponding to a harmonic excitation in an unbounded domain and the Stoke's fundamental solution, which corresponds to a concentrated body force. The former has been utilized, among others, by Cruse and Rizzo (1968), Manolis and Beskos (1981), and Abdalla (1984), and leads to a frequency domain formulation. In the present time-domain formulation, therefore, Stoke's fundamental solution for an infinite domain is employed instead.

Thus, for prescribed initial displacements and velocities $\underline{u}(\underline{x}, 0) = u_o(\underline{x})$; $\dot{\underline{u}}(\underline{x}, 0) = v_o(x)$ in Ω and surface tractions $t(\underline{x}, t)_{(n)i} = t_{ij}(\underline{x}, t)\, n_j$ on Γ the three-dimensional displacement solution of equation (5.1) is obtained in the form of Love's integral identity stated as (Eringen and Suhubi 1975)

$$\begin{aligned} \underline{\varepsilon}(\underline{\xi})\, u_k(\underline{\xi}, t) = & \int_{\Gamma} \{ \bar{u}_{ik}[x, t;\underline{\xi}|\, t_{(\underline{n})\,i}(x, t)] - \bar{t}_{(\underline{n})\,ik}[x, t;\underline{\xi}|\, u(x, t)] \}\, d\Gamma \\ & + \rho \int_{\Omega} \bar{u}_{ik}[x, t;\xi|f_i(\underline{x}, t)]\, d\Omega \\ & + \rho \int_{\Omega} [\, v_{oi}(x)\, U_{ik}(\underline{x}, t;\underline{\xi}) + u_{oi}(\underline{x})\, \dot{U}_{ik}(\underline{x}, t;\underline{\xi}))\,]\, d\Omega \end{aligned} \qquad (5.2)$$

where,

$$\underline{\varepsilon}(\underline{\xi}) = \begin{cases} 1 & \text{if } \underline{\xi} \in \Omega \\ \frac{1}{2} & \text{if } \underline{\xi} \in \Gamma \\ 0 & \text{if } \underline{\xi} \notin \Omega \cup \Gamma \end{cases} ;$$

u_i and $t(\underline{n})_i$ are the displacements and tractions on the boundary , u_{oi} and v_{oi} are the initial displacements and velocities in Ω ; $(\underline{n})$ represents the unit outward normal vector on the boundary and $\bar{u}_{ik}$, $\bar{t}_{(\underline{n})\,ik}$ and U_{ik} are the fundamental singular solutions with i, k equal to 1, 2, 3. $\bar{u}_{ik}$ expresses the displacement component in the i-direction at the point $\underline{x}$ due to a concentrated force of magnitude f(t) acting at point $\underline{\xi}$ in the k-direction and has the form (Eringen and Suhubi 1975)

$$\bar{u}_{ik}(x, t;\underline{\xi}|f) = \frac{1}{4\pi\rho}\left\{\left(\frac{3r_i r_k}{r^3} - \frac{\delta_{ik}}{r}\right)\int_{c_2}^{c_1}\frac{1}{c^3}f(t-\frac{r}{c})\,dc\right.$$

$$\left. + \frac{r_i r_k}{r^3}\left[\frac{1}{c_1^2}f(t-\frac{r}{c_1}) - \frac{1}{c_2^2}f(t-\frac{r}{c_2})\right] + \frac{\delta_{ik}}{rc_2^2}f\ (t-\frac{r}{c_2})\ \right\} \tag{5.3}$$

where r is the distance between points $\underline{x}$ and $\underline{\xi}$ i.e. $r_i = x_i - \xi_i$ and $r^2 = (x_i - \xi_i)(x_i - \xi_i)$ and δ_{ij} is Kronecker delta. It is implicitly assumed in equation (5.3) that $f(t - \lambda)$ is a time-retarded function defined as non-zero if $t - \lambda > 0$ and zero otherwise. $\bar{t}(\underline{n})_{ik}$ represents the corresponding stress tensor and can be obtained from the constitutive equation (Eringen and Suhubi 1975)

$$\bar{t}_{(\underline{n})\,ik} = \bar{t}_{ijk}n_j = \rho\{(c_1^2 - 2c_2^2)u_{km,m}\delta_{ij} + c_2^2(\bar{u}_{ki,j} + \bar{u}_{kj,i})\} \tag{5.4}$$

Additionally, U_{ik} is defined as

$$U_{ik}(\underline{x}, t;\underline{\xi}) = \bar{u}_{ik}[\underline{x}, t;\underline{\xi}|\,\delta(t)] \tag{5.5}$$

where $\delta(t)$ is the Dirac delta function.

For the foundation problem considered herein, the body force and the initial condition terms vanish, thus the volume integrals in equation (5.2) disappear and equation (5.2) reduces to the following boundary equation

$$\underline{\varepsilon}(\underline{\xi})u_k(\underline{\xi}, t) = \int_\Gamma \{\bar{u}_{ik}[\underline{x}, t;\underline{\xi}|\,t_{\underline{n}(i)}(\underline{x}, t)] - \bar{t}_{(\underline{n})\,ik}[\underline{x}, t;\underline{\xi}|\,u_i(\underline{x}, t)]\}\,d\Gamma \tag{5.6}$$

For a two-dimensional problem, such as the soil-structure interaction analysis for a gravity dam or vibrations of a strip footing, this equation decouples into two equations representing the in-plane and out-of-plane motions. Assuming the x_3-axis of the Cartesian coordinate system to coincide with the length of the strip footing and the half-space to occupy the region $x_2 \geq 0$ as shown in Figure 5.1, the governing boundary integral equation

becomes

$$\frac{1}{2}u_\beta(\xi,t) = \int_\Gamma \{\bar{u}_{\alpha\beta}[x,t;\underline{\xi}|\,t_{(n)\alpha}(x,t)] - \bar{t}_{(n)\alpha\beta}[x,t;\underline{\xi}|\,u_\alpha(x,t)]\}\,d\Gamma \qquad (5.7)$$

where α and β assume values 1 and 2 only.

It is to be observed that boundary Γ is the surface of the half-space, i.e. x_1-x_3 plane, for the present foundation problem. Since, for the two-dimensional problems considered herein, the tractions and displacements are independent of x_3, the corresponding integration can be transformed to an integration with respect to time (Niwa et al. 1980), thereby reducing the spatial integration to integration with respect to x_1 only. This reduction together with the numerical treatment of equation (5.7) is given below.

5.3 NUMERICAL TREATMENT

A numerical treatment of boundary integral equation (5.7) requires discretization of boundary tractions and displacements in both space and time. The time axis is divided into small intervals Δt and the boundary values are assumed constant over each interval. Since the spatial integration is to be reduced to the x_1-axis, the surface of the half-space is discretized into a number of line boundary elements, each of length δl and lying along the x_1-axis. To change the x_3-integration to a time integration, it should be observed that the time retarded nature of the fundamental solutions appearing in equation (5.7) ensures the displacements $u_\alpha(\xi,t)$ to be affected only by the boundary displacement and by the traction at point x at time t - r/c, where c is the wave velocity. Thus, at any time the boundary integration in equation (5.7) reduces to integration over a finite region on the surface of the half-space. However, the limits of this spatial integration are to be carefully decided.

For a receiver element R_e at time $t = N\Delta t$, the effective elements, called the source elements S_e, are those which satisfy the condition $x\text{-}x_R \leq cN\Delta t$, where x represents the x_1-coordinate of any point in the source element and x_R is the corresponding value for the centre of the receiver. In other words, the x_1-integration is obtained at any time as the sum

of integration over boundary elements satisfying the above conditions. The corresponding integration over x_3, in view of the previous discussion, is then obtained as the sum of integration over N subregions with integration limits from $\sqrt{[c(k-1)\Delta t]^2 - [x-x_R]^2}$ to $\sqrt{[ck\Delta t]^2 - [x-x_R]^2}$ for k=1,2....N.

Thus, the first term on the right hand side of equation (5.7) is written as

$$\int_{\Gamma} \{ \bar{u}_{\alpha\beta}[\underline{x}, t;\underline{\xi}|\, t_{(\underline{n})\alpha}(\underline{x}, t)] \}\, d\Gamma = \int_{x_1 x_3} \{ \bar{u}_{\alpha\beta}[\underline{x}, t;\underline{\xi}|\, t_{(\underline{n})\alpha}(\underline{x}, t)] \}\, dx_1 dx_3 \qquad (5.8)$$

Substituting the expression for $u_{\alpha\beta}$ from equation (5.3) and expressing integration over x_1 and x_3 in discretized form one obtains:

$$\int_{x_1 x_3} \{ \bar{u}_{\alpha\beta}[\underline{x}, t;\underline{\xi}|\, t_{(\underline{n})\alpha}(\underline{x}, t)] \}\, dx_1 dx_3 = \sum_{s=1}^{M} \sum_{k=1}^{N} \bar{u}_{\alpha\beta}\left[x, k; t_{\alpha}^{(N-k+1),x}\right]$$

$$= \frac{2}{4\pi\rho} \sum_{s=1}^{M} \sum_{k=1}^{N} \{ \int_{\Delta l} \int_{c_1}^{c_2} \frac{1}{c^3} \int_{Z_{k-1,c}}^{Z_{k,c}} \left(\frac{3 r_\alpha r_\beta}{r^3} - \frac{\delta_{\alpha\beta}}{r} \right) dZ dc dx_1$$

$$+ \int_{\Delta l} \frac{1}{c_2^2} \int_{Z_{k-1,c_2}}^{Z_{k,c_2}} \left(\frac{\delta_{\alpha\beta}}{r} - \frac{r_\alpha r_\beta}{r^3} \right) dZ dx_1 + \int_{\Delta l} \frac{1}{c_1^2} \int_{Z_{k-1,c_1}}^{Z_{k,c_1}} \frac{r_\alpha r_\beta}{r^3} dZ dx_1 \}\, t_{\alpha}^{(N-k+1),x} \qquad (5.9)$$

where $Z_{k,c} = \sqrt{(ck\Delta t)^2 - (x-x_R)^2}$; $t_{\alpha}^{(N-k+1),s}$ denotes the α-direction traction at time step N-k+1 acting over element s; and M represents the total number of boundary elements. The factor 2 in above equation comes from the fact that spherical waves contained in the three-dimensional fundamental solution propagate on both sides of the x_1-x_2 plane; stated otherwise, the x_3-dimension in the fundamental solution extends to infinity on both sides of the x_1 -x_2 plane. The traction tensor obtained from equation (5.4) can be discretized in the same way and equation (5.7) can be written at time step N and for boundary element R_e, as a system of linear algebraic equations

$$\frac{1}{2}\{u^{N,R_c}\} = \sum_{s=1}^{M}\sum_{n=1}^{N}\left[\,[G^{n,s}]\,\{t^{(N-n+1),s}\} - [T^{n,s}]\,\{u^{(N-n+1),s}\}\right. \\ \left. + [H^{n,s}]\,\{\dot{u}^{(N-n+1),s}\}\,\right] \tag{5.10}$$

where $\{u^{N,R_c}\}$ represents the displacement vector of receiver element R_c (=1, 2....M) at time step N. For the present two-dimensional problem, matrices [G], [T] and [H] in equation (5.10) are of dimension 2 x 2. The elements $G^{n,s}_{\alpha\beta}$ of the matrix [G] are given by equation (5.9). The elements for [T] and [H] can be written as

$$T^{n,s}_{\alpha\beta} = n_\gamma \frac{1}{2\pi}\{-6\cdot c_2^2\cdot \int_{\Delta l}\int_{c_2}^{c_1}\int_{Z_{k-1,c}}^{Z_{k,c}}\{\frac{5r_\alpha r_\beta r_\gamma}{r^5} - \frac{1}{r^3}(\delta_{\alpha\gamma}r_\beta + \delta_{\alpha\beta}r_\gamma + \delta_{\beta\gamma}r_\alpha)\}\,dZdcdx_1$$

$$-\int_{\Delta l}\int_{Z_{k-1,c_1}}^{Z_{k,c_1}}\{2\left(\frac{c_2}{c_1}\right)^2\{\frac{5r_\alpha r_\beta r_\gamma}{r^5} - \frac{1}{r^3}(\delta_{\alpha\gamma}r_\beta + \delta_{\alpha\beta}r_\gamma + \delta_{\beta\gamma}r_\alpha)\} + \left(1 - 2\left(\frac{c_2}{c_1}\right)^2\frac{\delta_{\alpha\gamma}}{r^3}r_\beta\right)\}\,dZdx_1$$

$$+\int_{\Delta l}\int_{Z_{k-1,c_2}}^{Z_{k,c_2}}\{\frac{1}{r^2}\left(\frac{12r_\alpha r_\beta r_\gamma}{r^3} - (2\delta_{\alpha\gamma}\frac{r_\beta}{r} + \delta_{\alpha\beta}\frac{r_\gamma}{r} + \delta_{\beta\gamma}\frac{r_\alpha}{r})\right)\}\,dZdx_1\} \tag{5.11}$$

and

$$H^{n,s}_{\alpha\beta} = n_\gamma\frac{1}{2\pi}\{(-\frac{1}{c_1})\int_{\Delta l}\int_{Z_{k-1,c_1}}^{Z_{k,c_1}}\{2\left(\frac{c_2}{c_1}\right)^2\frac{r_\alpha r_\beta r_\gamma}{r^4} + \left(1 - 2\left(\frac{c_2}{c_1}\right)^2\frac{\delta_{\alpha\gamma}}{r^2}r_\beta\right)\}\,dZdx_1$$

$$+\frac{1}{c_2}\int_{\Delta l}\int_{Z_{k-1,c_2}}^{Z_{k,c_2}}\{\frac{2r_\alpha r_\beta r_\gamma}{r^4} - (\delta_{\alpha\beta}r_\gamma + \delta_{\beta\gamma}r_\alpha)\}\,dZdx_1\} \tag{5.12}$$

Equation (5.10) can now be solved for unknown values of boundary displacements or tractions. In the above expressions for kernels G, H and T, it should be noted that $r = \sqrt{x_1^2 + Z^2}$ for two-dimensional surface footings. In expressions for $G^{n,s}_{\alpha\beta}$, $T^{n,s}_{\alpha\beta}$ and $H^{n,s}_{\alpha\beta}$ the various integrals are to be carefully evaluated. In order to reduce computational

errors inherent in the numerical integration, the integral should be evaluated analytically wherever possible. Carefully observing equations (5.10), (5.11) and (5.12) it can be seen that the integration over Z can be performed analytically. Carrying out this integration, the expression for the kernels, say $G_{22}^{n,s}$, can be expressed in the form

$$G_{22}^{k,s} = \frac{1}{2\pi\rho}\left(\int_{\Delta l}\int_{c_2}^{c_1}\frac{1}{c^3}\left\{-ln\left(\left(Z_{k,c}+\sqrt{x_1^2+Z_{k,c}^2}\right)/\left(Z_{k-1,c}+\sqrt{x_1^2+Z_{k-1,c}^2}\right)\right)\right\}dcdx_1\right.$$
$$\left.+\int_{\Delta l}\frac{1}{c_2^2}\left\{ln\left(\left(Z_{k,c_1}+\sqrt{x_1^2+Z_{k,c_1}^2}\right)/\left(Z_{k-1,c_1}+\sqrt{x_1^2+Z_{k-1,c_1}^2}\right)\right)\right\}dx_1\right)$$

The other kernels can be similarly evaluated and the remaining integrals can be obtained numerically. It is useful to observe that since the integrands are oscillatory, particularly severe at higher frequencies, a larger number of integration points is required over an element than is needed commonly in elastostatics, where the integrands vary less rapidly. However, for small element lengths oscillations can be accommodated adequately with relatively few integration points. For the purpose of the present application problems, the integrals were evaluated using a highly efficient adaptive quadrature where the requisite number of integration points is based on the behavior of the integrand over a particular interval. When receiver element R_e coincides with source element S_e, the singularity of kernels G, T and H needs to be treated carefully. For this purpose, it should be observed that this singularity occurs only at the first time step and can be treated by evaluating the integrals in their principal value sense. No significant error is thus introduced because the principal value of the logarithmic integrand is negligible.

The occurrence of this singularity at the first time-step is a distinct advantage in deducing the two-dimensional formulation from the three-dimensional fundamental solutions. If the two-dimensional fundamental solution were employed instead (Mansur 1984) the resulting kernels become singular at each time step.

5.4 APPLICATIONS

Equation (5.10) represents a generalized form of boundary integral equation for a two-dimensional elastodynamic system and can be used directly for the analysis of a soil-structure system. However, in the present study the application of the formulation is limited to simple examples for which numerical or analytical results are available in the literature; the purpose here being to verify the accuracy of the formulation and computer implementation, as well as, to demonstrate its usefulness and efficiency for application to general two-dimensional foundation interaction problems.

5.4.1 Response of a half-plane to external dynamic stresses

The boundary of the half-plane is discretized into a number of boundary elements and the given stress distribution is then discretized in both space and time to give the vector $t^{(N-k+1),s}$ at all time steps. The only unknowns are the displacements u and velocity $\dot{u}$. Velocity $\dot{u}$ can be expressed as displacement by using a backward difference in time; thus

$$\{\dot{u}^{(N-n+1),s}\} \equiv \frac{1}{2\Delta t}\left[3\{u^{(N-n+1),s}\} - 4\{u^{(N-n),s}\} + \{u^{(N-n-1),s}\}\right] \quad (5.13)$$

The unknown displacements can then be obtained at each time step by solving equation (5.10).

5.4.2 Surface rigid strip foundation

Consider a rigid massless foundation of rectangular cross-section and infinite length along the x_3-axis to be resting on the surface of an elastic half- space. Dynamic stiffness K_{ij} or compliance C_{ij} of this foundation can be obtained by applying a dynamic rigid body displacement under the footing and using equation (5.10) to calculate the resulting dynamic contact stresses. Since the infinite space fundamental solutions are

used, both the contact length and the free surface of the boundary need to be discretized. However, since the influence of free field elements on the foundation response decreases with distance (Alarcon and Dominguez 1980), only a relatively small length beyond the soil-foundation interface needs to be discretized. Both relaxed and welded contact conditions can be considered.

(i) Welded contact: The footing is considered bonded to the soil and therefore coupling exists between the horizontal and rocking motions. Thus for welded contact, compatibility between displacements of the soil and displacement of the footing itself requires

$$u_2(x_1(i)) = \Delta V + \phi x_1(i) \tag{5.14}$$

$$u_1(x_1(i)) = \Delta H \tag{5.15}$$

where i refers to a point under the footing; ΔV denotes the amplitude of vertical displacement at the centre of the footing; ϕ represents the amplitude of rocking; and ΔH is the amplitude of the horizontal displacement of the footing.

(ii) Relaxed contact: In the case of relaxed contact, the following condition are prescribed at the contact surface in order to simplify the complete mixed boundary value problem. For vertical and rocking vibrations a frictionless contact is assumed between the footing and the soil and, for horizontal vibration the normal force developed under the footing is assumed to be zero. This results in effective decoupling of the modes of vibration and for vertical and rocking motions one can write

$$P_1(x_1(i)) = 0 \tag{5.16}$$

$$u_2(x_1(i)) = \Delta v + \phi x_1(i) \tag{5.17}$$

while for horizontal motion

$$P_2(x_1(i)) = 0 \tag{5.18}$$

$$u_1(x_1(i)) = \Delta H \tag{5.19}$$

where $P_1(x_1(i))$ and $P_2(x_1(i))$ are the amplitude of horizontal and vertical forces at point i.

Thus the welded response of the footing can be obtained by solving equation (5.10) with boundary conditions given by equation (5.14) and (5.15). The corresponding relaxed response of the footing can be obtained by using equation(5.16) - (5.19) together with equation (5.10).

5.4.3 Embedded rigid strip foundation

Boundary integral equation (5.10) is modified to consider the effect of embedment of a rigid strip footing with little extra effort because of its inherent generality. The required modification is easily achieved if it is realized that the distance r is now given by $r = \sqrt{(x_1 - x_R)^2 + (x_2 - x_R)^2 + Z^2}$. The determination of the embedded response follows the same general steps as for the surface foundation with the only difference that matrices [G], [H] and [T] are now less sparse.

5.5 NUMERICAL RESULTS

In order to demonstrate the usefulness, accuracy and applicability of the methodology numerical examples are now presented. The accuracy of the technique is evaluated by comparing the results obtained by the present analysis with available analytical and numerical results. In the following examples each boundary element in the discretization is further divided into subelements (Karabalis 1984). Thus, the spatial integrations are performed over each subelement and their contributions are added to obtain the influence of the element. In this manner, a higher degree of computational accuracy is achieved without sacrificing the computer storage.

(i) Half-space under discontinuous prescribed stress distribution

In this example, the problem of a half-space subjected to a strip stress distribution

of width 2b applied as a step pulse is considered as shown in Figure 5.2(a). This transient electrodynamic problem was solved by Cruse (1968) in the transformed domain using the Laplace transform. Various distinct values of the Laplace parameter were obtained by the boundary element method and numerical inversion was employed to find the time-domain solutions. Mansur (1984) solved the same problem using the two-dimensional fundamental solutions. Unfortunately, the latter are inefficient to integrate numerically and also require the evaluation of the singularities at every time step. By comparison, the present study employs a two dimensional formulation derived from the three-dimensional fundamental solution, and thus represents a more accurate and efficient solution since the singularities are encountered only once in the time marching scheme when receiver element coincides with source element at the first time step. Employing the same numerical values for the constants and identical discretization, the response of the half-space is obtained by the present method. Figure 5.2(b) shows the time history of vertical displacement at stations 0, 2b and 4b from the load center line. Close agreement with results obtained by Mansur (1984) is evident.

(ii) Half-space under continuous prescribed stress distribution

This example presents the problem of a half-space which is initially at rest but is disturbed by a vertical pressure distribution continuous in both space and time. The results obtained from the present analysis are compared against the solution given by Ahmad and Banerjee (1988). The problem specification is shown in Figure 5.3. Ahmad and Banerjee (1988) solved this problem using a transient dynamic formulation in a transformed domain. The numerical solution consisted of a series of solutions for a steady-state dynamic problem with a number of discrete values of the transformed parameter. The final solution was obtained by numerically inverting the transformed domain solutions to the time-domain. The material properties of the half-space are: modulus of elasticity E = 138.7 MPa; Poisson's ratio ν = 0.15; and mass density ρ = 2100 kg/m^3. Time history of

vertical displacement at point A, plotted in Figure 5.3(b), is clearly in very good agreement with the results of Ahmad and Banerjee(1988).

(iii) Surface rigid strip footing under harmonic vibrations

The present formulation is now applied to determine the response of a surface rigid strip footing under harmonic vibrations. In the analytical results presented herein, the following properties of the soil medium are used: modulus of elasticity E = 96.5 MPa, Poisson's ratio $\nu = 0.25$; and mass density of soil $\rho = 2160$ kg/m^3. The footing is 1.52 m wide and boundary discretization under the footing as well as of the free field, is as shown in Figure 5.4(a). The results are presented in terms of the dynamic stiffness K_{ij} or compliance C_{ij} (the inverse of stiffness), where

$$K_{ij} = P_i/\pi G V_j \tag{5.20}$$

$$C_{ij} = 1/K_{ij} \tag{5.21}$$

plotted against the frequency factor a_0 defined as

$$a_o = \omega b/c_2 \tag{5.22}$$

where ω = forcing frequency; P_i = summation of forces in the i-direction under the footing and G = modulus of rigidity of the soil; and V_j = component of footing displacement in the j-direction. It should be noted that equation (5.21) is applicable only for the relaxed contact condition. For welded contact, where the horizontal and rocking degrees-of-freedom are coupled, the compliance functions are obtained by inverting the 3x3 stiffness matrix with coefficients given by equation (5.20).

Figure 5.4(b) shows the effect of the R/b ratio on the footing vertical stiffness for relaxed contact, where R represents the distance on either side of the footing where the boundary element discretization is terminated and b denotes the half width of the footing. The results for R/b=0, 3 are almost identical, thus confirming the adequacy of contact surface boundary discretization. Figure 5.5(a) shows the dynamic vertical stiffness of the

footing for relaxed contact compared with the analytical results of Karasudhi et al (1968). Excellent agreement between the two sets of results is observed. For the welded contact condition the vertical compliance has been computed to compare directly with the work of Luco and Westmann (1972). These results presented in Figure 5.5(b), show equally good agreement. A comparison of the vertical stiffness for relaxed and welded contact conditions, shown in Figure 5.5(c), confirms that the difference due to the two assumptions is negligible (Luco and Westmann 1972). Figure 5.6 shows the corresponding results for the horizontal vibrations of the footing and Figures 5.7 for the rocking mode of vibration. Comparison of these results with the analytical results given by Karasudhi et al (1968) and Luco and Westmann (1972) shows good agreement. The coupled horizontal rocking compliance for welded contact of the footing is presented in Figure 5.8 and also shows good correlation with the results of Luco and Westmann (1972).

(iv) Embedded rigid strip footing under harmonic vibrations

Figure 5.9(a) shows a rigid strip footing of width 2b embedded to a depth e in the surface of the half-space. The boundary element discretization employed to obtain the dynamic stiffness of the footing is also depicted in this figure. The width of the footing and properties of the half-space are the same as those used previously for the surface footing. Only relaxed contact conditions are considered herein and all the three vibration modes (i.e. vertical, horizontal and rocking modes) are analyzed. To verify the present time-domain formulation for the analysis of embedded footings, comparisons are made with results from the frequency domain analysis reported by Alarcon and Dominguez (1980). Figure 5.9(b) shows the comparison for dynamic rocking stiffness plotted against frequency factor $a_o = \omega b/c_2$, where ω is the forcing frequency. Good agreement between the two formulations is observed.

The present formulation is next applied to study the effect of embedment on the dynamic stiffnesses of the foundation in the rocking, horizontal and vertical translational

modes. For vertical vibration, Figure 5.10(a) shows that increase in stiffness with increase in embedment is insignificant. However, for horizontal and rocking modes of vibrations Figure 5.10(b) and 5.10(c) show significant increase in stiffness with embedment, particularly for the rocking mode. It is also of interest to note that the stiffness increases almost linearly with increase in the embedment ratio e/b.

5.6 FUTURE IMPLEMENTATION FOR DAM-FOUNDATION INTERACTION

Numerical examples presented in the preceding Section demonstrate the accuracy of the present time-domain boundary element formulation for modelling the dynamic behavior of a two-dimensional elastodynamic foundation medium. Although the presented applications considered only rigid strip footings, the applicability of the procedure to two-dimensional flexible footings, as representation of the behavior at the base of a concrete gravity dam, is equally straightforward. Furthermore, the force-displacement relationship at the surface of the half-space, given by equation (5.10), can be utilized to include also the interaction effects of the foundation rock in crack propagation analysis of a dam. Since, in the present fracture analysis, the dam is also modelled by boundary elements, it might appear that the two sub-systems, i.e. the dam and the foundation medium, could be analyzed as a single system. This is, however, not possible because of the different fundamental solutions employed in their modelling. As already noted, for the modelling of the dam, the static fundamental solution was employed because it avoids integration over the domain of the dam. However, as evident in equation (5.2), the latter would have been required if the time-dependent fundamental solution (Stoke's solution pair) were employed instead. Similarly, as discussed in Section 5.3, the use of the static fundamental solution in the modelling of dynamic characteristics of the foundation soil sub-system is also not adequate.

In view of the above, a procedure based on sub-structuring is proposed to carry out the dam-foundation interaction analysis utilizing the present boundary element

formulations for the two sub-systems. In this approach, the dynamic stiffness or compliance of the foundation sub-structure is obtained following the methodology presented earlier in this Chapter and the other sub-structure, the cracked dam, is idealized by employing the boundary element formulation of Chapter II.

The merits of sub-structuring in performing the dam-foundation interaction analysis have been demonstrated by Vaish and Chopra (1974) and Chandrashaker and Humar (1994). The frequency-domain formulations employed in these studies, however, require significant additional effort in analyzing the interaction under the practical case of earthquake loads because a discrete Fourier transform of the ground motion data is first required. The time-domain sub-structuring proposed herein avoids this additional effort and, unlike the foregoing frequency-domain procedures, also provides the response at the early times.

In the present case, it should be noted that the interaction will not be accounted for in an exact manner because the relative stiffness of the two sub-structures changes due to the increased flexibility of the dam with increase in the extent of cracking during the seismic response. The approximation is however not likely to be significant, particularly in the range of frequencies contained in ground motions experienced at rock sites, where concrete dams are usually founded. This can be observed from the data presented by Chopra and Gupta (1982), as well as from that by Abdalla (1984), which indicate that the relative stiffness of the foundation medium *vs* that of the dam does not influence significantly the response of the dam for excitation frequencies of 10 Hz and greater.

Although implementation is beyond the scope of this study, the proposed sub-structure procedure for including foundation interaction in the fracture analysis of dams is outlined below.

5.6.1 Time-domain sub-structure analysis of dam-foundation system

The dynamic equations of motion for a dam founded on flexible rock and idealized

as a planar two-dimensional boundary element system are

$$[M]\{\ddot{u}_r\} + [C]\{\dot{u}_r\} + [K]\{u_r\} = -[M]\left[\{I^x\}^T\{a_g^x\} + \{I^y\}^T\{a_g^y\}\right] + \{R\} \tag{5.23}$$

in which [M], [C] and [K] represent, respectively, the mass, damping and stiffness matrices corresponding to the boundary element discretization of the dam and derived following the procedure presented in Chapter II; $\{u_r\}$ is the vector of nodal displacements relative to the free-field displacement at the dam-rock interface, composed of

$$\{u_r\}^T = \{u_{r1}^x \quad u_{r1}^y \quad u_{r2}^x \quad u_{r2}^y \quad \cdots \quad u_{r(n+n_b)}^x \quad u_{r(n+n_b)}^y\}^T$$

where u_m^x and u_m^y are the x- and y-components of displacement at nodal point 'm' and $n+n_b$ represents the total number of nodes in the boundary element discretization of the dam, with n_b denoting the number of nodes on the dam-rock interface. Unit vectors $\{I^x\}$ and $\{I^y\}$ are given by

$$\{I^x\}^T = \{1\ 0\ 1\ 0\ \cdots\ 1\ 0\}^T$$
$$\{I^y\}^T = \{0\ 1\ 0\ 1\ \cdots\ 0\ 1\}^T$$

Also in equation (5.23): a_g^x and a_g^y are the horizontal and vertical components, respectively, of the free-field ground acceleration assumed to be identical at all nodal points on the interface and; $\{R\}$ is the vector of forces due to dam-foundation interaction possessing non-zero elements corresponding to the interface degrees-of-freedom only.

In order to obtain a time step-by-step solution of this equation the nodal displacement, velocity and acceleration vectors are discretized in time such that they remain constant over a small time interval Δt. Using the same discretization in time for the ground acceleration and the interaction forces and partitioning the relative displacement vector $\{u_r\}$ into $\{u\}$, the vector of displacements of nodal points not on the interface, and $\{u_b\}$, the interaction displacement vector at the dam-rock interface, equation (5.23) at time

t=NΔt is expressed as

$$\begin{bmatrix} M_{dd} & M_{db} \\ M_{bd} & M_{bb} \end{bmatrix} \begin{Bmatrix} \ddot{u}^N \\ \ddot{u}_b^N \end{Bmatrix} + \begin{bmatrix} C_{dd} & C_{db} \\ C_{bd} & C_{bb} \end{bmatrix} \begin{Bmatrix} \dot{u}^N \\ \dot{u}_b^N \end{Bmatrix} + \begin{bmatrix} K_{dd} & K_{db} \\ K_{bd} & K_{bb} \end{bmatrix} \begin{Bmatrix} u^N \\ u_b^N \end{Bmatrix} = \begin{Bmatrix} P^N \\ P_b^N \end{Bmatrix} + \begin{Bmatrix} 0 \\ R_b^N \end{Bmatrix} \quad (5.24)$$

where $\{P^N\}=\{P^N\ P_b{}^N\}^T$ represents the force vector due to applied accelerations a_g^x and a_g^y and; $\{R_b\}$ denotes the interaction forces acting on the dam at the interface.

Equation (5.24) can be solved for each time NΔt in a time marching scheme. The still unknown interaction forces R_b are obtained from the analysis of the foundation sub-structure. Treatment of these forces in equation (5.24), however, requires careful consideration as discussed below.

Since uplift at the dam base is not considered herein and full contact is assumed between the dam and the surface of the half-space, compatibility of displacements and equilibrium of forces must be ensured at all the nodes along the dam-foundation interface. Since the numerical implementation of Section 5.4 discretizes the foundation medium surface employing constant boundary elements whereas quadratic boundary elements are used for the cracked dam, the boundary nodes corresponding to the dam base are made to coincide with the nodes of the boundary element mesh used for the foundation/rock surface (Figure 5.11) by the compatibility condition

$$\{u_b^N\} = \{u_s^N\} \quad (5.25)$$

Correspondingly, equilibrium of tractions yields

$$\{t_b^N\} = -\{t_s^N\} \quad (5.26)$$

where subscript s refers to the surface of the half-space. Tractions t_b^N are related to R_b^N in equation (5.24) by the expression

$$\{R_b^N\} = [L]\{t_b^N\} \quad (5.27)$$

where [L] is a diagonal matrix whose elements l_{ii} represent the length 'l' of the constant boundary element 'i' used in the discretization of the half-space. Equation (5.27) is valid because traction on each such boundary element is also assumed to be constant.

Equations (5.25) to (5.27) relate the interaction forces and displacements between the dam and the underlying medium. These equations, in conjunction with equation (5.10), can be used obtain the interaction force vector $\{R_b\}$ required in equation (5.24). The latter can then be solved for the response of a cracked dam with the foundation interaction effects included in the analysis.

5.7 CONCLUDING REMARKS

A time domain boundary element formulation is presented in this Chapter to model the semi-infinite elastodynamic foundation medium of a concrete gravity dam. Although the mathematical manipulations and the computer coding of the procedure are left for future undertaking, this formulation can be employed to include dam-foundation interaction in the crack propagation analysis of concrete dams. The main advantage of the formulation is its generality in modelling the two-dimensional half space in an accurate and efficient manner. Given the importance of non-linear tensile cracking in seismic analysis of dams, the implementation of the formulation described in this Chapter in the fracture analysis procedure introduced in Chapter II constitutes a natural extension of the current work. This and other recommendations for future work in the area, together with the principal conclusions of the present research, are summarized in the next Chapter.

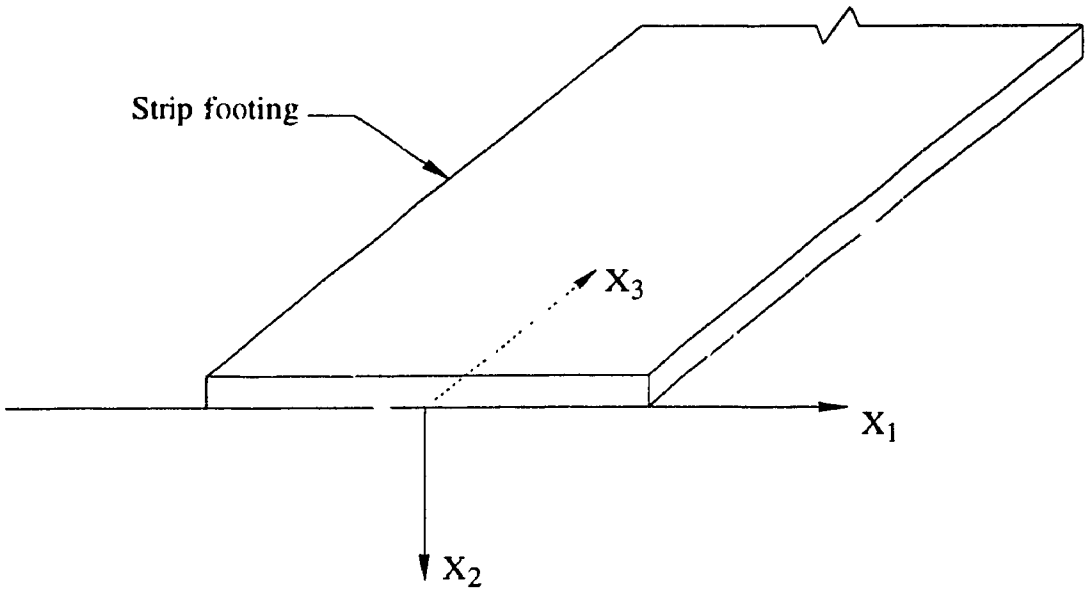

Figure 5.1 Strip footing on the surface of half-space

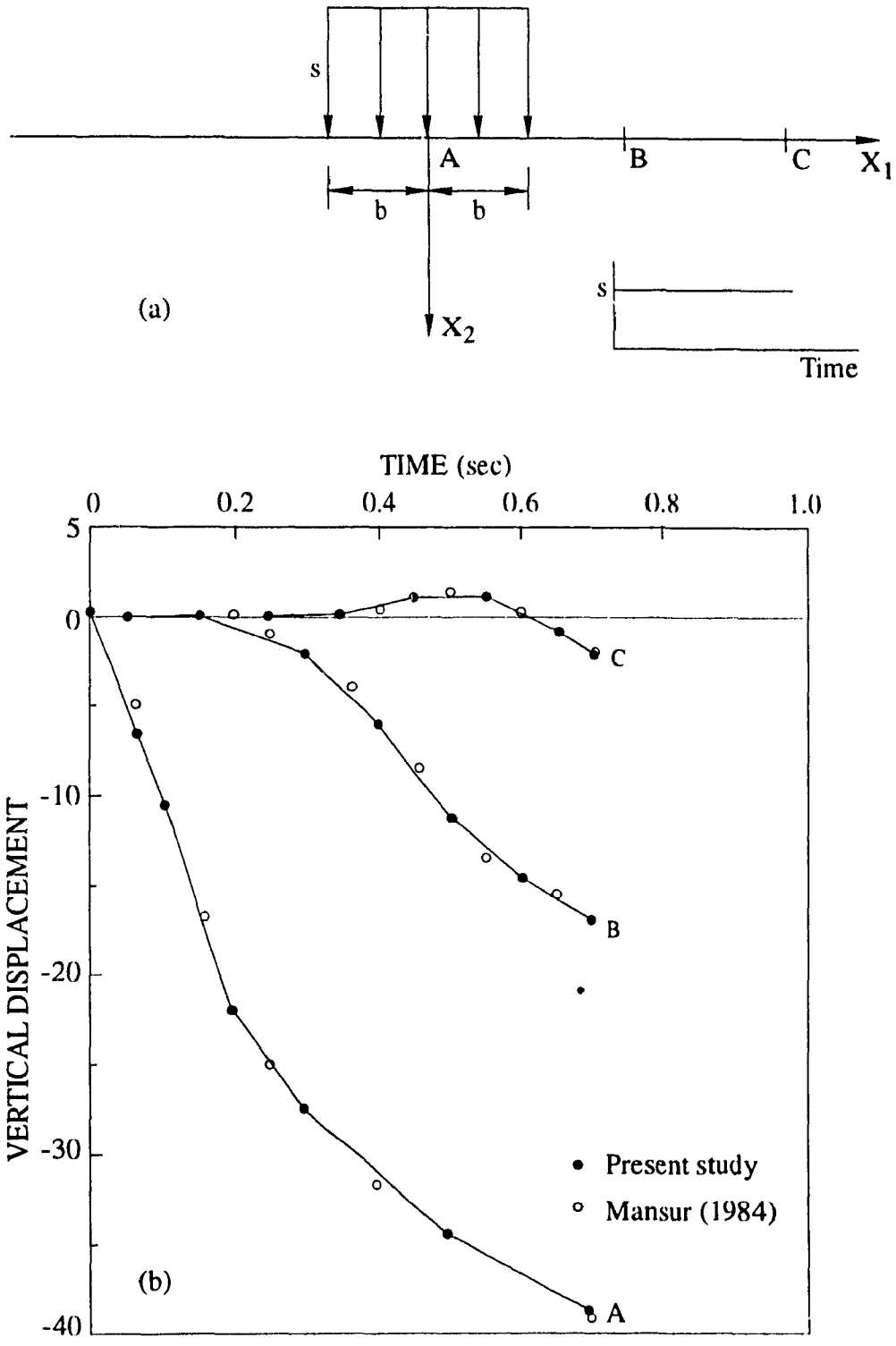

Figure 5.2 Strip stress distribution on half-space: (a) applied loading (b) time histories of vertical displacements

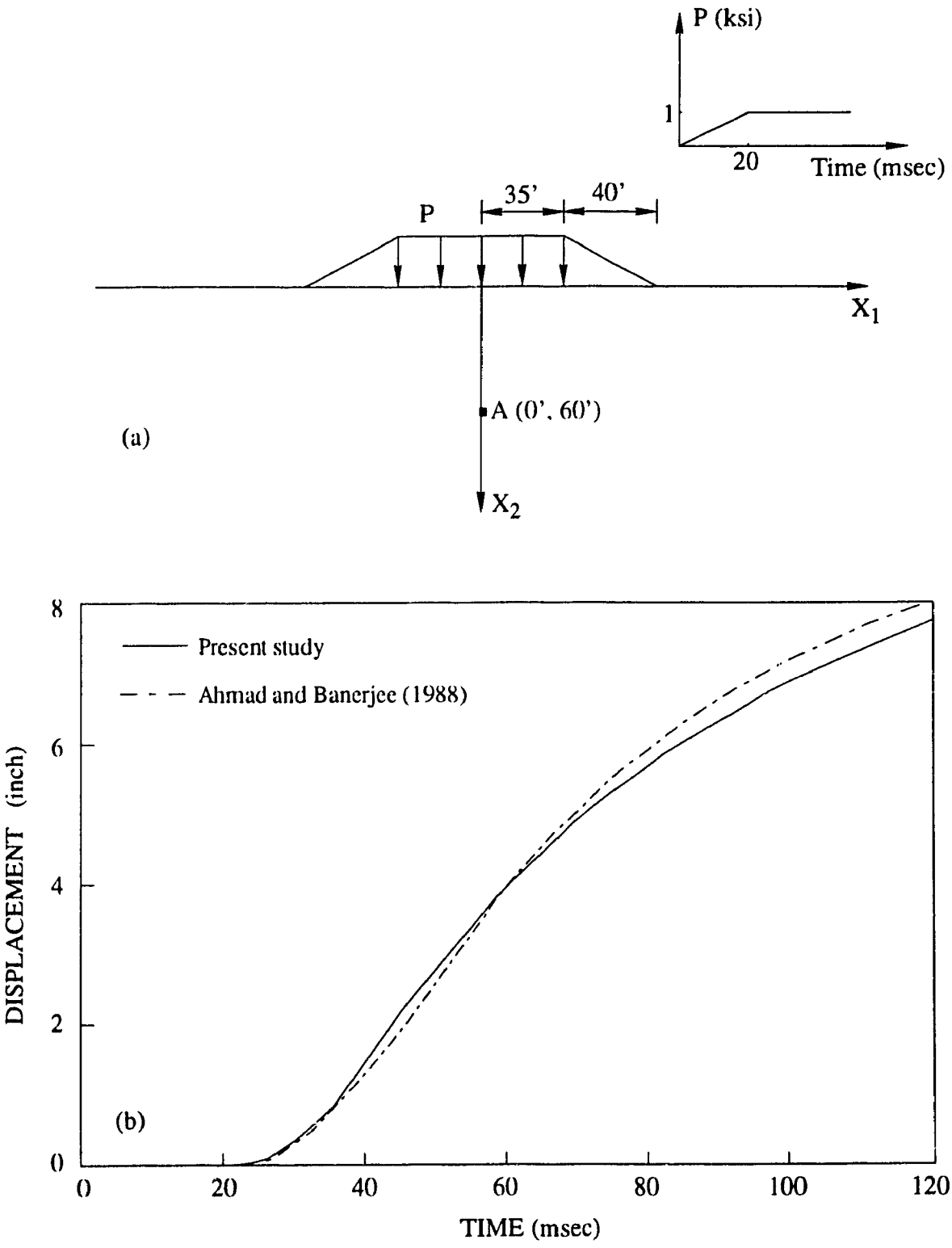

Figure 5.3 Half-space subjected to discontinuous stress: (a) loading; (b) time-history of displacement at point A

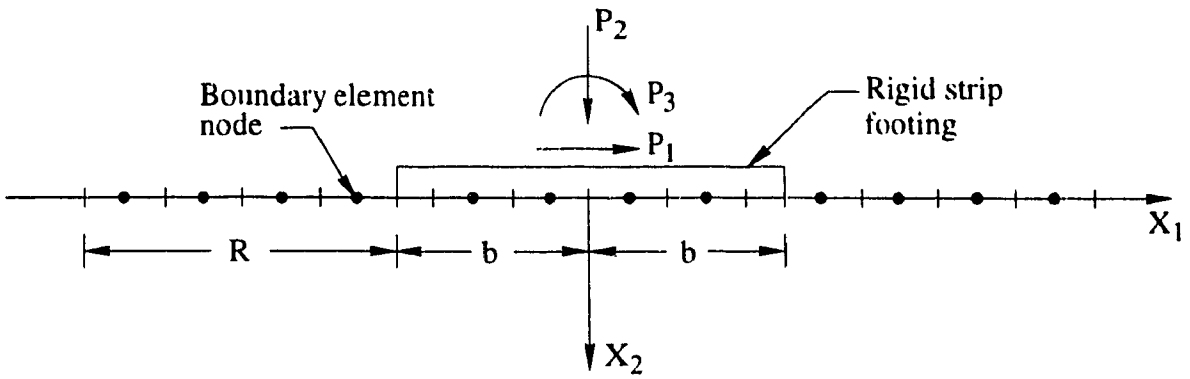

(a)

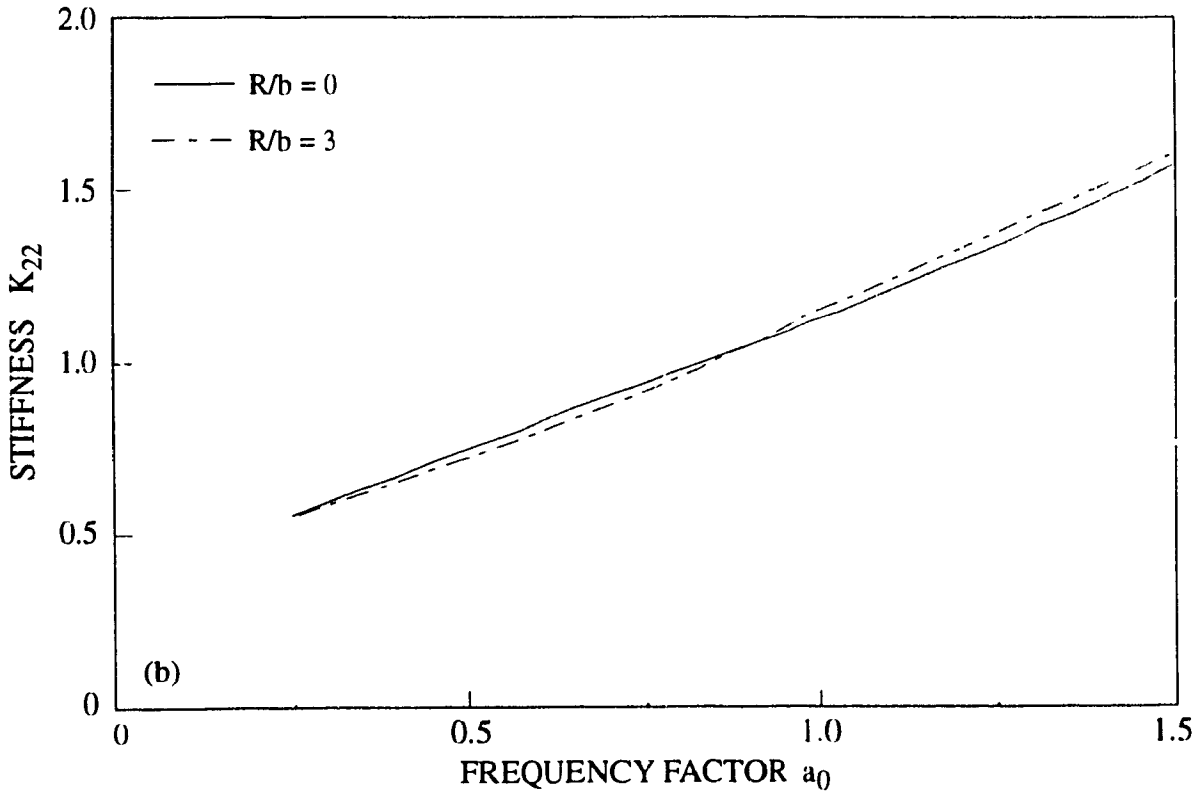

Figure 5.4 Harmonic vibration of rigid strip foundation: (a) boundary discretization; (b) effect of mesh truncation on vertical stiffness

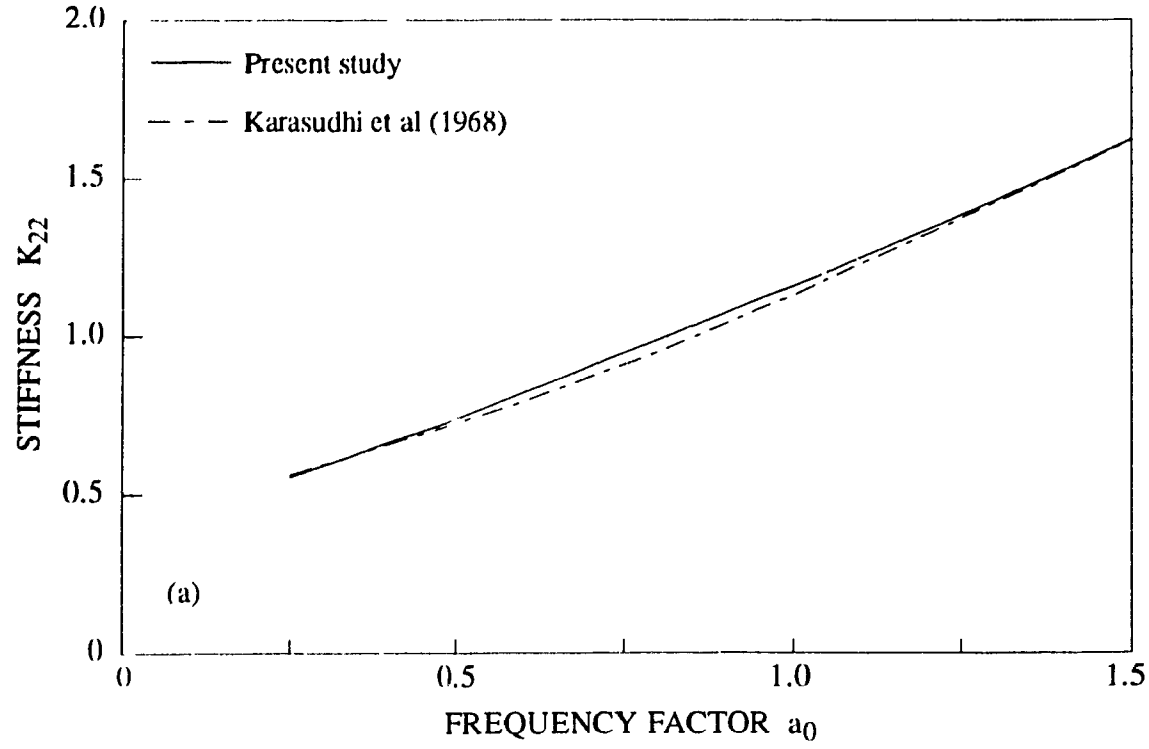

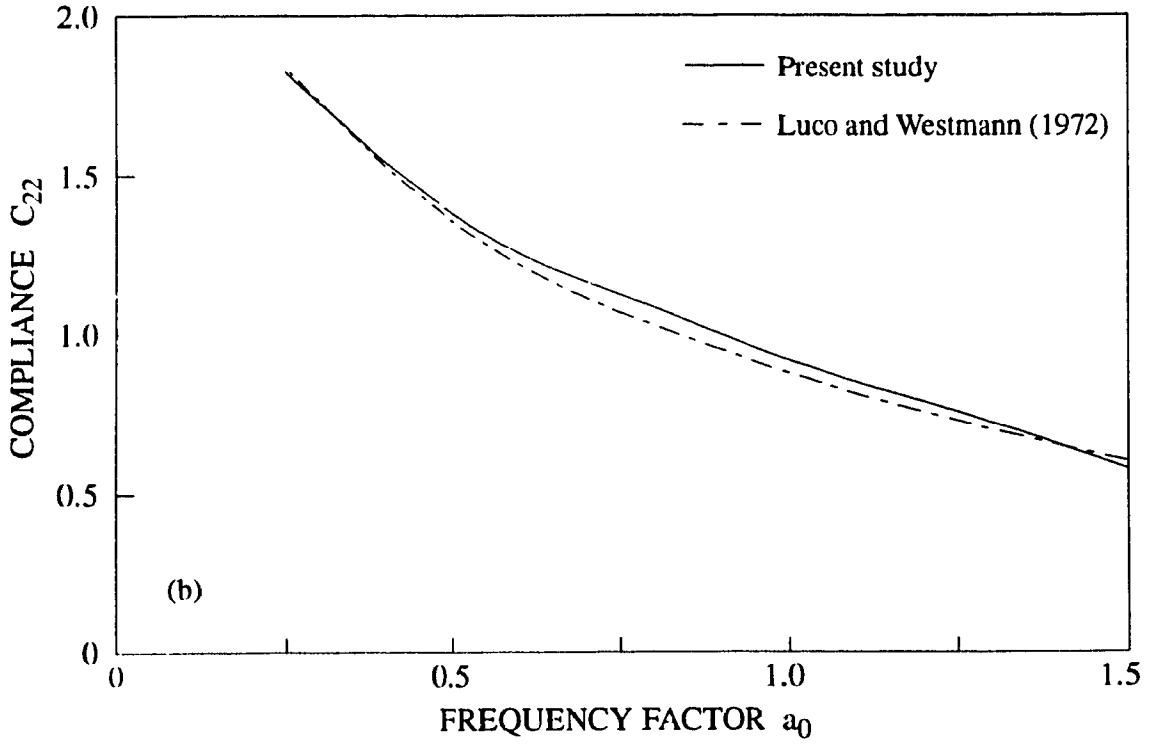

Figure 5.5 Harmonic vibration of surface rigid strip footing: (a) vertical stiffness for relaxed contact; (b) vertical compliance for welded contact

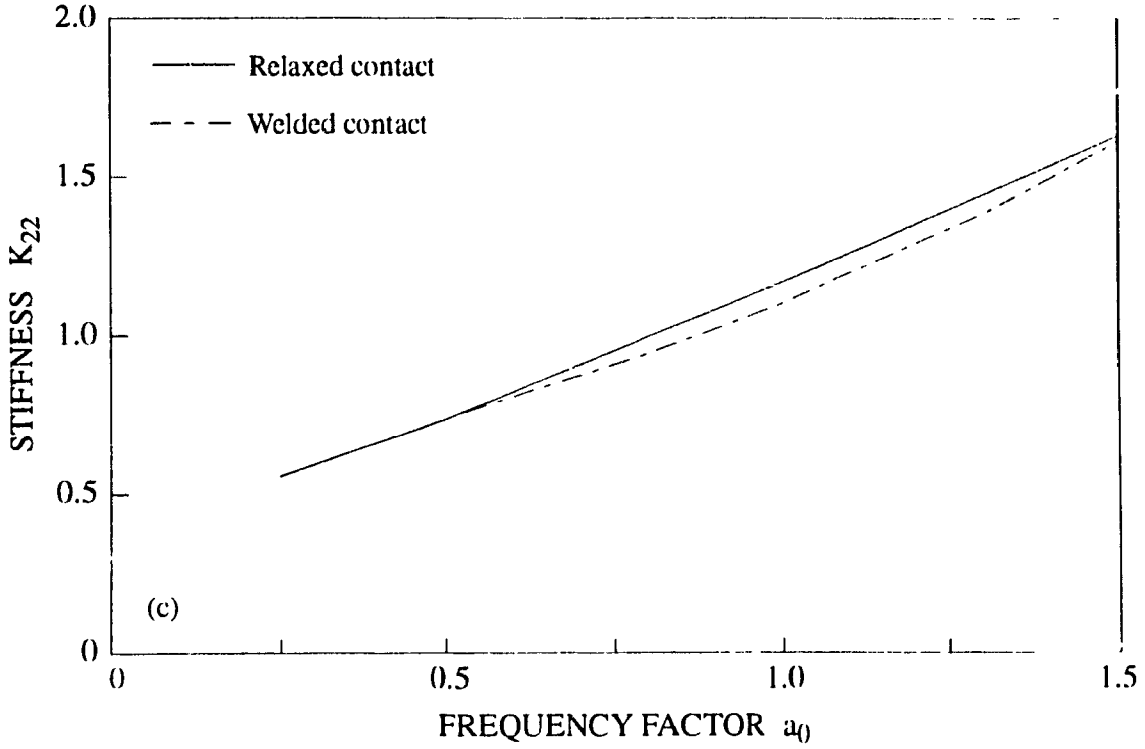

Figure 5.5 (c) comparison of vertical stiffness for welded and relaxed contact

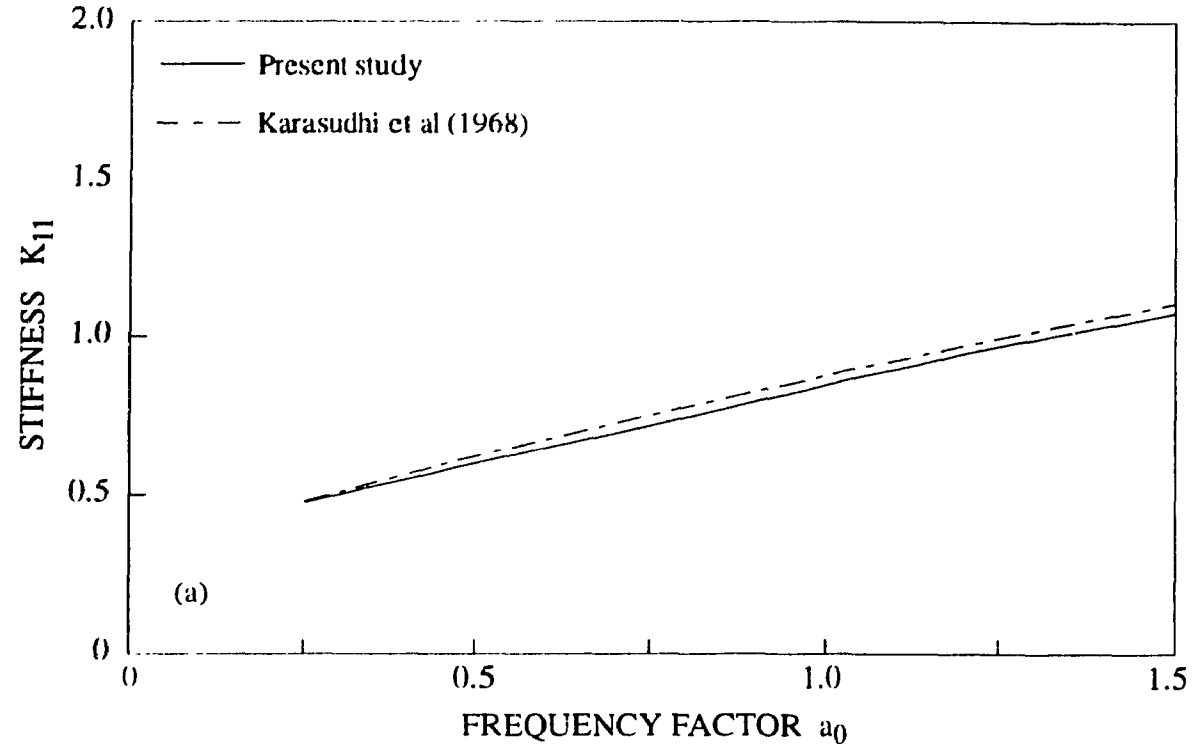

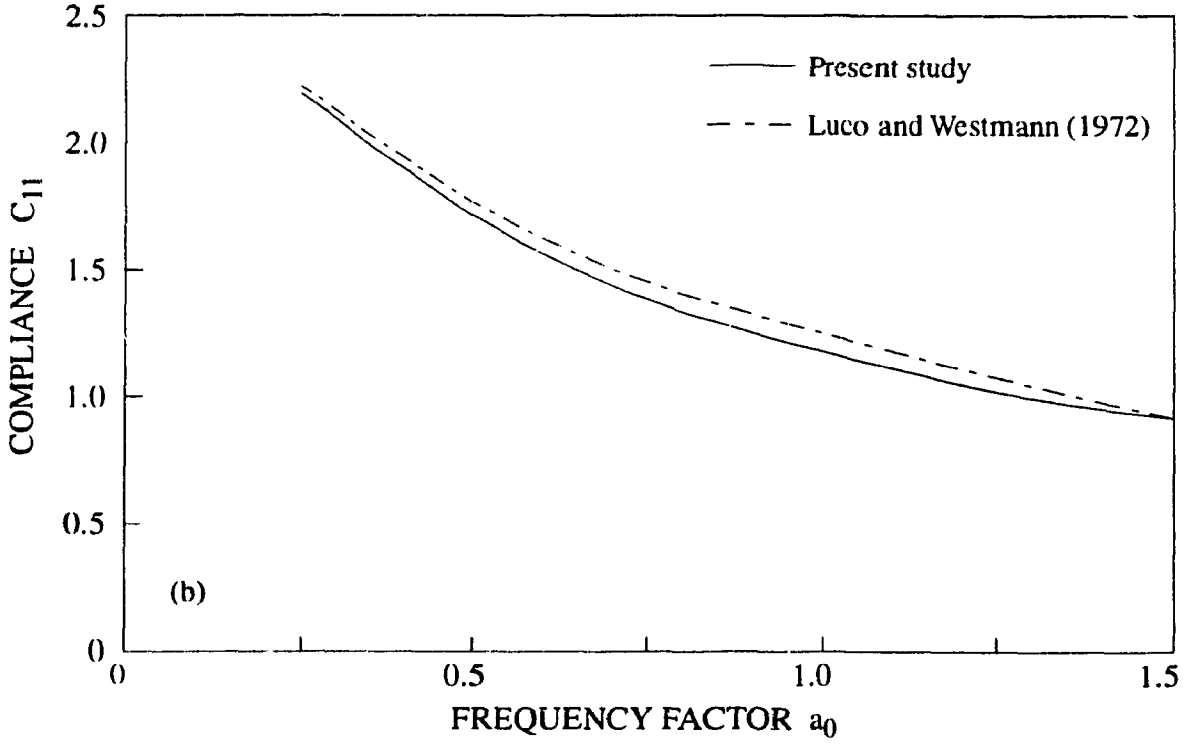

Figure 5.6 Harmonic vibration of surface rigid strip footing: (a) horizontal stiffness for relaxed contact; (b) horizontal compliance for welded contact

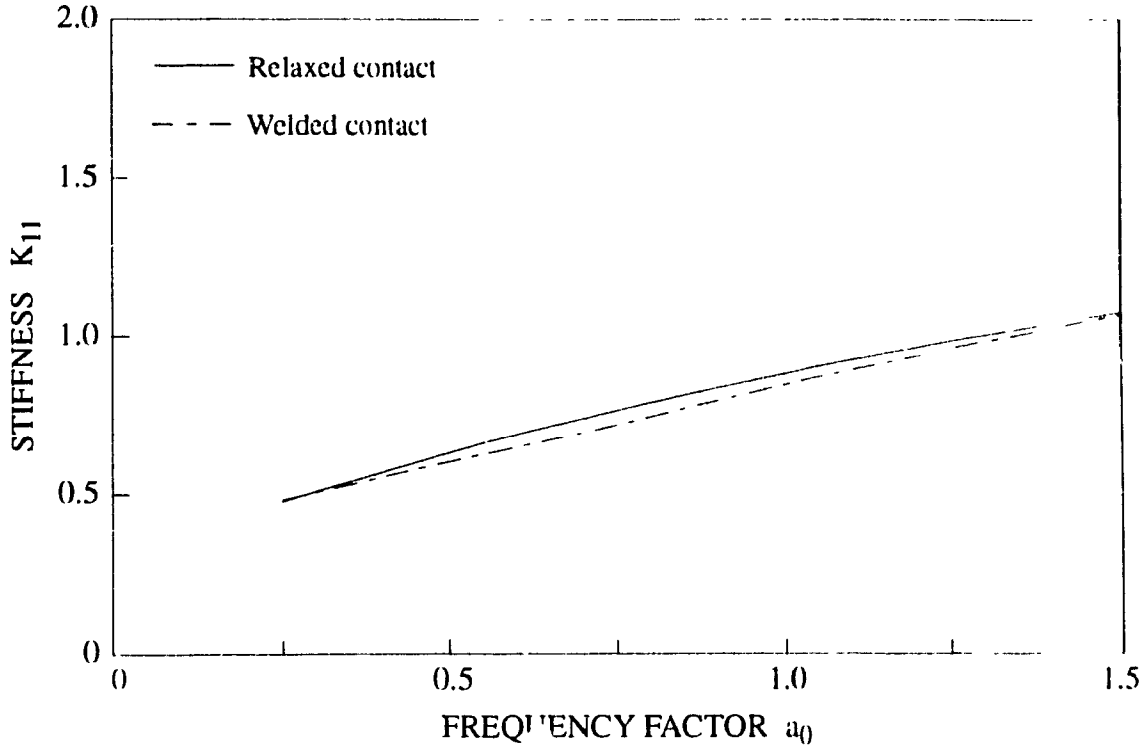

Figure 5.6 (c) comparison of horizontal stiffness for welded and relaxed contact

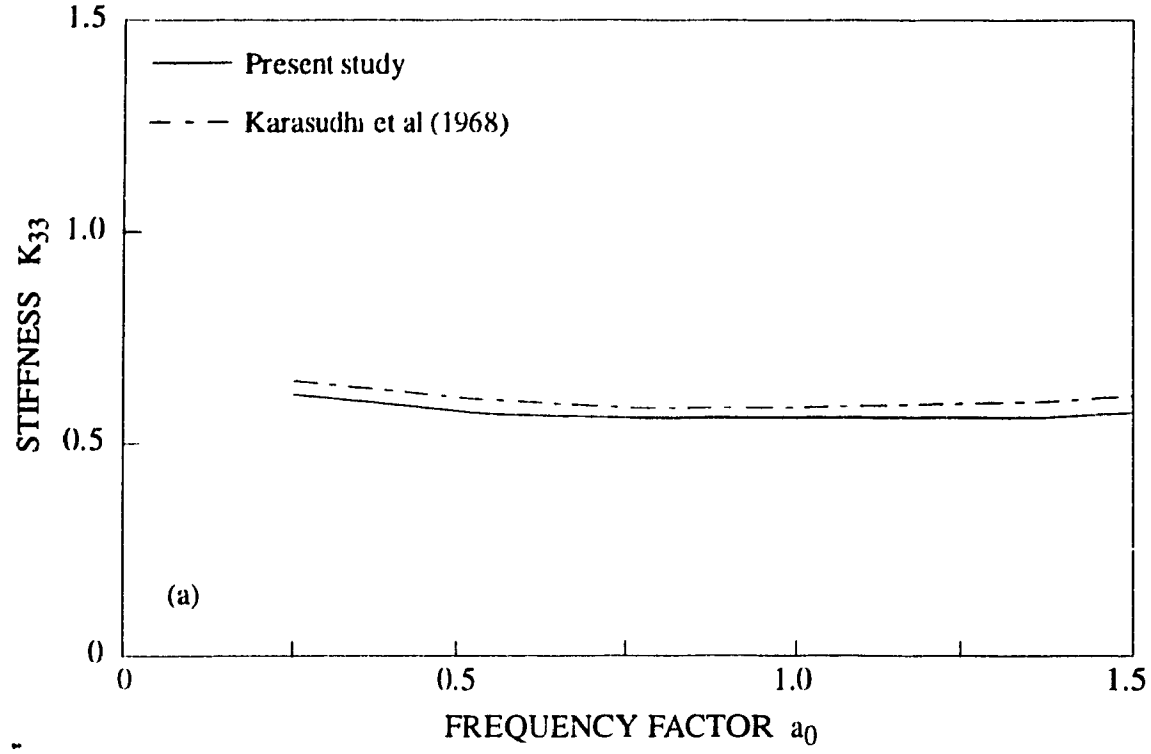

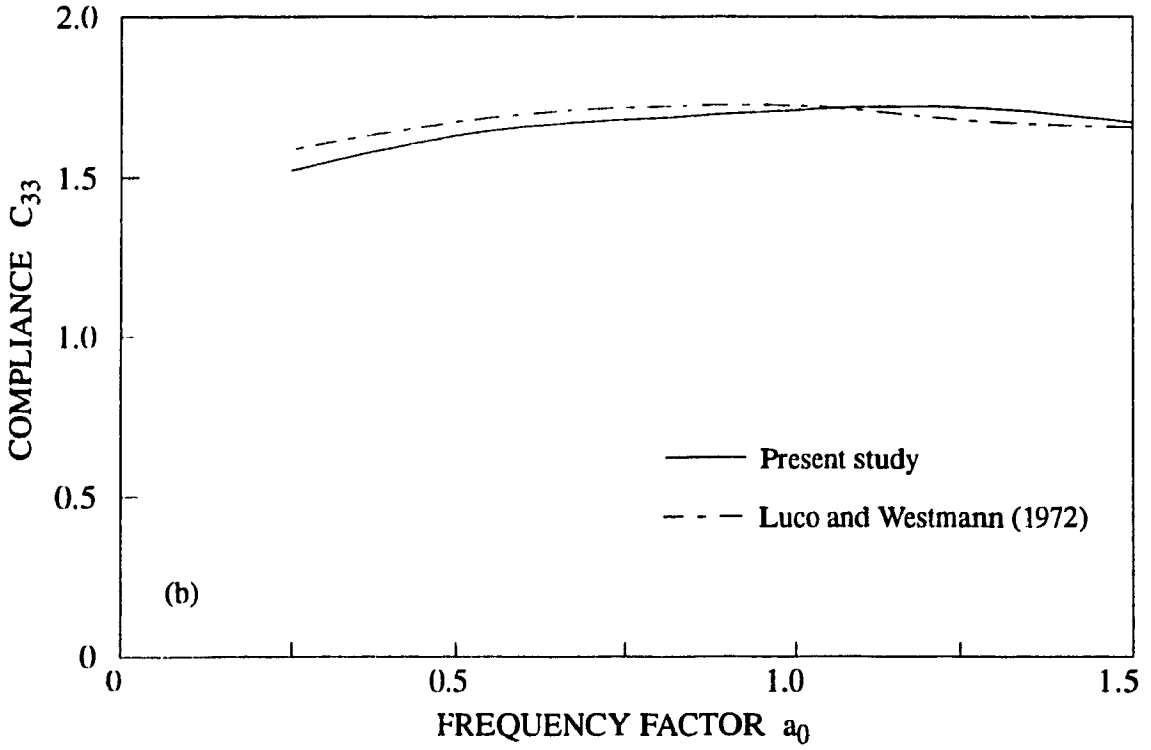

Figure 5.7 Harmonic vibration of surface rigid strip footing: (a) rocking stiffness for relaxed contact; (b) rocking compliance for welded contact

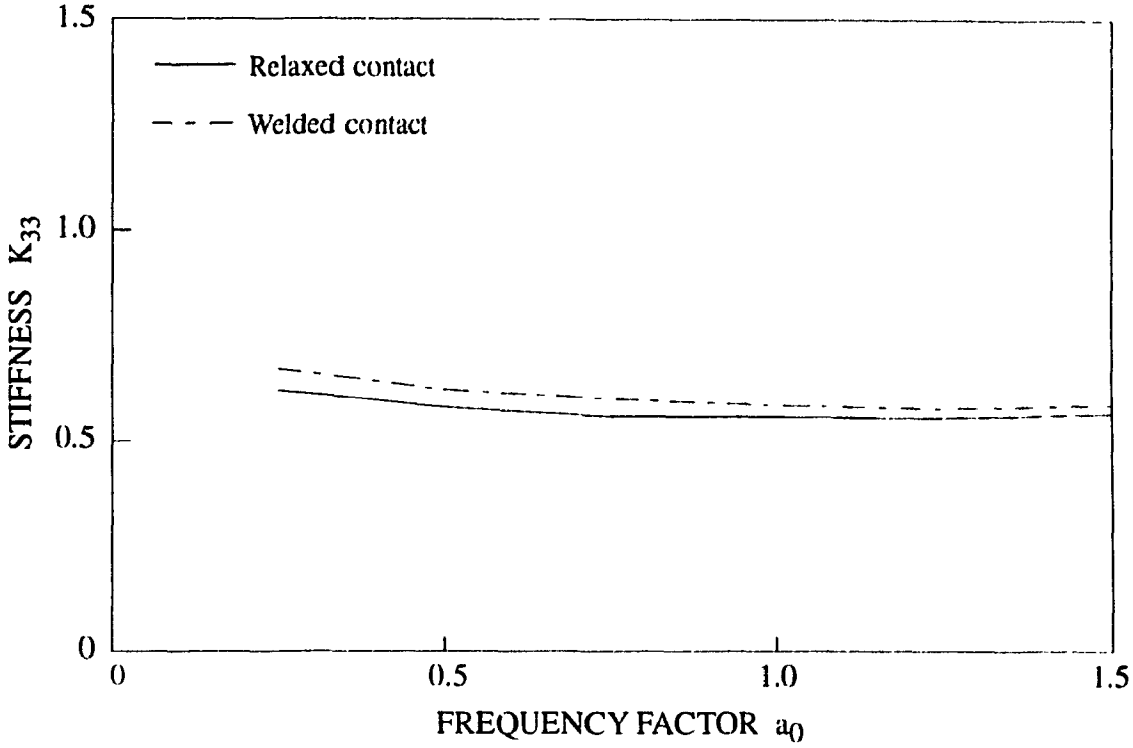

Figure 5.7(c) comparison of rocking stiffness for welded and relaxed contact

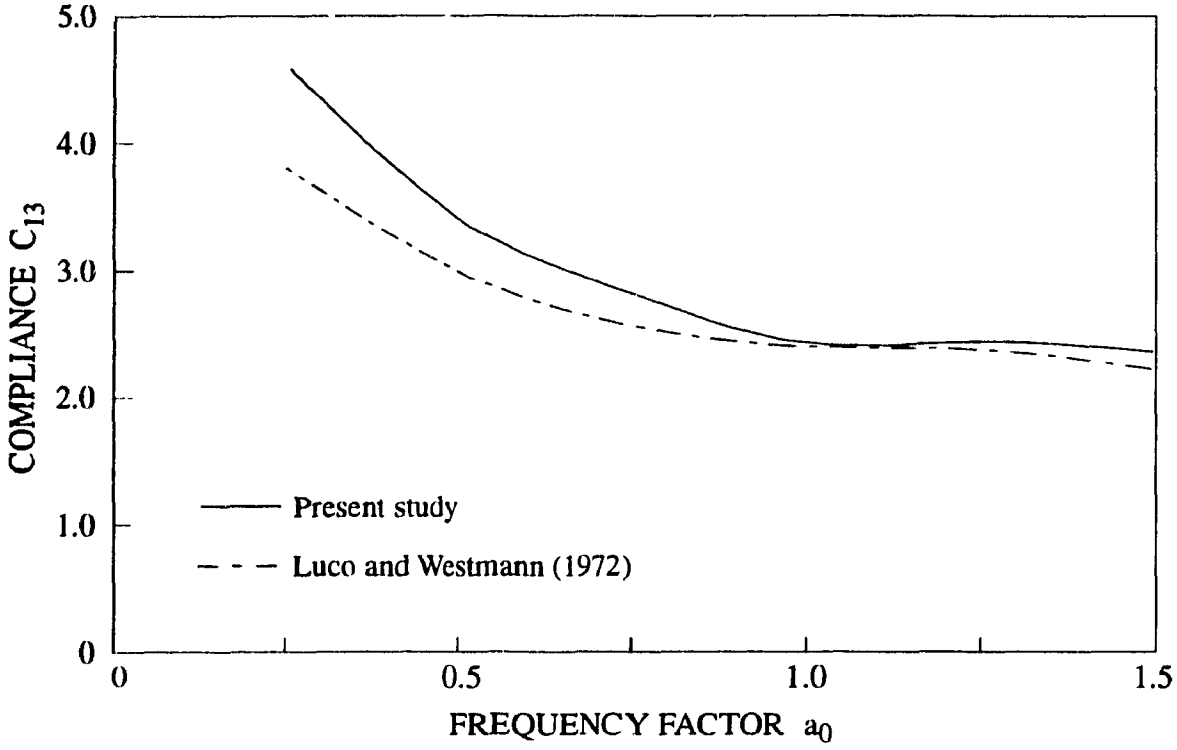

Figure 5.8 Coupled horizontal-rocking compliance for surface rigid strip footing

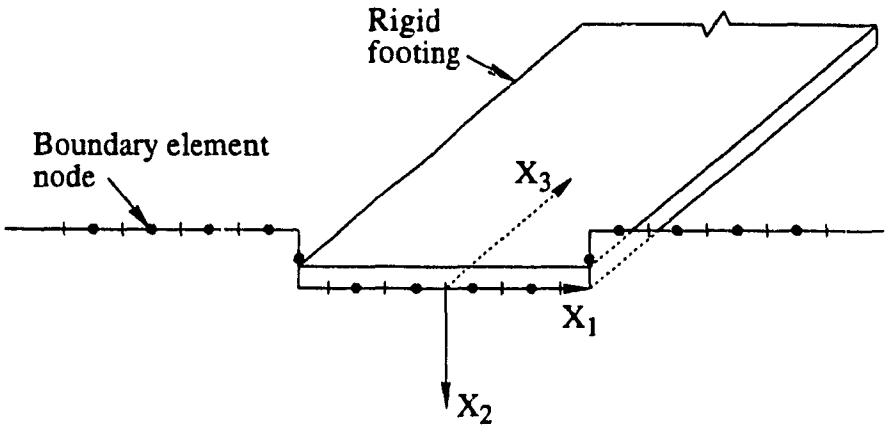

(a)

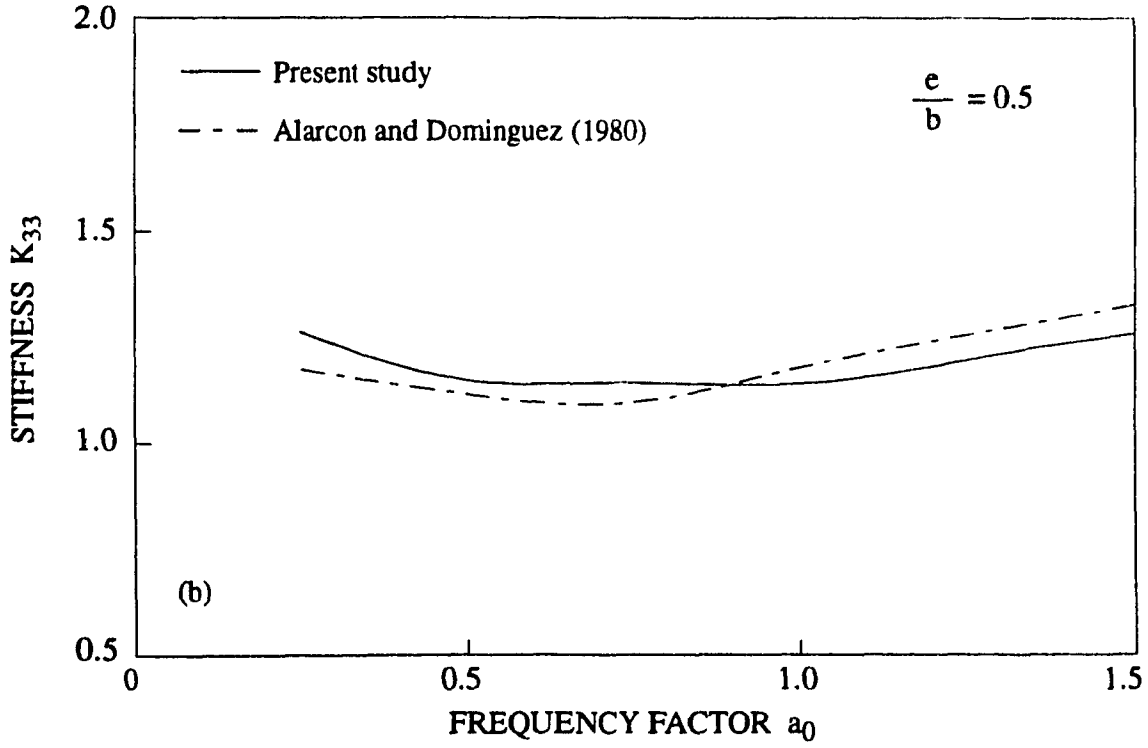

Figure 5.9 Harmonic vibration of embedded rigid strip footing: (a) strip footing and BE discretization; (b) time *vs* frequency domain analysis

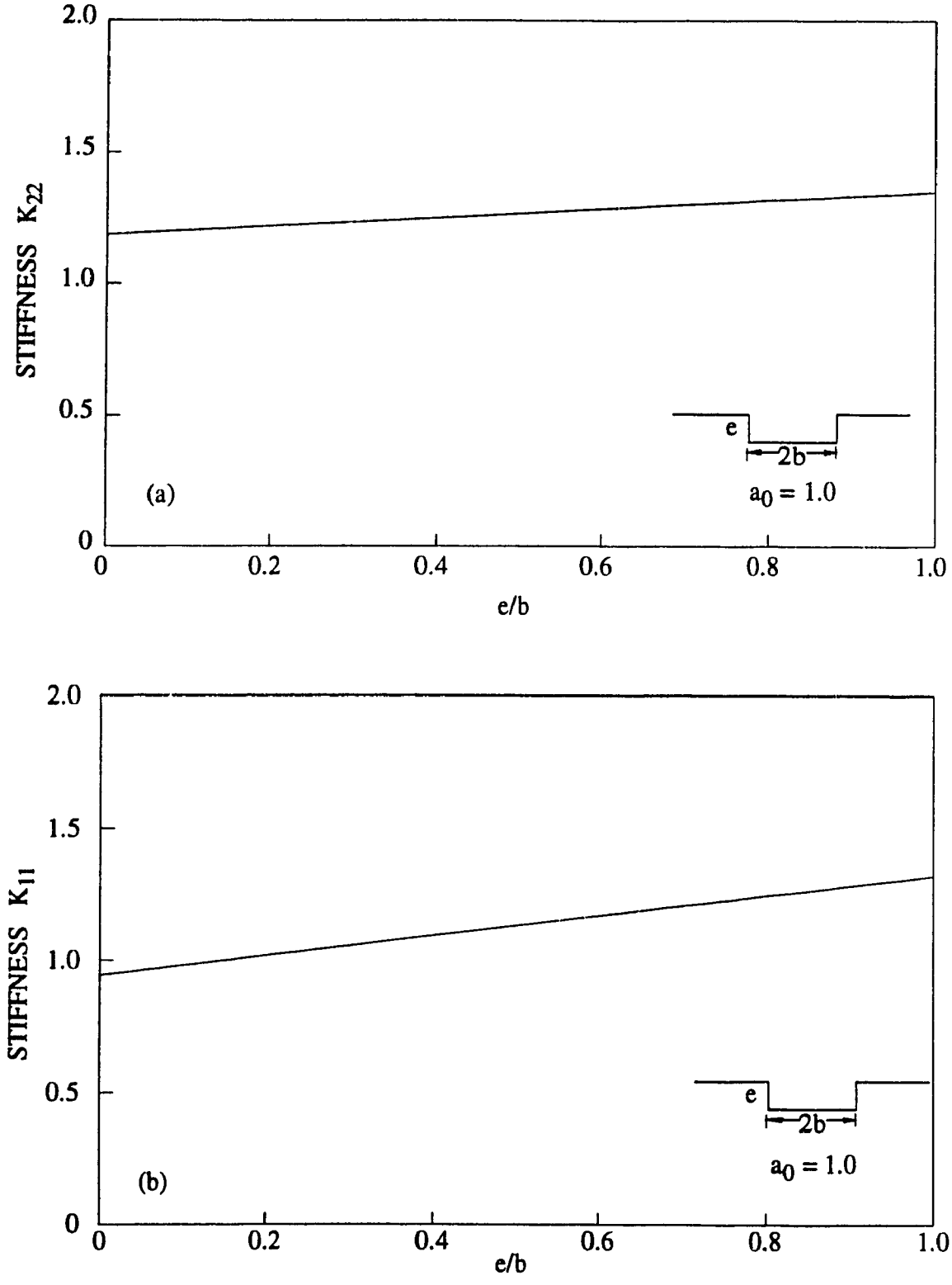

Figure 5.10 Effect of embedment on the harmonic response of rigid strip footing: (a) vertical stiffnes; (b) horizontal stiffness

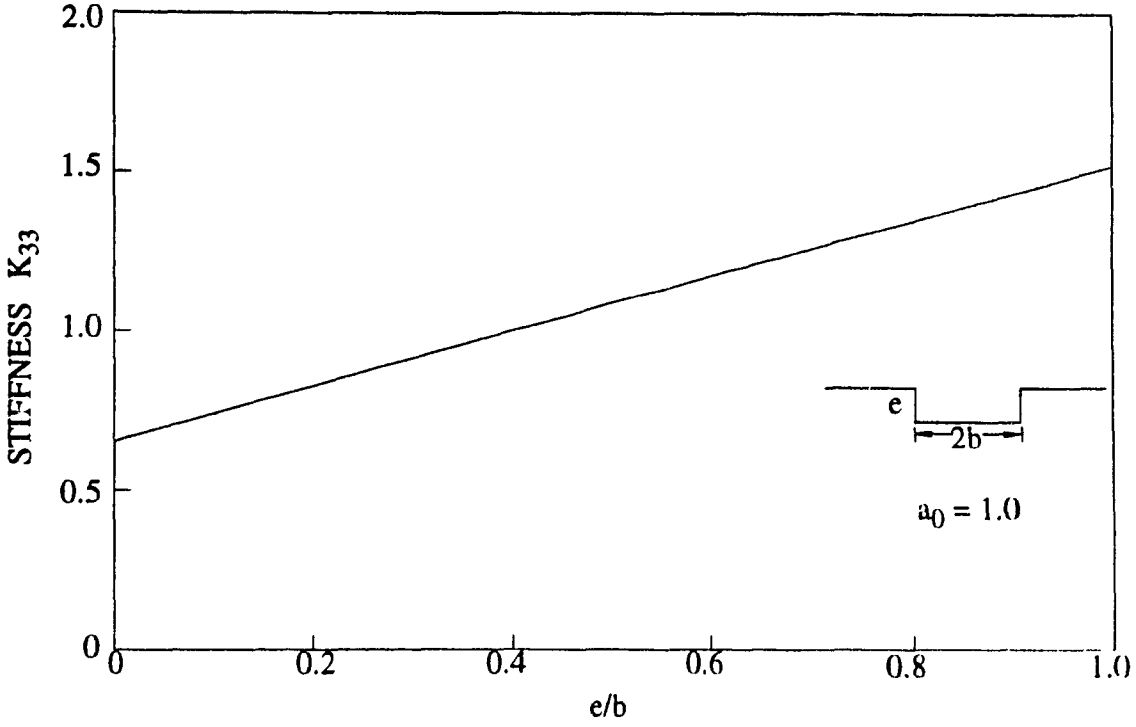

Figure 5.10 (c) rocking stiffness

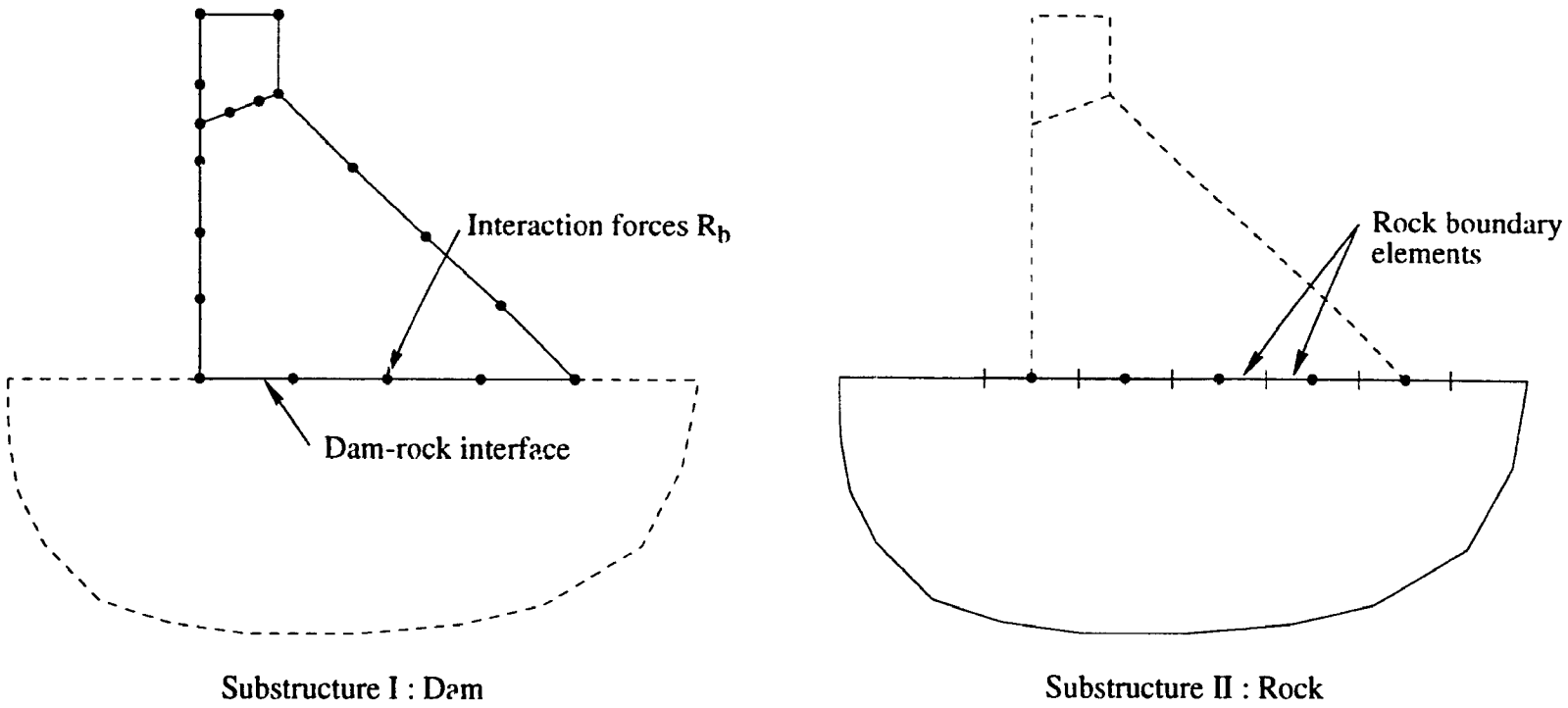

Figure 5.11 Dam-foundation system

CHAPTER VI

CONCLUSIONS AND RECOMMENDATIONS

6.1 CONCLUSIONS

The dynamic boundary element procedure for fracture analysis developed in the present study has been demonstrated to perform well in the investigation of seismic cracking in concrete gravity dams. From the analyses and results presented in this thesis, the following principal conclusions have been derived:

(i) The dynamic boundary element procedure based on the dual reciprocity approach, which employs the static fundamental solution, is adequate with boundary-only discretization for seismic fracture analysis of dams. Additional collocation at interior points in domains is not required for such analyses.

(ii) Static forces acting on a gravity dam, comprising such loads as the self-weight of the dam concrete and the hydrostatic pressure of the reservoir water, do not influence significantly the final profile of seismic cracking in the dam. Initiation of the propagation of cracks is, however, delayed if such loads act in a direction as to oppose the opening of the crack. Cyclic opening and closing of the crack under dynamic loading is also seen to be affected by the presence of static loads.

(iii) The present discrete crack propagation process appears to be not sensitive to the selected increments of crack extensions at each stage of crack growth. The piecewise increase in crack length should, of course, be restricted to a sufficiently small magnitude in order to limit the fracture energy released at each extension.

(iv) The magnitude of the fracture toughness of concrete influences significantly the fracture process. Increasing the fracture toughness delays the initiation of propagation of cracks in a dam. The final profile of cracking is, however, not significantly affected by the magnitude of the toughness, particularly for the case of a single crack propagating through the dam. Even for multiple cracking, the final rupture pattern is found to be almost unchanged when the fracture toughness is increased within a reasonable range. Furthermore, for sufficiently high magnitude of toughness, a widely distributed pattern of cracking is likely to develop. However, also a consequence of such high magnitude of toughness, cracking is likely to remain confined mostly to the surface of the dam.

(v) For the Koyna dam, the critical cracking pattern appears to be associated with a crack originating on the downstream face at the elevation of slope change and propagating almost instantaneously to the opposite face. Furthermore, irrespective of whether a single or multiple fracture model is used, the final rupture pattern for the dam is found to be identical and involves complete separation of the upper portion.

(vi) Although seismic cracking in a concrete gravity dam will originate at the heel and in the neck region near the crest, only cracking in the upper portion is found to be critical. The pattern of cracking in this region, however, does not seem to be influenced by the shape and size of the crest block.

(vii) Regarding the development of hydrodynamic uplift pressure in cracks on the upstream face of a dam, the data indicate that this phenomenon is expected to be much more significant during the post-rupture phase than prior to rupture. In the time preceding rupture, the openings of the upstream cracks remain sufficiently

small for the water pressure not to penetrate.

6.2 RECOMMENDATIONS FOR FUTURE WORK

The following recommendations are made for future extension of the present work and for further research in the area of seismic cracking in dams:

(i) The present crack propagation analysis procedure should be extended to included the interaction of the dam with the surrounding media, namely the reservoir water and the foundation rock. For the latter, the time domain formulation proposed in Chapter V can be incorporated in this future work. Regarding the interaction of the reservoir with a dam undergoing seismic cracking, an appropriate time-domain boundary element formulation needs to be incorporated also.

(ii) Although in large structures, such as concrete gravity dams, the zone of micro-cracking in front of a discrete crack is small compared to the dimensions of the structure, no conclusive evidence of the necessity of including the resulting non-linear behavior in the analysis of dams is available in the literature. Nevertheless, the presence of micro-cracks, together with the associated strain-softening behavior, suggests that non-linear fracture mechanics be employed for studying concrete fracture. The present cracking analysis procedure can therefore be modified to include non-linear fracture mechanics. More importantly, the procedure, apart from being more realistic, will be applicable to the fracture analysis of smaller concrete structures also.

(iii) Since it has been demonstrated in the present study that significant hydrodynamic pressure can be expected to develop inside cracks on the water retaining face of a dam during the post-rupture response, a formulation needs to be developed to

include rigorously these effects in the seismic crack propagation analysis.

(iv) Prediction of the post-rupture response of the dam during the remaining time-history of the same earthquake or even during aftershocks is extremely important. A formulation is therefore needed to perform such analysis. It should be noted that the boundary element method is ideally suited for analyzing efficiently contact problems such as posed by this phase of the seismic response.

(v) The multi-domain discretization scheme adopted herein for the representation of discrete cracks poses some limitation in the case of multiple cracks occurring close to each other. The artificial inter-domain boundary lines emanating from different crack tips may interfere with one another, thus requiring a redefinition of the initial mesh. An adaptive procedure, such as recommended recently by Portela et al. (1993), is better suited for this situations because the inter-domain boundary is not required and can be easily implemented.

(vi) A further possible improvement in the procedure may take the form of automatic crack initiation. The linear elastic analysis required at present to identify the potential cracking zones will thus be avoided, with cracks being automatically introduced at locations where the tensile strength is exceeded.

(vii) Crack propagation under static loading is not included in the present computer program. Implementation of cracking under static loads, together with treatment of static water pressure inside cracks, will make the current computer code very useful for the professional engineering community.

REFERENCES

Abdalla, M.A.M. **1984**. 'Dynamic soil structure analysis by boundary element method', Ph.D. Thesis, Carleton University, Ottawa.

Ahmad, S. and Banerjee, P.K. **1985**. 'Free vibration analysis by BEM using particular integrals', Journal of the Engineering Mechanics Division, ASCE, 112 (7), 682-695.

Ahmad, S. and Banerjee, P.K. **1988**. 'Multi-domain BEM for two-dimensional problems of elastodynamics', International Journal for Numerical Methods in Engineering, 26, 891-911.

Ahmadi, M. T. and Khoshrang, Gh. **1992**. 'Sefidrud dam's dynamic response to large near-field earthquake of June 1990', Dam Engineering, III (2), 85-115.

Alarcon, E. and Dominguez, J. **1980**. 'Impedance of foundation using the boundary integral equation method', Proceedings of the International Symposium on Innovative Numerical and Applied Engineering Science, 264-280.

Ayari, M.L. and Saouma, V.E. **1990**. 'A fracture mechanics based seismic analysis of concrete gravity dams using discrete cracks', Engineering Fracture Mechanics, 35 (1/2/3), 587-598.

Bazant. Z.P. and Cedolin, L. **1979**. 'Blunt crack band propagation in finite element analysis', Journal of the Engineering Mechanics Division, ASCE, 105 (2), 297-315.

Bazant, Z.P. and Oh, B.H. **1983**. 'Crack band theory for fracture of concrete', Materials and Structures, 16(93), 155-177.

Bhattacharjee, S.S. and Léger, P. **1993**. 'Seismic cracking and energy dissipation in concrete gravity dams', Earthquake Engineering and Structural Dynamics, 22, 991-1007.

Blandford, G.E., Ingraffea, A.R. and Liggett, J.A. **1981**. 'Two-dimensional stress intensity factor computations using the boundary element method', International Journal for Numerical Methods in Engineering, 17, 387-404.

Bruhwiler, E., Broj, J.J. and Saouma, V.E. **1991**. 'Fracture model evaluation of dam concrete', Journal of Materials in Civil Engineering, ASCE, 3(4), 235-251.

Bruhwiler, E. and Wittmann, F.H. **1990**. 'Failure of dam concrete subjected to seismic loading conditions', Engineering Fracture Mechanics, 35(1/2/3), 117-126.

Chandrashaker, R. and Humar, J.L. **1994**. 'Fluid-foundation interaction in the seismic response of gravity dams', Earthquake Engineering and Structural Dynamics, 22, 1067-1084.

Chapuis, J., Rebora, B. and Zimmermann, Th. **1985**. 'Numerical approach of crack propagation analysis in gravity dams during earthquakes', 15th Congress of the International Commission on Large Dams, Lausanne, 57(26), 451-473.

Chopra, A.K. **1987**. 'Earthquake analysis, design and safety evaluation of concrete dams', 5th Canadian Conference on Earthquake Engineering, Ottawa, 39-62.

Chopra, A.K. and Chakrabarti, P. and Gupta, S. **1980**. 'Earthquake response of concrete gravity dams including hydrodynamic and foundation interaction effects'. Report No. UCB/EERC-80/01, Earthquake Engineering Research Center, University of California, Berkeley.

Chopra, A.K. and Gupta, S. **1982**. 'Hydrodynamic and foundation interaction effects in frequency response functions for concrete gravity dams', Earthquake Engineering and Structural Dynamics, 10, 89-106.

Cruse, T.A. **1968**. 'A direct formulation and numerical solution of the general transient elastodynamic problem: II', Journal of Mathematical Analysis and Applications, 22, 341 - 355.

Cruse, T.A. **1978**. 'Two-dimensional BIE fracture mechanics analysis', Applied Mathematical Modelling, 2, 287-293.

Cruse, T.A. and Rizzo, F.J. **1968**. 'A direct formulation and numerical solution of the general transient elastodynamic problem', Journal of Mathematical Analysis and Applications, 22, 244-258.

Damisah F.O. **1981**. 'The application of boundary integral method to foundation dynamics', Ph.D.Thesis, Imperial College of Science and Technology, London, England.

Dasgupta, G. and Chopra, A.K. **1979**. 'Dynamic stiffness matrices for viscoelastic half planes', Journal of the Engineering Mechanics Division, ASCE, 105 (5), 729-745.

Dominguez, J. and Chirino, F. **1986**. 'BEM for dynamic crack problems in two dimensions', BETECH '86 (Eds. J.J. Connor and C.A. Brebbia), Computational Mechanics Publication, Springer-Verlag, New York, 619-632.

Donolon, W.P. and Hall, J.F. **1991**. 'Shaking table study of concrete gravity dam monoliths', Earthquake Engineering and Structural Dynamics, 20, 769-786.

El-Aidi, B. and Hall, J.F. **1989a**. 'Non-linear earthquake response of concrete gravity dams Part 1: Modelling', Earthquake Engineering and Structural Dynamics, 18, 837-851.

El-Aidi, B. and Hall, J.F. **1989b**. 'Non-linear earthquake response of concrete gravity dams Part 2: Behavior', Earthquake Engineering and Structural Dynamics, 18, 853-865.

Erdogan, F. and Sih, G.C. **1963**. 'On the crack extension in plates under plane loading and transverse shear', Journal of Basic Engineering, 85, 519-527.

Eringen A.C. and Suhubi E.S. **1975**. '*Elastodynamics - Volume II Linear Theory*', Academic Press, N.Y.

Fan, W.X. **1983**. 'Circumferential strain factor criterion for complex brittle fracture', Applied Mathematics and Mechanics (Beijing), 3(2), 211-224.

Fan, T.Y. and Hahn, H.G. **1985**. 'An application of the boundary integral equation method to dynamic fracture analysis', Engineering Fracture Mechanics, 21(2), 307-313.

Feltrin, G., Galli, M. and Bachmann, H. **1992**. 'Influence of cracking on the earthquake response of concrete gravity dams with reservoir', Proceedings of the 10th World Conference on Earthquake Engineering, 8, Madrid, 4627-4632.

Feng, L. **1994**. 'Fracture analysis of concrete dams by boundary element method', Ph.D. Thesis, Concordia University, Montreal.

Graves, R.H. and Derucher, K.N. **1987**. 'Interface smeared crack model analysis of concrete dams in earthquakes', Journal of the Engineering Mechanics Division, ASCE, 113 (2), 1678-1693.

Guyan, R.J. **1964**. 'Reduction of stiffness and mass matrices', AIAA Journal, 3(2), 380.

Hall, J.F. **1986**. 'Study of earthquake response of Pine Flat dam', Earthquake Engineering and Structural Dynamics, 14, 281-295.

Ingraffea, A.R., Gerstle, W.H. and Peruchio, R. **1989**. 'Fracture analysis with interactive computer graphics', Boundary Element Method in Structural Analysis (Ed. D.E. Beskos), Patras, Greece, 235-272.

Kanaan, A.E. and Powell, G.H. **1973**. 'General purpose computer program for inelastic dynamic response of plane structures', Report No. EERC 73-6, Earthquake Engineering Research Center, University of California, Berkeley.

Kanninen, M. F. and Popelar, C. H. **1985**. *Advanced Fracture Mechanics*, Oxford University Press, London.

Karabalis, D.L. **1984**. 'Dynamic response of 3-D foundations', Ph.D. Thesis, University of Minnesota, Minnesota.

Karasudhi, P., Keer, L.M. and Lee, S.L. **1968**. 'Vibratory motion of a body on an elastic half plane', Journal of Applied Mechanics, ASME, 35, 697-705.

Keegstra, P.N.R., Head, J.L. and Turner, C.E. **1976**. 'A two dimensional dynamic linear-elastic finite element program for the analysis of unstable crack propagation and arrest', Numerical Methods in Fracture Mechanics (Eds. D.R.J. Owen and A.R. Luxmoore), Swansea, England, 634-646.

Liang, V.C. **1974**. 'Dynamic response of structures in layered soil', Research Report No. R74/10, MIT.

Luco, J.E. and Westmann, R.A. **1972**. 'Dynamic response of rigid footing bonded to an elastic half space', Journal of Applied Mechanics, ASME, 39, 527-534.

Lysmer, J. and Khulemyer, R.L. **1969**. 'Finite dynamic model for infinite media,' Journal of the Engineering Mechanics Division, ASCE, 95, 859-877.

Mall, S. **1980**. 'Finite element analysis of stationary cracks in time dependent stress fields', Numerical Methods in Fracture Mechanics (Eds. D.R.J. Owens and A.R. Luxmoore), Swansea, England, 539-551.

Manolis, G.D. and Beskos, D.E. **1988**. *Boundary Element Method in Elastodynamics*, Unwin-Hyman, Boston, 102-107.

Manolis, G.D. and Beskos, D.E. **1981**. 'Dynamic stress concentration studies by boundary integral and Laplace transform', International Journal of Numerical Methods in

Engineering, 17, 573-599.

Mansur, W.J. **1984**. 'A time stepping technique to solve wave propagation problems using the boundary element method', Ph.D. Thesis, University of Southampton, Southampton U.K.

Mlakar, P.F. **1987**. 'Nonlinear response of concrete gravity dams to strong earthquake-induced ground motion', Computers and Structures, 26 (1/2), 165-173.

Medina, F., Dominguez, J. and Tassoulas, J.L. **1990**. 'Response of dams to earthquakes including effects of sediments', Journal of Structural Engineering, ASCE, 116(11), 3108-3121.

Mettu, S.R. and Nicholson, J.W. **1988**. 'Computation of dynamic stress intensity factor by time domain boundary integral equation method-II. Examples', Engineering Fracture Mechanics, 31(5), 769-782.

Mindess, S. **1984**. 'Fracture toughness testing of cement and concrete', Fracture Mechanics of Concrete: Material Characterization and Testing, (Eds. A. Carpinteri and A.R. Ingraffea), 67-110.

Nardini, D. and Brebbia, C.A. **1982**. 'A new approach to free vibration analysis using boundary elements', Boundary Element Method in Engineering (Ed. C.A. Brebbia), Proceedings of the 4th International Seminar, Southampton, 312-326.

Niwa, A. and Clough, R.W. **1980**. 'Shaking table research on concrete dam models', Report No. UCB/EERC-80/05, Earthquake Engineering Research Center, University of California, Berkeley.

Niwa, Y., Fukui, T., Kato, S. and Fujiki, K. **1980**. 'An application of the integral equation method to two-dimensional elastodynamics', Theory and Applications of Mechanics, 28, 281 -290.

Ottenstreuer, M. and Schmid, G. **1981**. 'Boundary elements applied to soil foundation interaction', Proceedings of the 3rd International Seminar on Recent Advances in B.E.M., California, 293-309.

Pal, N. **1976**. 'Seismic cracking of concrete gravity dams', Journal of Structural Engineering, ASCE, 102(9), 1827-1843.

Pekau, O.A., Zhang, C. and Feng, L. **1991**. 'Seismic fracture analysis of concrete gravity dams', Earthquake Engineering and Structural Dynamics, 20, 335-354.

Portela, A., Aliabadi, M.H. and Rooke, D.P. **1993**. 'Dual boundary element incremental analysis of crack propagation', Computers and Structures, 46(2), 237-247.

Raphael, J.M. **1984**. 'Tensile strength of concrete', Journal of American Concrete Institute, 81, 158-165.

Rots, J.G. **1991**. 'Smeared and discrete representations of localized fracture', International Journal of Fracture, 51, 45-59.

Saouma, V.E., Bruhwiler, E. and Boggs, H.L. **1990**. 'A review of fracture mechanics applied to concrete dams', Dam Engineering, I (1), 41-57.

Sih, G.C. and Macdonald, B. **1974**. 'Fracture mechanics applied to engineering problems strain energy density fracture criterion', Engineering Fracture Mechanics, 6, 361-386.

Skrikerud, P.E. and Bachmann, H. **1986**. 'Discrete crack modelling for dynamically loaded, unreinforced concrete structures', Earthquake Engineering and Structural Dynamics, 14, 297-315.

Smith, R.N.L. and Mason, J.C. **1982**. 'A boundary element method for curved cracked problems in two dimensions', Boundary Element Method in Engineering (Ed. C.A. Brebbia), Proceedings of the 4th International Seminar, Southampton, 472-484.

Snyder, M.D. and Cruse, T.A. **1975**. 'Boundary-integral equation analysis of cracked anisotropic plates', International Journal of Fracture, 11(2), 315-328.

Tinawi, R. and Guizani, L. **1994**. 'Formulation of hydrodynamic pressures in cracks due to earthquakes in concrete dams', Earthquake Engineering and Structural Dynamics, 23, 699-715.

Underwood, P. and Geers, T.L. **1981**. 'Doubly asymptotic boundary element analysis of dynamic soil structure interaction', International Journal of Solids and Structures, 17, 687-697.

United States Bureau of Reclamation, **1976**. 'Design of gravity dams', Department of the Interior, Denver, Colorado.

United States Federal Energy Regulatory Commission, **1991**. 'Engineering guidelines for the evaluation of hydropower projects', Office of Hydro Power Licensing, Washington D.C.

Saini, S.S. and Krishna, J. **1974**. 'Overturning of top profile of the Koyna dam during severe ground motion', Earthquake Engineering and Structural Dynamics, 2, 207-217.

Vaish, A.K. and Chopra, A.K. **1974**. 'Earthquake finite element analysis of structure-foundation systems', Journal of the Engineering Mechanics Division, ASCE, 100(6), 1101-1116.

Vargas-Loli, L.M. and Fenves, G.L. **1989**. 'Effects of concrete cracking on the earthquake response of gravity dams', Earthquake Engineering and Structural Dynamics, 18, 575-592.

Veletsos, A.S. and Verbic, B. **1974**. 'Basic response function for elastic foundation', Journal of the Engineering of Mechanics Division, ASCE, 100(1),189-202.

Waas, G. **1972**. 'Analysis method for footing vibrations through layered media', Ph.D. Thesis, University of California, Berkeley.

Wepf, D., Skrikerud P., and Bachmann, H. **1984**. 'Influence of cracking on the seismic response of concrete gravity dams', Proceedings of the 8th World Conference on Earthquake Engineering, San Francisco, 95-102.

Wolf, J.P. and Darbre, G.R. **1984a**. 'Dynamic stiffness matrix of soil by boundary element method: conceptual aspects', Earthquake Engineering and Structural Dynamics 12, 385-400.

Wolf, J.P. and Darbre, G.R. **1984b**. 'Dynamic stiffness matrix of soil by boundary element method: embedded foundations', Earthquake Engineering and Structural Dynamics 12, 401-416.

Zhou, J. and Lin, G. **1992**. 'Seismic fracture analysis and model testing of concrete gravity dams', Dam Engineering, III (1), 35-47.

APPENDIX A

STANDARD FUNCTIONS AND PROCEDURES USED IN THE BOUNDARY INTEGRAL FORMULATION

A1 FREQUENCY INDEPENDENT FUNDAMENTAL SOLUTION

The frequency independent fundamental solution from elastostatics is the Kelvin solution, which for a plane strain problem is given by

$$u^*_{ij}(\xi, x) = \frac{-1}{8\pi(1-\upsilon)G}\{(3-4\upsilon)\ln(r)\,\delta_{ij} - \frac{\partial r}{\partial x_i}\frac{\partial r}{\partial x_j}\}; \quad \text{(A1)}$$

$$p^*_{ij}(\xi, x) = \frac{-1}{4\pi(1-\upsilon)r}\{\left[(1-2\upsilon)\,\delta_{ij} + 2\frac{\partial r}{\partial x_i}\frac{\partial r}{\partial x_j}\right]\frac{\partial r}{\partial n} - (1-2\upsilon)\,(\frac{\partial r}{\partial x_i}n_j - \frac{\partial r}{\partial x_j}n_i)\} \quad \text{(A2)}$$

where r is the distance between points ξ and x; δ_{ij} the Kronecker delta; n_1 the unit outward normal at x; G the shear modulus and ν the Poisson's ratio. The above expressions are valid for plane stress problem if ν is replaced by $\nu'=\nu/(1+\nu)$.

A2 DISPLACEMENT FIELD AND TRACTIONS CORRESPONDING TO FUNCTIONS $f^j = C - R(\xi_j - x)$

The set of functions $f^j(x)$ employed to transform the inertial domain integral are related to the static problem for which the displacement field is

$$\psi^j_{li} = \left[\frac{1-2\upsilon}{5-4\upsilon}C + \frac{r}{30(1-\upsilon)}\right]x_l x_i - \frac{9-10\upsilon}{90(1-\upsilon)}\delta_{li}r^3 \quad \text{(A3)}$$

The corresponding stress field can be obtained from the following relation

$$\tau^j_{ijk} = \delta_{ij}\left[\frac{2G}{1-2\nu}\{(1-2\nu)\frac{\partial\psi^j_{jk}}{\partial x_i} + \nu\frac{\partial\psi^j_{kl}}{\partial x_l}\}\right] + (1-\delta_{ij})\left[G\{\frac{\partial\psi^j_{jk}}{\partial x_i} + \nu\frac{\partial\psi^j_{ik}}{\partial x_j}\}\right] \quad \text{(A4)}$$

with tractions $\eta^j_{li} = \tau^j_{lim} n_m$; where n_m represents the component of outward normal vector on the boundary.

A3 BODY FORCE DUE TO SELF-WEIGHT

The domain integral corresponding to the body force representing the self-weight of concrete is given by

$$B_i = \int_{\Omega} u^*_{ij} b_j d\Omega \tag{A5}$$

where b_j is the constant gravitational force; u^*_{ij} denotes the Kelvin fundamental displacement solution and Ω represents the domain. In order to reduce this domain integral to the boundary, the Galerkin tensor G^*_{ij}, which is related to the Kelvin fundamental solution by the following expression

$$u^*_{ij} = G^*_{ij,\,kk} - \frac{1}{2(1-\nu)} G^*_{ik,\,kj}, \tag{A6}$$

is used in the present study. Using this expression in equation (A5), the body force integral of equation (A5) becomes

$$B_i = \int_{\Omega} (G^*_{ij,\,kk} - \frac{1}{2(1-\nu)} G^*_{ik,\,kj})\, b_j d\Omega \tag{A7}$$

For a two-dimensional plane strain problem, the Galerkin tensor has the form

$$G^*_{ij} = \frac{1}{8\pi G} r^2 ln\,(\frac{1}{r})\,\delta_{ij} \tag{A8}$$

and the corresponding fundamental displacement becomes

$$u^*_{ij} = \frac{-1}{8\pi(1-\nu)G}\{(3-4\nu)\ln(r)\,\delta_{ij} - r_i r_j + (\frac{7-8\nu}{2})\,\delta_{ij}\} \qquad \text{(A9)}$$

which differs from equation (A1) by a constant. Equations (A8) and (A9) are used to transform the domain integral in equation (A5), which reduces to the following boundary integral expression

$$B_i = \int_\Gamma (\frac{r}{8\pi G}\left[2\ln(\frac{1}{r}) - 1\right]\left[b_i n_k \frac{'}{\partial x_k} - \frac{1}{2(1-\nu)} b_k \frac{\partial r}{\partial x_k} n_i\right]) d\Gamma \qquad \text{(A10)}$$

A4 UPDATING OF STIFFNESS MATRIX IN CRACK PROPAGATION ANALYSIS

In the crack propagation analysis, the stiffness matrix [k] changes as a crack extends in length. For a given configuration of crack(s), the stiffness matrix is evaluated using the procedure discussed in Chapter II. At the time step when the crack instability is incurred, the crack length is extended and a new tangent stiffness matrix is computed for the corresponding discretization of the boundary element mesh. Response calculations are repeated at this same time step with the new tangent stiffness matrix. The use of unbalance forces in the subsequent time step, as used in the case of stiffness modification due to crack closure, is therefore not required.

APPENDIX B

SEISMIC MULTIPLE CRACKING ANALYSIS OF PINE FLAT DAM

B1 INTRODUCTION

The Koyna dam analyzed in the present study has been noted earlier to have a cross-section which is not typical for gravity dams. The unusual characteristic which differentiates this dam from other gravity-type dams is the relatively large crest block and the abrupt change in slope of the downstream face at approximately two-thirds the height of the bulkhead. As a result, it is possible that the conclusions based on the analytical observations made for this dam may not hold true for concrete gravity dams in general. In view of this, fracture response of a more typical gravity dam, namely the Pine Flat dam, has also been investigated and is summarized here. This dam was selected because, as the Koyna dam, it is located in an active seismic area and, because the seismic cracking response of this dam has been studied previously by a number of other researchers using both analytical and experimental techniques.

B1.1 Past investigations of cracking in the Pine Flat dam

Located in Kern County, California, the Pine Flat concrete gravity dam consists of 37 monoliths with a crest length of 560 m. The cross-section of a non-overflow monolith of the dam is shown in Figure B-1(a) and represents a typical section for a gravity-type concrete dam. The dam has been analyzed for earthquake induced cracking by Chapuis et al (1985) employing the finite element method and a hybrid smeared-discrete cracking model. Hydrodynamic forces obtained from dam-reservoir interaction analysis for an uncracked dam were used in the fracture analysis. The dam-foundation interaction was, however, not considered. Fracture response of the dam was investigated for an artificial

accelerogram with peak ground acceleration of 0.1 g and applied in the horizontal direction. The maximum principal tensile stress criterion incorporating the principles of linear elastic fracture mechanics was employed for crack extension, with the concrete fracture toughness assumed to be 1.0 MPa.m$^{1/2}$. Cracking was predicted at two locations: at the heel and on the upstream face near the base of the crest block. The crack originating at the heel was, however, found to be not critical. The crack originating on the upstream face near the crest propagated horizontally for more than half the width of the section before turning downwards into the body of the dam. The crack propagation, however, could not be completed due to the geometric constraints imposed by the coarseness of the finite element mesh. Seismic analysis of the dam by El-Aidi and Hall (1991a; 1991b) featured the investigation of the fracture behavior along pre-determined planes of weakness. Smeared crack technique was used for modelling cracks in a finite element mesh. Dam-foundation-reservoir interaction, as well as the cavitation effects in the water, were included. The automated smeared crack propagation analysis, however, resulted in unrealistic crack profiles, which were subsequently guided in the desired direction by incorporating the analyst's intervention in the program. The size of the finite elements in the mesh was, nevertheless, still found to influence the results.

Detailed cracking analysis of the dam has also been performed by Vargas-Loli and Fenves (1989), who adopted smeared crack modelling together with the crack band theory to conserve the fracture energy released by cracked finite elements. However, due to the limitations on the size of finite elements resulting from economic considerations, the concrete fracture energy could not be conserved at a realistic level. Cracking analyses were performed for the 1951 Taft and the 1971 Pacoima earthquakes with the ground motions scaled to different peak accelerations. Critical cracking in the dam was predicted primarily in the top region which cracked extensively, but the computed cracking pattern was very diffused.

Laboratory investigation of the fracture response of this dam has been reported by

Donolon and Hall (1991). They performed shaking table tests on three small scale models of the top portion of the dam and monitored crack propagation by using high speed photography. Cracking occurred near the base of the crest block which was found to extend from one face to the other. The completely separated section also showed significant stability even under the subsequent very strong shake table excitation.

In the following, earthquake-induced multiple cracking in the dam is investigated employing the boundary element method and the dynamic crack propagation analysis procedure presented in this study. Results for the fracture response of the dam, as well as data concerning crack opening/closing behavior, are presented. The investigation and the presentation of results follow the same general format as used for the multiple fracture analysis of the Koyna dam in Chapter IV, so that appropriate comparisons can be drawn between the predicted cracking response for these two dams with significantly different geometries.

B2 NUMERICAL RESULTS

In the present study, the tallest monolith of the dam, shown in Figure B1(a), is selected to investigate the seismic cracking behavior of the dam. The following material properties are employed for the mass concrete of the dam: modulus of elasticity = 22400 MPa, Poisson's ratio = 0.2 and density = 2400 kg/m^3. In the absence of test values, the dynamic tensile strength of the concrete is assumed to be 3.66 MPa, which is also the value used by Vargas-Loli and Fenves (1989). Damping associated with the first two modes of vibration of the dam is taken to be 5% each, of critical damping. Three different values of the dynamic fracture toughness of concrete, namely K_{Id} = 2.0, 5.5 and 9.0 MPa.m$^{1/2}$ are employed for this dam also, in order to permit direct comparison of results with those obtained earlier for the Koyna dam. As before, the lowest value is employed for the detailed investigation of cracking in the dam and the influence of higher magnitudes of toughness on the fracture response is examined separately.

The depth of impounded water is taken to be 116 m, which corresponds to the full reservoir condition. The dam-reservoir interaction is approximated by adding water mass to appropriate nodes on the upstream face. The base of the dam is considered fixed, thus neglecting the dam-foundation interaction. For the reasons mentioned previously, water pressure effects in cracks on the upstream face of the dam are not considered in the present case also.

The S69E component of the ground motion recorded at the Taft Lincoln School Tunnel during the Kern County, California, earthquake of July 21, 1952, is selected as the excitation for the fracture analysis of the dam. Only the horizontal component of the ground motion, acting in the stream-wise direction, is used in this study. The peak acceleration of the record is 0.18g.

B2.1 Linear response analysis and locations of potential cracking

In order to identify the zones of potential cracking, a linear elastic analysis of the dam is performed for 6 sec of the ground motion. Peak tensile stress in the dam is, however, found not to exceed the assumed tensile strength of concrete. Therefore, in order to induce cracking, the ground acceleration is scaled-up by a factor of 2.5 for which the corresponding envelope of principal tensile stresses on the faces of the dam is depicted in Figure B1(b). Three potential zones of cracking can be identified from this figure; two in the top portion of the dam, zones 1 and 2, and one (zone 3) near the heel. It is interesting to note that the predicted regions of higher tensile stress in the upper part of the dam are located near the base of the crest block for this dam also, irrespective of its rather smooth downstream profile compared to the Koyna dam.

Based on the above stress distribution, multiple crack propagation analysis of the dam should be performed considering cracks originating in all three zones. However, as mentioned above, it has already been demonstrated by Chapuis et al (1985) that cracking in zone 3 is not critical. Consequently, the following multiple crack propagation analysis

of the dam considers two pre-assigned cracks, one each in zones 1 and 2. Thus 1 m long C1 and C2 initial cracks are introduced, respectively, on the downstream and the upstream faces of the dam. Crack C1 is modelled at elevation 98 m, whereas crack C2 on the upstream face is taken at elevation 102 m. The corresponding boundary element discretization of the dam with initial cracking is shown in Figure B2. The mesh comprises 180 nodes and 117 boundary elements, with the usual traction-singular dicretization near the tips of cracks. Crack propagation analysis is conducted also for the scaled ground motion with a time step of 0.003 sec.

B2.2 Analysis of fracture response

Results for the fracture response of the dam are presented in Figure B3. The final profiles for the two initial cracks are depicted in Figure B3(a). As shown, complete separation of the crest block is predicted with cracks C1 and C2 propagated to merge within the body of the dam. It is worth noting that the computed final profile of crack C1 is almost perpendicular to the downstream face and matches the profile of a similar crack obtained in the laboratory rupture test of the dam by Donolon and Hall (1989). Furthermore, the final rupture pattern in Figure B3(a) is almost identical to the fracture pattern obtained for the multiple cracking in the Koyna dam in Figure 4.8(a).

Influence of the presence of a long crack on the path followed by a crack on the opposite face of the dam is also evident from Figure B3(a). Thus, the upstream crack C2, which propagates later [Figure B3(b)] begins to extend horizontally but reorients itself towards the tip of the already propagated crack C1 during the subsequent growth. As previously noted for the Koyna dam, this change in propagation direction is a consequence of the change in stress field orientation due to the increase in shear stress in the intact concrete between the two crack tips. The downward growth of crack C2, however, also brings the tip of this crack sufficiently close to the crack C1 to result in complete rupture of the dam cross-section.

Corresponding time histories of crack lengths for C1 and C2 are shown in Figure B3(b), and, as can be seen, the propagation process for the two cracks is almost instantaneous. The propagation of the downstream crack C1, which begins to grow first, is completed in a single phase in only 0.04 sec, while the corresponding elapsed time for the propagation of C2 is 0.05 sec.

Time history of horizontal displacement of the dam crest is presented in Figure B3(c), where the corresponding data from the linear elastic analysis of the uncracked dam is also depicted. Although the fracture process can be seen to influence the crest displacement, it is evident that the deviation in the two time histories is not significant over most of the time-history. However, with the dam cross-section nearly ruptured, larger magnitude of the crest displacement is computed and the maximum difference in the peak crest displacement is approximately 7 mm at rupture. Noting that the positive displacement indicates movement toward downstream, it is also observed in Figure B3(c) that the crest is displaced in the upstream direction when the downstream crack C1 begins to propagate, and that crack C2 becomes unstable in the same cycle when the crest movement reverses. The corresponding maximum openings of the two crack mouths [Figure B3(d)] are, however, not proportional to the displacement magnitudes of the crest.

Examining the crack mouth opening data in Figure B3(d), it is evident that the two cracks open and close alternately, with comparable magnitudes for the entire time history until rupture. The mouth opening magnitude at initiation of propagation of downstream crack C1 is 0.45 mm and the crack continues to open to a maximum magnitude of 1.46 mm while also extending in length. For the instability of crack C2 also, comparable opening magnitude of 0.525 mm is predicted and the maximum magnitude of the opening of this crack during the rupture phase is 1.38 mm. Furthermore, it is also worth noting that the first major opening for each crack coincides with crack instability and results in complete rupture, which, as noted above, occurs in a single reversal of the crest movement. It is interesting to recall that similar behavior was predicted for the single

fracture models for the Koyna dam.

B2.3 Behavior with higher concrete fracture toughness

Results for the multiple crack propagation analysis with two higher values of the fracture toughness are presented in Figure B4, where the final profiles of cracks C1 and C2 for K_{Id} = 5.5 and 9.0 MPa.m$^{1/2}$ are shown. Comparing these crack profiles with those for K_{Id} = 2.0 MPa.m$^{1/2}$ in Figure B3(a), it is evident that final cracking in the dam is significantly different for the three values of the concrete fracture toughness. For K_{Id} = 9.0 MPa.m$^{1/2}$, the two cracks propagate deep into the body of the dam, but neither do they penetrate the cross-section independently nor merge with each other to result in complete rupture. On the other hand, for K_{Id} = 5.5 MPa.m$^{1/2}$, although the propagating crack C2 in Figure B4(a) appears to be heading toward the downstream crack C1, the fracture analysis could not be completed because the tip of this crack approaches to intersect the subdomain boundary emanating from crack C1. Further rediscretization with the current boundary element mesh could not therefore be performed.

From other crack propagation data (not shown) for the two higher magnitudes of the fracture toughness, it is observed that the initiation of crack extension is delayed as the fracture toughness is increased. As a result, larger envelope values of tensile stresses are also predicted in this dam for the higher magnitudes of concrete toughness. For example, it can be seen from Figure B5 that the envelope tensile stresses computed on the two faces of the dam for K_{Id} = 9.0 MPa.m$^{1/2}$ exceed the tensile strength of concrete in the top part of the dam. Distributed surface cracking is thus likely to occur for this dam also, provided the fracture toughness is sufficiently high.

B2.4 Approximate post-cracking behavior

Since the hydrodynamic uplift pressure in upstream crack C2 can also build-up during the remaining time history of the earthquake excitation after rupture, the

corresponding opening data for this crack is obtained by performing approximate post-rupture analysis. The analysis is performed only for K_{Id} = 2.0 MPa.$m^{1/2}$, for which complete rupture is predicted. Hypotheses involved in such continuation of the time history analysis have already been discussed for the case of Koyna dam.

The resulting time history of crack mouth opening for the 6 sec of ground excitation is presented in Figure B6. Clearly, the opening magnitude for upstream crack C2 is much larger during the post-rupture phase compared to that at rupture. Since complete penetration of the dam cross-section occurs at an early stage of the earthquake excitation, the remaining strong ground motion results in significant movement of the dam crest and consequent large crack openings. Although downstream crack C1 experiences very large openings (maximum opening = 80 mm), the more relevant upstream crack C2 also undergoes a number of opening phases with significant opening magnitudes. The durations of these openings are, however, small and the almost completely separated top part of the dam continues to exhibit a stable response. The maximum opening of upstream crack C2 in the post-rupture phase is 22.3 mm compared to 1.38 mm during the rupture phase. Furthermore, magnitudes greater than 10 mm can also be noticed in four other cycles during the post-rupture phase, although the opening durations are all of the order of 0.1 sec.

B2.5 Summary of observations concerning hydrodynamic pressure build-up in crack C2

In order to predict the possible build-up of dynamic water pressure in upstream crack C2 during the three phases of the fracture response of the dam, corresponding mouth opening data are summarized in Table B1. As can be seen, the crack openings during the pre-rupture and the rupture phases of this dam are small. The maximum opening of 1.38 mm during the rupture process itself, combined with the very short duration of 0.05 sec, appears to be inconsequential for hydrodynamic pressure development in the crack. On the other hand, crack openings during the post-rupture phase are an order of magnitude

larger and probably sufficient to allow the water pressure to penetrate the crack and affect the dam response following rupture.

B3 CONCLUDING REMARKS

From the results presented above it is observed that, irrespective of the geometry, seismic cracking in a concrete gravity dam appears to be concentrated near the base of the crest block. Furthermore, the final cracking pattern is likely to result in complete rupture of the dam cross-section. Moreover, due to the almost instantaneous propagation of the cracks, the rupture process itself is also short. Increasing magnitudes of fracture toughness of concrete influence the final cracking pattern in the dam and, for sufficiently high toughness values, cracking is more distributed due to the delay in the propagation of already existing cracks. Openings of the upstream crack during the pre-rupture and the rupture phases are found to be too small for the hydrodynamic pressure to build-up. However, during the post-rupture response greatly increased magnitudes are predicted making possible that dynamic uplift pressure will develop in such cracks during this phase of the response. The consequence of such pressure development is that the post-rupture stability of the separated upper portion of the dam will be influenced by this pressure.

Finally, the data from the fracture analysis of the Pine Flat dam presented in this Appendix has served to confirm that the observations/conclusions arising out of the Koyna dam investigation presented in Chapter IV can be viewed as generally applicable.

Table B1 Crack mouth opening data for C2

K_{Id} ($MPa.m^{1/2}$)	Mouth opening data	Pre-rupture	Rupture	Post-rupture
2.0	Magnitude (mm)	0.33	1.38	22.03
	Duration (sec)	0.10	0.05	0.08
	Time (sec)	2.24	2.68	4.89

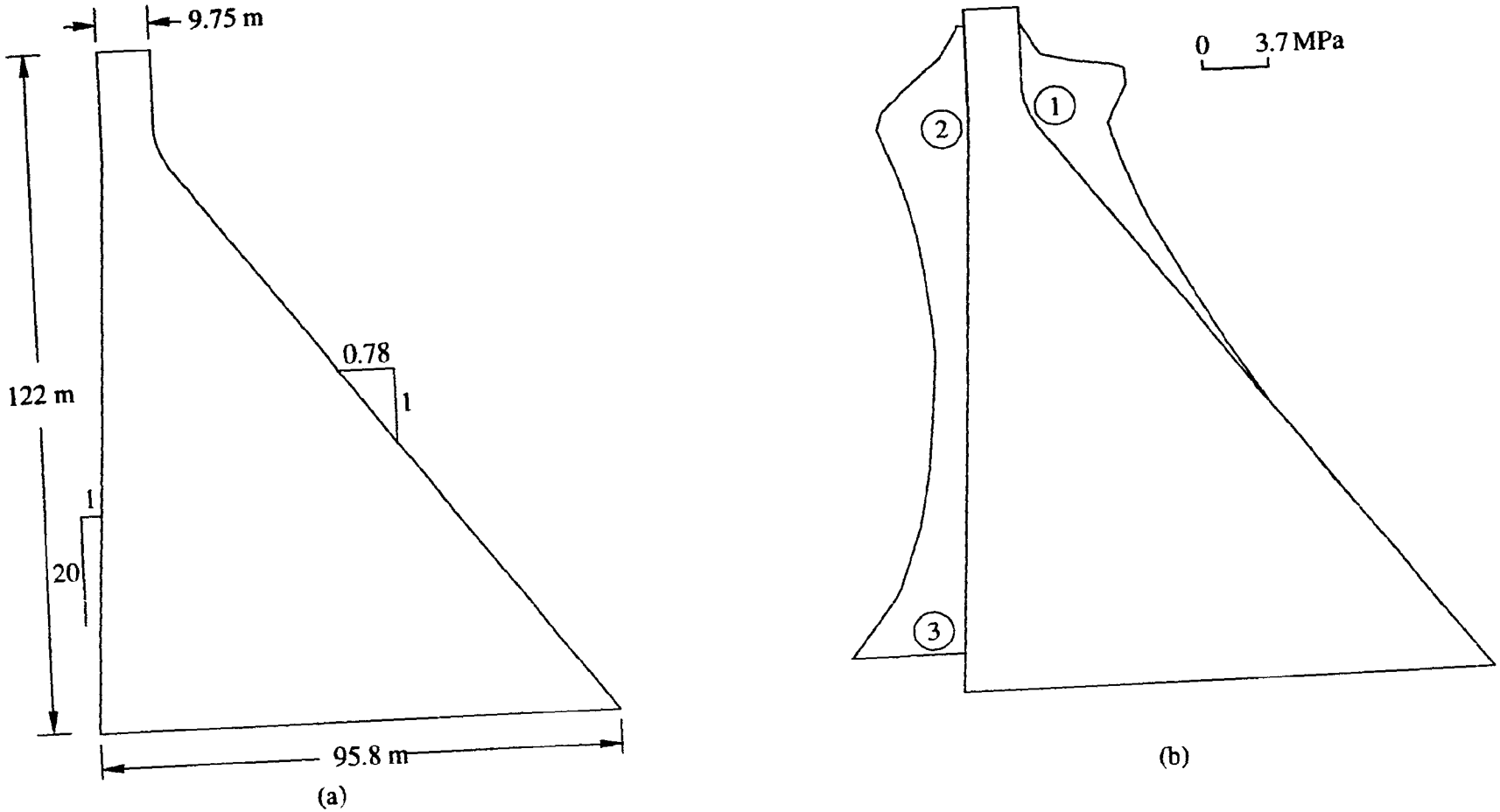

Figure B1 Pine Flat dam : (a) tallest non-overflow monolith: (b) envelope of principal tensile stresses for seismic analysis without cracks

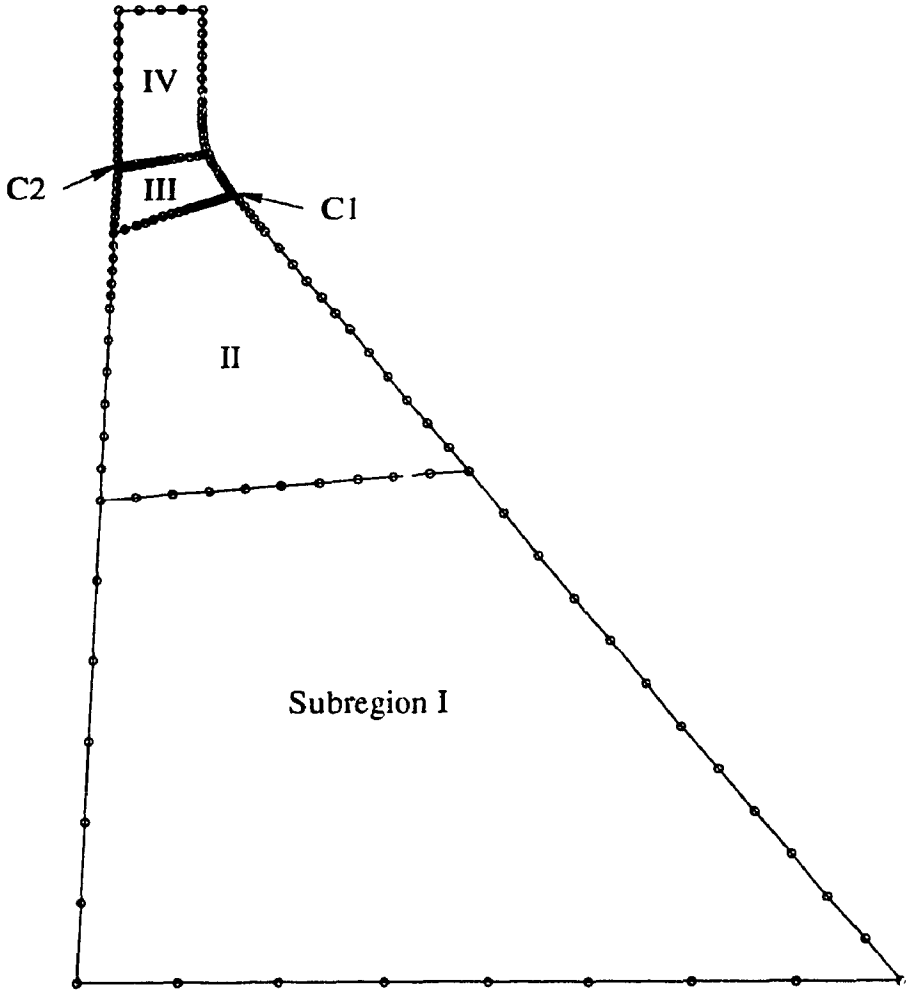

Figure B2 Boundary element discretization of Pine Flat dam with multiple cracking

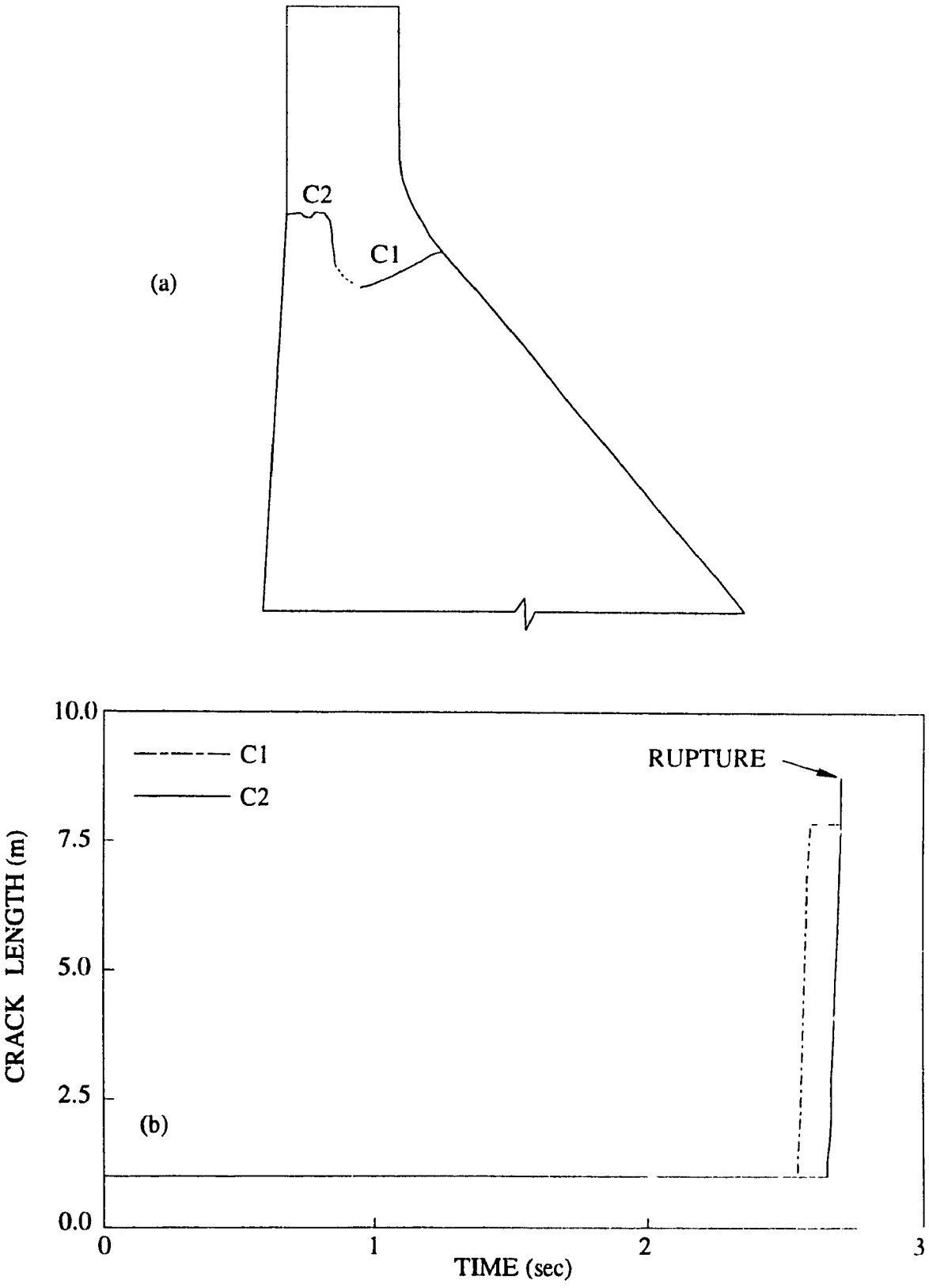

Figure B3 Fracture process for K_{Id} =2.0 MPa.m$^{1/2}$: (a) final cracking profile; (b) time-histories of crack lengths

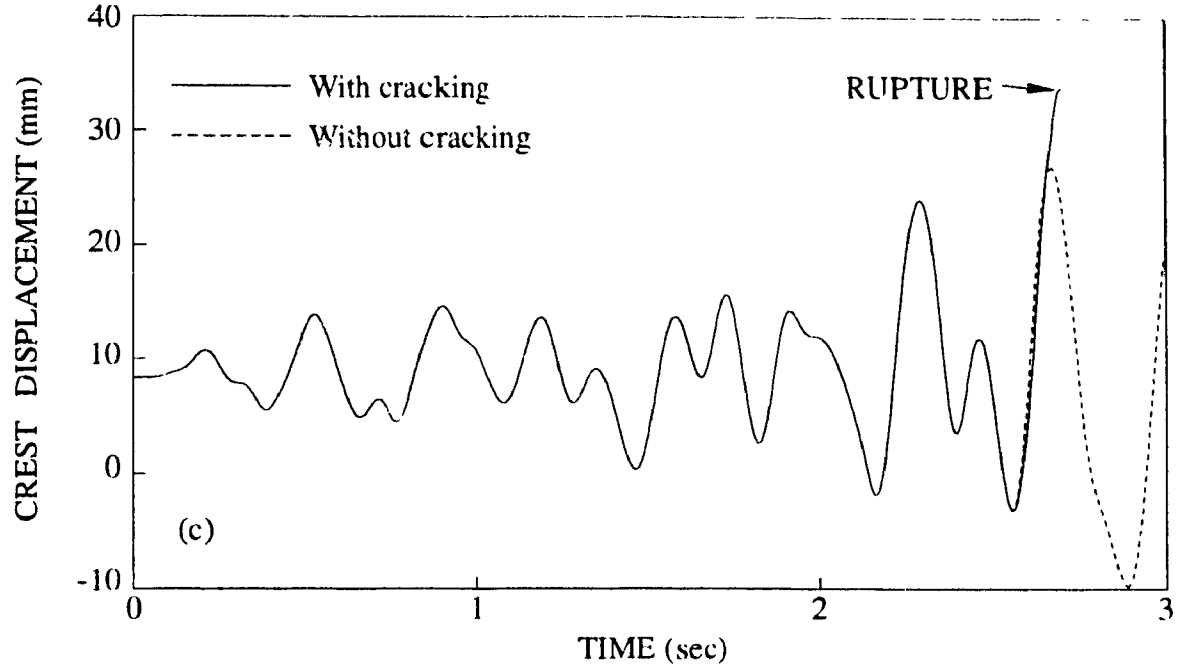

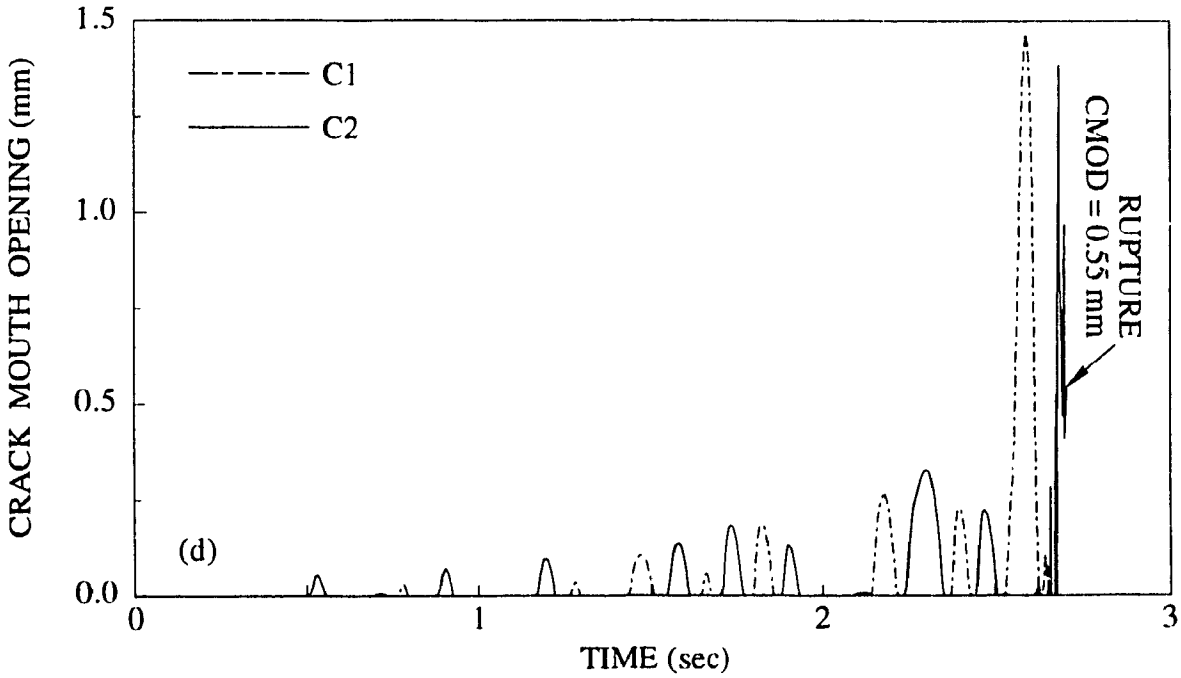

Figure B3 Continued: (c) time history of crest displacement; (d) time histories of crack mouth openings

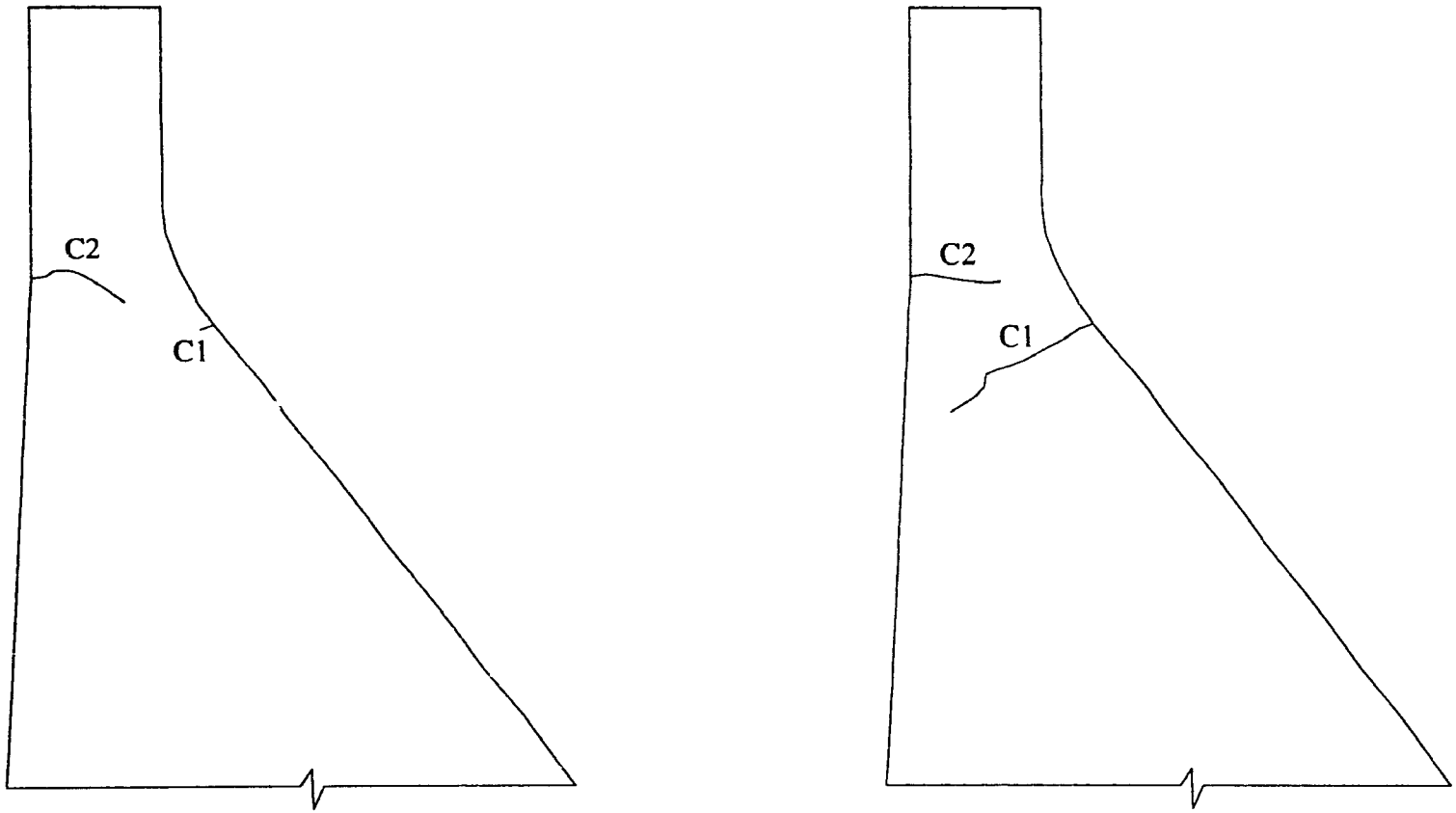

Figure 34 Final cracking profiles for higher magnitudes of dynamic fracture toughness: (a) $K_{Id} = 5.5$ MPa.m$^{1/2}$; (b) $K_{Id} = 9.0$ MPa.m$^{1/2}$

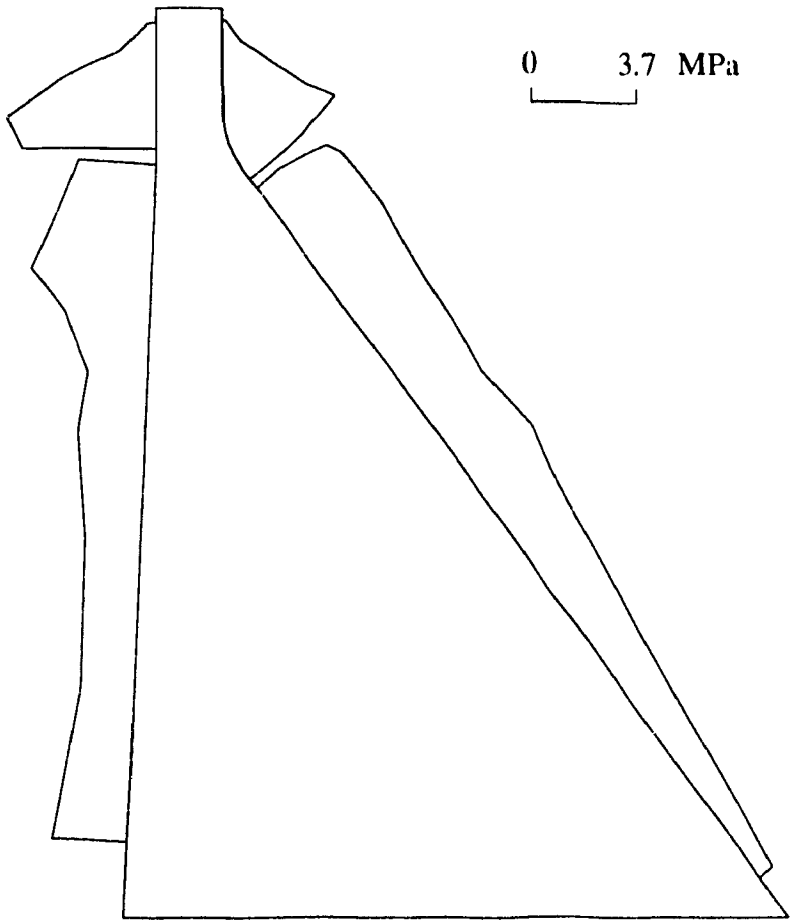

Figure B5 Envelope of principal tensile stresses for $K_{Id} = 9.0$ MPa.m$^{1/2}$

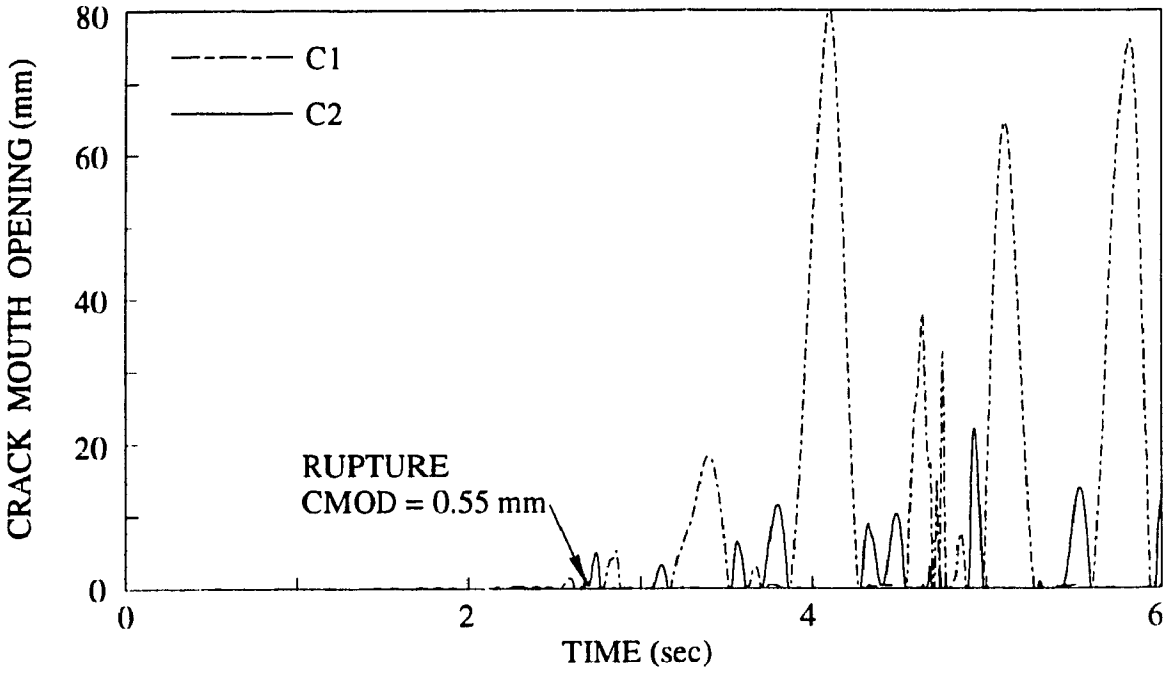

Figure B6 Post-rupture behavior for K_{Id} = 2.0 MPa.m$^{1/2}$